An Internal Model Principle Approach to Modeling Predictive Human Motor Behavior

by

Steven Cutlip

A dissertation submitted in partial fulfillment
of the requirements for the degree of
Doctor of Philosophy
(Biomedical Engineering)
in the University of Michigan
2021

Doctoral Committee:

Professor Brent Gillespie, Chair
Professor Cindy Chestek
Professor James Freudenberg
Professor James Weiland

Steven Cutlip

scutlip@umich.edu

ORCID iD: 0000-0003-4849-0435

© Steven Cutlip 2021

TABLE OF CONTENTS

List of Figures . . . . . **v**

List of Tables . . . . . **ix**

Abstract . . . . . **x**

Chapter

1 Introduction **1**

2 Haptic Feedback and the Internal Model Principle **8**

2.1 INTRODUCTION 8
2.2 Model Development 9
2.2.1 Open Loop Strategies For Driving Oscillations 10
2.2.2 Closed Loop Strategies For Driving Oscillations 12
2.3 Methods 16
2.3.1 Participants and Apparatus 16
2.3.2 Experiment Conditions 16
2.4 Results 17
2.4.1 Raw Signals 17
2.4.2 Fast Fourier Transform (FFT) 17
2.4.3 Signal Energy 17
2.4.4 Phase Plots 18
2.5 Discussion and Conclusion 18

3 Respecting the Coupled Dynamics: Haptic Feedback Carries both Power and Information **21**

3.1 INTRODUCTION 21
3.2 Model Development 22
3.2.1 Hand Model 23
3.2.2 Coupled Hand-Oscillator Model 23
3.2.3 Decoupled Hand-Oscillator Model 24
3.2.4 Coupled Virtual Hand-Oscillator Model 25
3.2.5 System Identification for Hand Model 26
3.2.6 Control Strategies 27
3.2.7 Model Simulation 27
3.2.8 Participants and Apparatus 28
3.2.9 Experiment Conditions 29

3.2.10 Experimental Measures . . . 29
3.3 Results . . . 30
3.3.1 Sample Data . . . 30
3.3.2 Summary Data . . . 30
3.4 Discussion and Conclusion . . . 30

4 An Internal Model Principle Based Approach to Modeling the Pursuit of Predictable Signals . . . 33

4.1 Introduction . . . 33
4.2 Background . . . 35
4.2.1 The Internal Model Principle . . . 35
4.2.2 IMP Example . . . 36
4.2.3 A Hybrid Dynamical System with IMP Controllers . . . 37
4.2.4 Our Proposed Model: The Feedforward Extended IMP Model . . . 39
4.2.5 Expected Model and Participant Behavior . . . 41
4.3 Simulation of the Feedforward Extended IMP Model . . . 41
4.3.1 Simulation Methods . . . 41
4.3.2 Simulation Results . . . 42
4.3.3 Simulation Discussion . . . 42
4.4 Human Participant Experiment . . . 43
4.4.1 Experimental Methods . . . 43
4.4.2 Experimental Results . . . 44
4.4.3 Survey Results . . . 46
4.4.4 Experimental Discussion . . . 46
4.5 Conclusion . . . 47

5 The Effects of Haptic Feedback and Transition Type on Transfer of Control between Drivers and Vehicle Automation . . . 49

5.1 Introduction . . . 49
5.2 Methods . . . 51
5.2.1 Participants . . . 51
5.2.2 Apparatus . . . 52
5.2.3 Automation System . . . 53
5.2.4 Secondary Task . . . 54
5.2.5 Transitioning Schemes . . . 55
5.2.6 Experiment Procedure . . . 56
5.2.7 Performance Metrics and Data Analysis . . . 57
5.3 Results . . . 58
5.3.1 Collisions . . . 58
5.3.2 Detection of unexpected automation failures . . . 58
5.3.3 Secondary Task Score . . . 59
5.3.4 Distance to Centerline $D_C(t)$ . . . 59
5.3.5 Intervention Period I_P . . . 61
5.3.6 NASA-TLX Score . . . 61
5.3.7 Subjective Ratings of Awareness of Automation Input . . . 63

5.4 Discussion 63
5.5 Conclusion 65
6 Conclusion **66**
6.1 Limitations and Future work 67
Bibliography **70**

LIST OF FIGURES

FIGURE

2.1 When rendered through a haptic device, a virtual torsional spring of stiffness K and inertia J_M can be used to study manipulation tasks akin to juggling. 9

2.2 The compliance of muscle encapsulated in stiffness k_1, along with damping b and mass m_1 that describe the backdrive impedance of the body, are driven by a motion source $\theta_r(t)$ to produce displacements $\theta_z(t)$ at the hand. The dynamics of an oscillator comprising stiffness k_2 and mass m_2, when rendered through the haptic device with force F_m, become coupled to the dynamics (biomechanics) of the body. By linearity, a persistent sinusoidal excitation $r(t)$ at frequency $\omega_0 = \sqrt{k_2/m_2}$ will produce, at steady-state, a sinusoid at $\omega_0 = \sqrt{k_2/m_2}$ in $\theta_w(t)$ and $\theta_z(t) \to 0$. Note: transitional diagram is standing in for what might be a rotational system 10

2.3 Without coupling, or if the haptic device motor is disabled, the dynamics of the virtual spring-mass system is driven by the motion source $\theta_z(t)$, the displacement of the haptic device handle. 11

2.4 (A) The coupled system displays a null response in the response of θ_z and a steady response in θ_w to sinusoidal excitation in θ_r at $\omega_0 = 0.6$ rad/s. (B) The uncoupled system, on the other hand, displays a steady response in θ_z and an unstable response in θ_w. 13

2.5 Time domain simulation results. (A) Coupled system, (B) Uncoupled system. Parameter values were selected as follows: $k_1 = 2.1$ N/m, $b = 0.27$ Ns/m, $m_1 = 0.00068$ kg, $m_2 = 0.2$ kg, $k_2 = 2.84$ N/m. 14

2.6 Block diagrams for the closed-loop controller based on the Internal Model Principle wrapped around the coupled system 14

2.7 Time domain simulation results for the closed-loop system shown in Fig. 2.6. The value 1 was used for the single free controller parameter C_0. 14

2.8 Raw Signals: EMG, Virtual Wheel $\theta_w(t)$, and Physical Wheel $\theta_z(t)$ position for Participant 4 (S4). The force $F_m(t)$ experienced by the user is proportional to the difference between $\theta_w(t)$ and θ_z(t) 16

2.9 Fast Fourier Transforms: Single Sided Amplitude Spectrum for EMG and Virtual Wheel Position for Subject 4 (S4) 17

2.10 In this figure $d\theta_W(t)/dt$ is plotted against θ_W for all three strategies and all 5 participants cr(t)eating phase plots. 19

3.1 Experimental Apparatus and Virtual Environment. A single-axis haptic device was used to render a virtual spring-inertia comprising stiffness k_2 and inertia m_2. 24
3.2 Coupled Hand-Oscillator Model. The spring k_1, damper b_1, and mass m_1 that together describe the backdrive impedance of the body are driven by a motion source $r(t)$ to produce displacements $z(t)$ at the hand. The oscillator is comprised of a stiffness k_2 and mass m_2. This translational schematic is standing in for a rotational system such as Fig 3.1. The corresponding block diagram is shown. Importantly, the diagram features a feedback signal F that represents the torque rendered through the haptic device to the dynamics of the body. 24
3.3 Decoupled Hand-Oscillator Model. Without coupling, or if the haptic device motor is disabled, the dynamics of the virtual spring-mass system is driven by the motion source $z(t)$, the displacement of the haptic device handle. Importantly, the diagram no longer features the feedback signal containing F as in Fig 3.2. 25
3.4 Coupled Virtual Hand-Oscillator Model. Haptic feedback has been removed and thus the mass-spring-damper biomechanics (in red) are no longer loaded by a reaction force from the oscillator. However, the double-mass task dynamics have been preserved by inserting a model of the hand (virtual hand, in black) into the virtual environment. . . 26
3.5 Simulation Results: The Decoupled Hand-Oscillator and Coupled Virtual Hand-Oscillator systems are simulated using a sinusoid generator. The first thirty seconds the system is excited at the natural frequency of the virtual spring mass and then the generator is shut off for thirty seconds. 28
3.6 Single Representative Participant Results: This figure shows representative data from the human subject experiment. The participant attempts to resonate the system at the oscillator's natural frequency for the first 30 seconds and then relaxes for the next 30. . 31
3.7 All Participants: means of metrics across all three conditions. Errors bars associated with each bar indicate variance. The amplitudes associated with the RMS values are in volts (EMG) and rad (hand, virtual hand, and oscillator). 32

4.1 Experimental conditions. A) Visual feedback of both the target and the cursor are available to the participant. B) Only visual feedback of the target is displayed; the cursor is blanked. C) No visual feedback is displayed on the monitor; both the cursor and target are blanked. 34
4.2 Standard feedback control block diagram. For an IMP based controller the poles of $C(s)$ include the poles of the reference signal generator $R(s)$. 36
4.3 State machine featuring two modes: A) IMP controller $M(s)$ with feedback B) IMP controller $M(s)$ without feedback. 38
4.4 Simulation of a system designed according to IMP described as a hybrid dynamic model (a state machine with continuous modes). Note that the mode of the state machine changes halfway through the simulation. Tracking is maintained despite the change in availability of $r(t)$. 39

4.5 A hybrid dynamical model of predictable reference tracking with three distinct modes depending on signal availability. Mode I) uses two Internal Model Principle controllers $M(s)$ and $C(s)$ working in parallel when both $r(t)$ and $y(t)$ are available; mode II) uses an IMP controller $M(s)$ while $C(s)$ acts as a signal generator without excitation when only $r(t)$ is available; and mode III) uses both IMP controllers $M(s)$ and $C(s)$ acting as signal generators without excitation when neither $r(t)$ nor $y(t)$ are available. 40
4.6 Results of IMP based model during signal blanking. Each 30 second interval is demarcated by a vertical grey bar; this indicates a change in the availability of $r(t)$ and/or $y(t)$. 42
4.7 Representative subject time signals: A) The raw positional data of the target (red) and the participant controller cursor (green), B) Shows the amplitude associated with the highest frequency in the cursor data, C) The frequency difference between the target (oscillating at 0.5 Hz) and the cursor, and D) The phase difference between the target and the cursor. 44
4.8 Summary Data: The box plots show average RMSE, frequency error, and phase error over all intervals, for all participants, and for both trials 45
4.9 Boxplots showing the difference in RMSE performance before and after exposure to y, r condition 46

5.1 A) Hardware setup B) Virtual driving environment and C) Top view of the driving track (navigated clockwise) 53
5.2 Screenshots of the secondary task that was presented on a tablet computer (in both cases above, the participant was required to swipe right) 55
5.3 Expected result of composing planned human and automation paths by transitioning scheme and obstacle-handling assignment. Under the schemes (top row) only one of the automation planned paths (in brown) or human planned paths (in green) is active (solid) while the other is inactive (dashed) at any given time. Thus the vehicle follows either the automation or human planned path around the obstacle. For the human-assigned obstacles (right group of four panels), the driver pushes a button to disengage and re-engage the automation, whose path is nominally through the obstacle. Under the schemes (bottom row), the vehicle follows a combination of the human and automation planned paths. The arrows indicate the direction and magnitude of haptic feedback presented to the human driver. Note that and have identical behavior in response to HA obstacles, however they have different performance in response to AA obstacles. The intent of the comparison between these two schemes is to understand which performs better overall when AA and HA are jointly considered. 56
5.4 A) An example of a typical trajectory traced by the vehicle around an obstacle with the metric $D_C(t)$ indicated between the trajectory and lane centerline. B) The metric I_P is defined as the time interval between crossing a 1 m threshold from the lane centerline. 57
5.5 Average total secondary task score accumulated 0 to 5s before obstacles. Error bars indicate standard error. 60
5.6 Distance to centerline $D_C(t)$ shown in overlay for all obstacles except for unexpected automation failures, separated by Obstacle Type and transitioning scheme. A) AA obstacles (shown to participant as red obstacles) and B) HA obstacles (shown to participant as green obstacles). The magenta trace is the average trajectory. 61

5.7 The mean distance to centerline $\overline{D_C}$ computed over a 20 second window centered at the obstacle. The error bars indicate standard error. 62
5.8 A) Average time interval I_P between 1 m threshold crossings before and after passing an HA obstacle. Error bars indicate standard error. B) Table indicating significant differences (*) across transition schemes 62

LIST OF TABLES

TABLE

2.1 Amplitude at 0.6 Hz and signal energy associated with EMG and θ_W for all three strategies and all 5 participants. 18

3.1 Simulation: Average RMS value of metrics (in rad) across all three conditions. 27

5.1 Transition schemes by type and feedback availability 55
5.2 Experiment design 57
5.3 Number of collisions occurring in the four transitioning schemes with HA obstacles. . 59

ABSTRACT

For the sensorimotor system to complete motor tasks it controls the body, it controls objects that the sensorimotor system acts upon within the environment, and it anticipates future states of the environment. The sensorimotor system is known to adapt and improve in performance with practice in response to predictable phenomena. The literature explains motor adaptation and performance improvement in terms of models, called internal models, of future loads. The theory of internal models has been investigated in the neuroscience and human motor behavior communities, where electrophysiological data and motor performance experiments have yielded rich data in support of the role of predictive modeling.

Internal models can be divided into two types: internal models of the plant and internal models of exogenous processes. While internal models of the plant have a rich history and have been studied extensively, literature on internal models of exogenous processes is less developed. This dissertation introduces the Internal Model Principle (IMP) as a tool for modeling internal models of exogenous processes. This dissertation further extends the usefulness of the IMP for modeling human motor control by extending the model to handle sensorimotor tasks that feature signal blanking.

Haptic feedback can be considered as an exogenous signal (a disturbance) whose features can be predicted because they are produced by the plant under control. Haptic feedback is an information signal providing the receiver feedback about the state of the system. However, haptic feedback is also a power signal; sufficient force due to haptic feedback can backdrive the biomechanics of a participant. In this dissertation these topics are explored in two studies, one in the context of driving oscillations in a spring-mass system and the other in the context of shared control design for semi-autonomous vehicles.

CHAPTER 1

Introduction

A healthy sensorimotor system adeptly controls the body to perform tasks in a manner that robotic systems struggle to replicate. Part of what makes the sensorimotor system able to perform motor tasks well is its ability to make predictions. Predictive behaviors of the sensoriotor system can be observed both in nature and laboratory settings with examples that include: predatory behaviors, [1, 2, 3], hiding in moving shelters [4], and in athletic and music performance [5]. In order to produce influences on the body that can be predicted, these tasks necessarily involve deterministic dynamics. To explain how the sensorimotor system is so adept and able to take advantage of these deterministic dynamics, a longstanding explanation has been developed with ample evidence and robust support: the sensorimotor system internalizes the environment and retains information in the form of models (internal models) to process and integrate sensory information and to plan motor action [6, 7, 8, 9]. Experimental support is available in: forcefield adaptation [10], reach and grasp tasks [11], adaptation to vestibular stimuli [12], visuomotor experiments [13, 14], electrophysiological measurements [15], the study of eye movements [16], and in general settings [9].

Internal Models and the Internal Model Principle

Internal models can be divided into to two types: models of plants and models of processes that generate predictable exogenous signals. These two internal model types specify different relationships between the modeller and the subject to be modeled, and as such, require different treatments. However, distinctions between the two types are often not clearly made. While internal models of the plant are not the topic of interest in this dissertation they are discussed here in order to make their distinction from internal models of exogenous processes clear.

An internal model of the plant describes an object that the sensorimotor system acts upon within the environment, such as a tool or object. As a consequence, to form an internal model of the plant, active exploration is available to understand its dynamics. For example, for someone who has never held a hammer, a hammer's weight, mass center, moment of inertia, and center of percussion

may be initially unfamiliar. Consequently, the amount of force and best means of manipulating a hammer to hammer a nail is initially unknown. With experience using the hammer, including active exploration, a model of the hammer is thought to be formed, allowing subsequent hammers to be wielded and subsequent nails to be hammered with ease and without much cognitive effort [17, 18]. Notably, the sensorimotor system has access to both input and output signals of a plant. An important distinction of internal models of the plant is that the dynamics in question lie within the control loop.

In addition to objects in the environment, the first type of internal model also includes models of one's own body. The sensorimotor system, with experience, is able to form internal models to compensate for one's own body in order to better perform tasks [19, 20]. For example often at a young age of development or after a long period of under-utilization, the unfamiliarity of the mechanical properties of one's own body may prove cumbersome, leading to frequent errors of control. The dynamics of the body are coupled to the sensorimotor system in a manner than can be compared to the coupling of a tool to the body. However, a major difference is that the sensorimotor system has had much more experience with the dynamics of the body, as it is continuously coupled to the body, whereas it is only intermittently coupled to tools. Because of these similarities, understanding whether internal models of tool and body are learned independently or whether the internal model of the arm is adapted continues to be a topic of research [20].

The second type of internal model, and topic of interest in this dissertation, is of exogenous signal processes. Exogenous signal processes are dynamics located in the external world to which the sensorimotor system is not dynamically coupled [8, 21]. The sensorimotor system only has access to the output signal of an exogenous signal generator. For example, an internal model of the anticipated trajectory of a baseball may be utilized to improve interception [22]. Another example of an exogenous process is a metronome where the timing of its sound cues may be internalized and used to improve the timing of keystrokes upon a piano. The metronome is an example of an exogenous process; a process that generates a signal which the sensorimotor system may use for control but is not mechanically coupled. The dynamics of the metronome are then not located within the control loop and are consequently not modeled through active exploration but are instead passively learned. As a result, internal models of exogenous signal generators must be treated in a manner very different to internal models of the plant.

By separating Internal Models into these two types it becomes clear that mathematical descriptions involving the plant are extensively studied [23, 10, 8, 6, 24] and those of exogenous processes are understudied [25]. This is likely due to the combination of several different causes: 1) The distinction between models of the plant and exogenous processes is subtle as has not been fully recognized by the motor behavior community 2) In practice, many signals have high noise, present without patterns, or have complex unrecognizable patterns 3) By definition, the controller only

has access to the output of an exogenous process, this makes recognizing patterns more difficult. Patterns often have to be limited to steps, ramps, or oscillations in order to be recognized. 4) Model based architectures tend to focus on models of the plant even within the control systems community. Literature on mathematically modeling human motor behavior has been influenced in large part by one of the earliest models of human control behavior, the McRuer Crossover model [26]. The McRuer Crossover model focuses on how the sensorimotor system is able to consider the first type of internal model involving plant dynamics [27]. Toward modeling human motor behavior in response to predictable exogenous signals however, the McRuer model falls short, as it is only applicable to internal models of the plant. McRuer did speculate about the possible existence of a synchronous generator in the feedforward path but did not go very far in studying this idea. Models of unpredictable tracking behavior based on McRuer have been extended to better capture predictable behavior through additions such as a feedforward path [28, 29, 26, 30, 31]. However, motor behavior literature has not yet sufficiently treated internal models of exogenous processes.

The first contribution of this dissertation is to introduce a promising and underutilized alternative for modeling human behavior called the Internal Model Principle (IMP) [25]. The Internal Model Principle states that perfect tracking of a reference signal can only be achieved with a model of the predictable signal within the control loop [32, 33]. Internal models of exogenous signals are precisely what the IMP requires in order for a system to achieve perfect tracking. In this dissertation I present the IMP as a means for modeling how human motor behavior might incorporate internal models of predictable exogenous processes within a control loop.

An Internal Model Principle Architecture to Handle Blanking

In this dissertation the applicability of the IMP is extended to motor control tasks where the predictable signals of interest are not always available to the sensory system. The ability to predict or anticipate a cue allows one to plan and execute motor behavior before a cue occurs. To study this behavior, a task paradigm has been developed wherein a reference signal of interest is temporarily hidden from the participant; this paradigm is also called signal blanking or simply blanking. The sensorimotor system has been shown to exhibit good reference tracking behavior even with intermittent visual access to the reference trajectory [16, 34].

In an effort to model these behaviors, feedforward extensions to compensatory control strategies have been proposed [29, 35, 31, 36]. While feedforward control is able to explain an increase in performance due to predictable proprieties of the reference signal, feedforward control no longer applies when the system is faced with signal blanking. In this dissertation my second contribution is to show how the IMP can be used to replicate human motor behavior in tasks that feature signal blanking.

Haptic Feedback: Power and Information

Haptic feedback introduces an additional challenge when trying to understand or explain how the sensorimotor system utilizes internal models [37, 38]. Suppose a user of a human-machine system is experiencing haptic feedback that is strong enough to backdrive their biomechanics. Haptic feedback can be thought of as comprising two signals: power and information. Haptic feedback as power is present through the transmission of power that backdrives the biomechanics of the user. Haptic feedback as information is evidenced through our ability to describe and utilize perceptions of what is being felt from the physical world in order to better perform motor tasks.

In the field of prosthetics this dual nature has great importance and continues to be explored. For example, mechanical body-powered prostheses provide certain advantages over myoeletric alternatives because of their ability to transmit appropriate haptic cues to the driving shoulder when being backdriven, resulting in a more intuitive perceptual experience [39]. To study human motor behavior, experiments have to be carefully designed to ensure the dynamics of the system one wishes to study are accurately portrayed. The experiment designer also has to mindfully construct the task itself as many tasks tend to present a multitude of reactive and predictive strategies that may be difficult to compare if the task is not constrained appropriately.

Often, those studying haptics focus on haptic feedback that is restricted to cutaneous stimulation rather than feedback capable of backdriving the limb segments and joints of its user. Knowledge of control system modeling within the haptics community, tends to focus on stability and passivity analyses of the device itself [40, 41, 42]. In the robotics and dynamic walking communities, an appreciation exists for coupled dynamics and the backdrivable nature of the human body [43, 44]. An exception exists in the study of haptic shared control where the coupled dynamics of the driver's biomechanics must be considered [45, 46]. However, a clear appreciation that the act of coupling dynamics changes the task from the perspective of the sensorimotor system remains to be stated.

As the prevalence of haptic technology grows and seeks to expand its impact, it will become increasingly important to combine insights from the robotics and dynamic walking communities. The third contribution of this dissertation highlights the importance of considering the dual roles of haptic feedback as well as offering a concrete study that illustrates both roles to the haptics community.

Studying Transitions of Control in a Simulated Semi-autonomous Vehicle

Finally, in separate but related work, I investigate the role of transitions and haptic feedback between humans and automation systems. When designing a successful human-machine system, the interactions between haptic feedback, information-carrying cues, control transitions, and authority paradigms have to be carefully considered. The cues generated by the system and displayed to

the user have to be constructed to allow the user to form the intended internal models of the human-machine system. When human and machine are mechanically coupled, each agent engages in a complex collaboration problem where, in order accomplish task goals, they have to negotiate with each other and react appropriately to visual or haptic cues [47, 48, 49, 50, 51]. In some cases, while each agent may be imbued with similar control abilities, each agent is thought to take on a specialized role causing each agent to exhibit different control behaviors; such as a student and teacher [52]. Perhaps the most ubiquitous example of a human-machine collaborative system is the semi-autonomous vehicle. Increasingly, the automation within a semi-autonomous vehicle is tasked with more and more responsibility. However, there are still instances where the human passenger is asked to transition to the role of driver [53, 54, 55]. Critical to the design and safety of these collaborative systems is understanding how to both keep the human prepared and maintain communications during transitions [56, 57]. For my final contribution, in the last chapter of my dissertation I investigate the role of haptic feedback and abruptness of transitions through a human participant study.

This thesis has four main contributions.

- **Contribution 1, Chapter 2:** Introduce the IMP to the human motor and haptics community by re-purposing the theory of IMP to describe human motor control behavior.
- **Contribution 2, Chapter 3:** Extend the IMP to model the robustness of human-motor behavior to signal blanking while tracking predictable signals.
- **Contribution 3, Chapter 4:** Delineate the dual roles of haptic feedback, power and information.
- **Contribution 4, Chapter 5:** Assess how haptic feedback affects performance during transitions of control within a semi-autonomous human machine system.

Relationship between Chapters and Contributions

Haptic Feedback and the Internal Model Principle: Contribution 1, Chapter 2

According to the Internal Model Principle from control engineering, error feedback together with a controller containing an internal model that generates an expected disturbance signal can achieve perfect delay-tolerant disturbance rejection using only modest loop gains. While internal models of plant dynamics have been central to the study of human motor control, internal models of reference or disturbance signal generators have received very little attention. The Internal Model Principle suggests a certain control strategy for achieving steady oscillatory motion in a virtual spring-mass. The strategy relies on haptic feedback in its dual roles of carrying power and information and this dual reliance may be used to derive numerous testable hypotheses. This chapter presents results from an initial study in which high time-correlation between surface electromyography and commanded torque signals suggests the adoption of a control strategy based on the Internal Model Principle.

An Internal Model Principle Based Approach to Modeling the Pursuit of Predictable Signals: Contribution 2, Chapter 3

Humans demonstrate an aptitude for recognizing and exploiting predictable patterns in the environment. Human behaviors that account for predictable environmental influences are called *predictive* and can be distinguished from *reactive* behaviors by their complete elimination of error and phase delay. Modeling this behavior would allow a robotic system to perceive the environment in a more human-like manner or allow a human-machine system to better understand and anticipate the actions of its operator. Existing models of human pursuit tracking behavior have focused on describing the tracking of unpredictable signals. Models of unpredictable tracking behavior have been extended, through additions such as a feedforward path, to capture some elements of predictable behavior. However, these extensions to not explicitly model predictable reference signals. We propose an alternative model utilizing the Internal Model Principle (IMP) that does explicitly model reference signals. The IMP was developed in the control community to allow mechatronic systems to track the patterns of reference signals or reject disturbances with known frequencies. A key component of the IMP architecture is an explicit dynamic model of the predictable reference dynamics within a feedback loop. This chapter motivates the advantages of this modeling approach by presenting and simulating an IMP based model and by conducting a human participant study for comparison.

Respecting the Coupled Dynamics: Haptic Feedback Carries both Power and Information: Contribution 3, Chapter 4

Haptic feedback provided in the axis of a motor task cannot be removed without changing the motor task itself. Haptic feedback couples the biomechanics of the backdrivable body to the dynamics of the environment and establishes a conduit for both power and information exchanges. To isolate the roles of haptic feedback in information exchange and power exchange, a task without haptic feedback was devised that preserved the motor challenge of controlling the coupled dynamics. We placed an identified model of a participant's biomechanics in the virtual environment and coupled it to the original task dynamics. Visual feedback was provided to substitute for the missing haptic feedback. The performance of participants in the same motor task was compared with and without haptic feedback and in the new task without haptic feedback. The presence of the coupled dynamics in the task predicted the match across conditions rather than the feedback modality. The results presented in this chapter provide support to the idea that rather than controlling their environment, humans control the coupled dynamics of their body and environment.

The Effects of Haptic Feedback and Transition Type on Transfer of Control between Drivers and Vehicle Automation: Contribution 4, Chapter 5

When driving conditions exceed the design limits of an automation system, transfers of control back to a human driver become necessary. Such transfers may compromise safety, since a driver typically requires time to get back into the loop. Various schemes for combining human and automatic control over steering have been proposed to address the challenges of transferring control smoothly. This chapter presents the findings from a simulator study that compared four such schemes. The driver initiated a transfer of control either by pressing a button and assuming full control of the vehicle (abrupt transition) or by overpowering an automation that continued to act on the vehicle (gradual transition). Two additional factors in the $2 \times 2 \times 2$ factorial design were the availability of haptic feedback and the inclusion of a secondary task. To examine the robustness of each scheme, all driving scenarios involved nominal and off-nominal conditions. The findings from this study demonstrate the benefits of Haptic Shared Control (i.e., overpowering transitions with haptic feedback) for facilitating transfers of control between a human driver and vehicle automation. Haptic feedback enhanced drivers' awareness of automation input and the status of the vehicle while the overpowering transitions improved the smoothness of interventions, compared to switching transitions.

CHAPTER 2

Haptic Feedback and the Internal Model Principle

2.1 INTRODUCTION

When haptic feedback is denied, performance in most manipulation tasks degrades significantly, often failing altogether. Thus we know that haptic feedback informs control strategies used to assess mechanical properties, to identify and sort objects, to guide manipulation processes, and to tune motor control strategies. But how exactly does the human motor system make use of haptic sensory feedback? Naturally, haptic feedback across a mechanical contact carries not only sensory information but also mechanical power. How does the motor control system make sense of these intertwined roles? These questions are of high interest for scientific reasons and to inform the design of control algorithms for autonomous robots, for robots that work cooperatively with humans, and for robots designed to train or rehabilitate human motor skill.

Juggling is a manipulation skill that has garnered significant study from the perspective of robotics, control, and neuroscience [58, 59, 60, 61, 62]. It has been found that haptic feedback is critical to stabilize and maintain a steady juggling height [62, 58]. A continuous system counterpart to juggling without discrete contacts is eliciting and maintaining oscillation in a mechanical oscillator. Examples of mechanical oscillators include a torsional spring-inertia system as shown in Fig. 3.1. The value of haptic feedback for eliciting oscillations in a spring-mass has been studied from an empirical standpoint [63]. Huegel and O'Malley used the challenge of maintaining oscillations at a specified amplitude as a task to be trained with haptic guidance [64]. Dingwell et al. [23] observed sophisticated model-based strategies for moving a mass from an initial to final rest position through a spring. The Internal Model Principle, a tenet in control engineering since the early 1970s [33], states that a feedback controller containing a model of the signal to be tracked or rejected (exogenous signals) can achieve, using only modest loop gains, perfect reference tracking or disturbance rejection. A model in the controller acts to generate the signal that precisely zeros out the error between desired and actual system response. The Internal Model Principle generalizes the manner in which integral control eliminates static steady-state error (the zero response of an integrator with a non-zero initial condition). Thus, to track a persistent sinusoidal reference at frequency ω_0, the

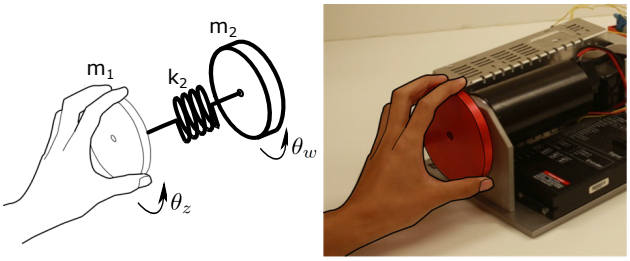

Figure 2.1: When rendered through a haptic device, a virtual torsional spring of stiffness K and inertia J_M can be used to study manipulation tasks akin to juggling.

Internal Model Principle posits that the controller should contain poles at $s = \pm j\omega_0$. In steady state, this controller will generate the excitation that produces perfect reference tracking.

The Internal Model Principle has its adherents in engineering practice, most notably in the disk drive industry [65]. However, as a hypothesis for biological control, the Internal Model Principle has found very little exploration to date with the exception of [25]. Contrast this unexplored territory to the use of internal models of plant dynamics (endogenous system), which has produced a very large literature [7, 9, 8]. Also not that the Internal Model Principle does not propose an *inverse model* in a feedforward controller (where it would be useful for cancelling plant dynamics). Instead, the Internal Model Principle proposes that a model of the expected reference or disturbance signal generator be placed in the control loop.

In this chapter the Internal Model Principle is used to generate hypotheses about human control strategies for driving oscillations in an undamped spring-mass system. We account for the dual roles of haptic feedback for power and information exchange in our system models (section 3.2) and undertake a human participant study to test the predictions produced by hypothesizing a neural controller based on the Internal Model Principle (sections 3.1 and 3.3). We conclude by observing that the Internal Model Principle gives a parsimonious explanation of how humans use haptic feedback to perform cyclic manipulation tasks.

2.2 Model Development

Due to compliance in muscle, the body's dynamics are liable to become coupled to the dynamics of objects being manipulated, especially when the impedance of the body and object are approximately matched. In such case the nervous system is faced not with the control of the object dynamics, but with the control of the coupled dynamics of body and object. Even in producing desired motions in a simple mass, it is necessary to devise a strategy that will arrest both the kinetic and potential energy in the coupled dynamics of body and mass. In essence the human motor system solves the crane operator's problem even when moving a rigid object, so long as the inertia forces

produce extensions in muscle [66]. All the while it may not "feel" like a sophisticated strategy, given that proprioception and force sensing is available at the hand, that distal attribution is likely at play [67], and that the brain's schemes may not be available for introspection.

Note that driving-point impedance can be modulated by co-contracting muscles or changing posture. Thus one might choose to eliminate compliance from the manipulation challenge by co-contracting muscles. However, such a strategy is generally reserved for the early stages of motor learning [68]. Studies have shown that humans prefer to adopt a modest compliance and a more sophisticated control strategy in the latter stages of learning [23] to save energy and increase performance.

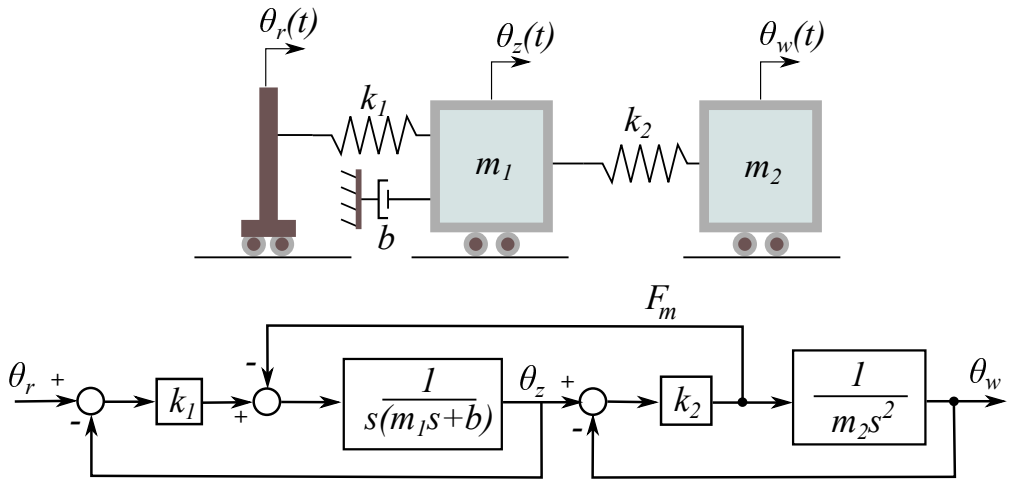

Figure 2.2: The compliance of muscle encapsulated in stiffness k_1, along with damping b and mass m_1 that describe the backdrive impedance of the body, are driven by a motion source $\theta_r(t)$ to produce displacements $\theta_z(t)$ at the hand. The dynamics of an oscillator comprising stiffness k_2 and mass m_2, when rendered through the haptic device with force F_m, become coupled to the dynamics (biomechanics) of the body. By linearity, a persistent sinusoidal excitation $r(t)$ at frequency $\omega_0 = \sqrt{k_2/m_2}$ will produce, at steady-state, a sinusoid at $\omega_0 = \sqrt{k_2/m_2}$ in $\theta_w(t)$ and $\theta_z(t) \to 0$. Note: transitional diagram is standing in for what might be a rotational system

2.2.1 Open Loop Strategies For Driving Oscillations

Consider now the manipulation of a non-rigid object like a spring-mass (without damping). And suppose the manipulation challenge is to maintain sustained oscillations in this mechanical oscillator. Given that a distal mass is part of the model for the driving point impedance of the hand [69, 70, 71], when the dynamics of a spring-mass are coupled to the body, a system with fourth-order dynamics results. Figure 2.2 shows a mass m_1 with displacement $\theta_z(t)$ along with stiffness k_1 and damping b that describes the driving point impedance at the hand. This second order driving point impedance is elaborated with a motion source $\theta_r(t)$ to describe volitional muscle action [71]. Figure 2.2 also shows the same model in the form of a block diagram, where the role of

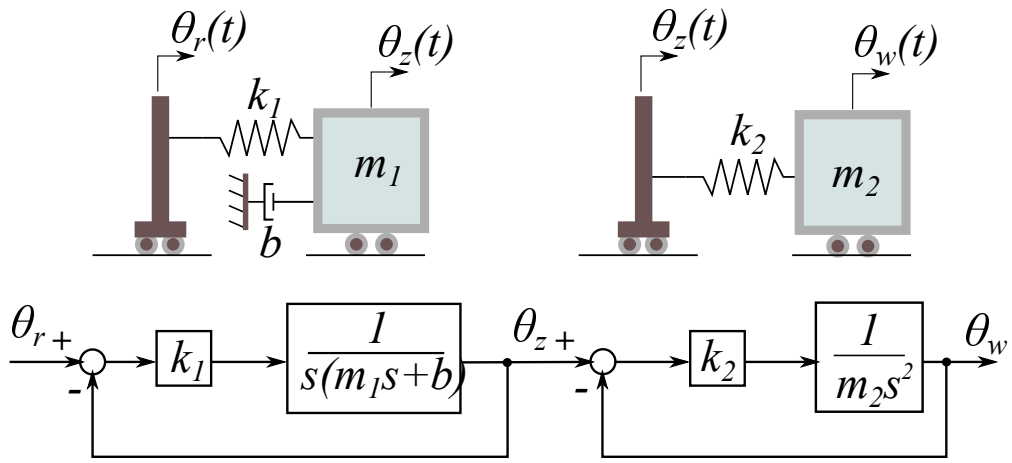

Figure 2.3: Without coupling, or if the haptic device motor is disabled, the dynamics of the virtual spring-mass system is driven by the motion source $\theta_z(t)$, the displacement of the haptic device handle.

the force F_m carried in the spring k_2 becomes apparent as a feedback path coupling the dynamics of the undamped oscillator with the dynamics of the body. The response of hand displacement $\theta_z(t)$ and oscillator displacement $\theta_w(t)$ to an excitation $\theta_r(t)$ may be obtained directly from the block diagram:

$$\frac{\theta_Z(s)}{\theta_R(s)} = \frac{G(s)}{1 + \frac{m_2}{k_2}s^2 G(s)H(s)} \tag{2.1}$$

$$\frac{\theta_W(s)}{\theta_R(s)} = \frac{G(s)H(s)}{1 + \frac{m_2}{k_2}s^2 G(s)H(S)}, \tag{2.2}$$

where $G(s) = \frac{k_1}{m_1 s^2 + bs + k_1}$ and $H(s) = \frac{k_2}{m_2 s^2 + k_2}$.

To make the poles and zeros of these transfer functions explicit, let us express $G(s)$ as a ratio of polynomials $\frac{N_G(s)}{D_G(s)}$ and $H(s)$ as $\frac{\omega_0^2}{(s^2+\omega_0^2)}$ (highlighting the undamped oscillator dynamics with natural frequency $\omega_0 = \sqrt{k_2/m_2}$). Then the transfer functions in Eqs. 2.1 and 2.2 can be re-written:

$$\frac{\theta_Z(s)}{\theta_R(s)} = \frac{N_G(s)(s^2 + \omega_0^2)}{D_G(s)(s^2 + \omega_0^2) + \frac{m_2\omega_0^2}{k_2}s^2 N_G(s)} \tag{2.3}$$

$$\frac{\theta_W(s)}{\theta_R(s)} = \frac{\omega_0^2 N_G(s)}{D_G(s)(s^2 + \omega_0^2) + \frac{m_2\omega_0^2}{k_2}s^2 N_G(s)}. \tag{2.4}$$

Note that the poles of $H(s)$ appear as zeros in the transfer function $\frac{\theta_Z(s)}{\theta_R(s)}$. See also the Bode plot in Fig. 2.4(A). These are called transmission zeros, and they suggest the following control strategy to achieve sustained oscillations in the oscillator: Simply excite the coupled dynamics with

a sinusoid at frequency ω_0. Given that $\frac{\theta_W(s)}{\theta_R(s)}$ is stable and linear, the steady-state response $\theta_w(t)$ to $\theta_r(t) = \sin \omega_0 t$ will be a sinusoid at ω_0 with possibly a different amplitude and phase. At the same time $\theta_z(t) \to 0$, precisely because of the presence of the transmission zeros in $\frac{\theta_Z(s)}{\theta_R(s)}$.

Note that the discussion so far also pertains to the manipulation of a virtual spring-mass rendered through a haptic device. The mass m_1 and damping b modeling human impedance may alternatively be lumped with the physical dynamics of a haptic device. Also, whether the damper b links mass m_1 to ground or to the motion source $r(t)$ is immaterial to the arguments that follow. What would be the behavior of the spring-mass oscillator without haptic rendering (if the haptic device motor were turned off)? When $F_m(t) = 0$, the user and spring-mass are no longer mechanically coupled, as shown schematically in Fig. 2.3. Information flows, in that the motion source $\theta_z(t)$ driving the virtual spring-mass is derived from the instrumented haptic wheel. But mechanical power is no longer exchanged across the haptic device. In this case the response $\theta_z(t)$ to a persistent sinusoidal excitation $\theta_r(t) = \sin \omega_0 t$ is given by $\theta_Z(s) = G(s)\theta_R(s)$ from which we see that the steady-state response $\theta_z(t)$ is a sinusoid at frequency ω_0 (see Fig. 2.4B). In turn, the spring-mass responds with an oscillation whose amplitude grows without bound.

Let us compare the control strategies available to a human user attempting to maintain steady oscillations in the virtual spring-mass in the cases of coupled and uncoupled dynamics (with and without haptic rendering). For the case of coupled dynamics, the smooth amplitude function $\frac{\theta_W(s)}{\theta_R(s)}$ in Fig. 2.4A serves as a map to select an amplitude for an open-loop strategy based on generating a persistent sinusoidal control input. The map can also be applied at frequencies other than ω_0. Note that this strategy is very robust and even insensitive to loop delays because it is, after all, an open-loop strategy. In that sense it may be considered a feed-forward control strategy. Note that this feedforward strategy does not make use of an inverse model of the spring-mass system, as in standard conceptions of model-based feedforward control [7].

2.2.2 Closed Loop Strategies For Driving Oscillations

What is available to the user if feedback is added to the open-loop strategy for the control of the coupled dynamical system described above? After all, haptic feedback is available as a neural signal, provided to the central nervous system by haptic sensory organs. We can now ask how closed-loop sensory feedback might enhance performance and additionally whether a feedback strategy would be sensitive to the loop delays inherent in human motor control.

We presume that a neural substrate is available to generate a sinusoidal command to muscle at a specified frequency and amplitude (this is represented in Fig 2.6 as the block $C(s) = C_0/(s^2 + w_0^2)$ which describes a sinusoid at frequency w_0 in the laplace domain). We also suppose that there exists a means of generating a signal $F_m^{exp}(t)$ that describes the expected haptic feedback, or the force $F_m(t)$ felt by the hand grasping the haptic device. An error signal $e(t)$ could be formed by

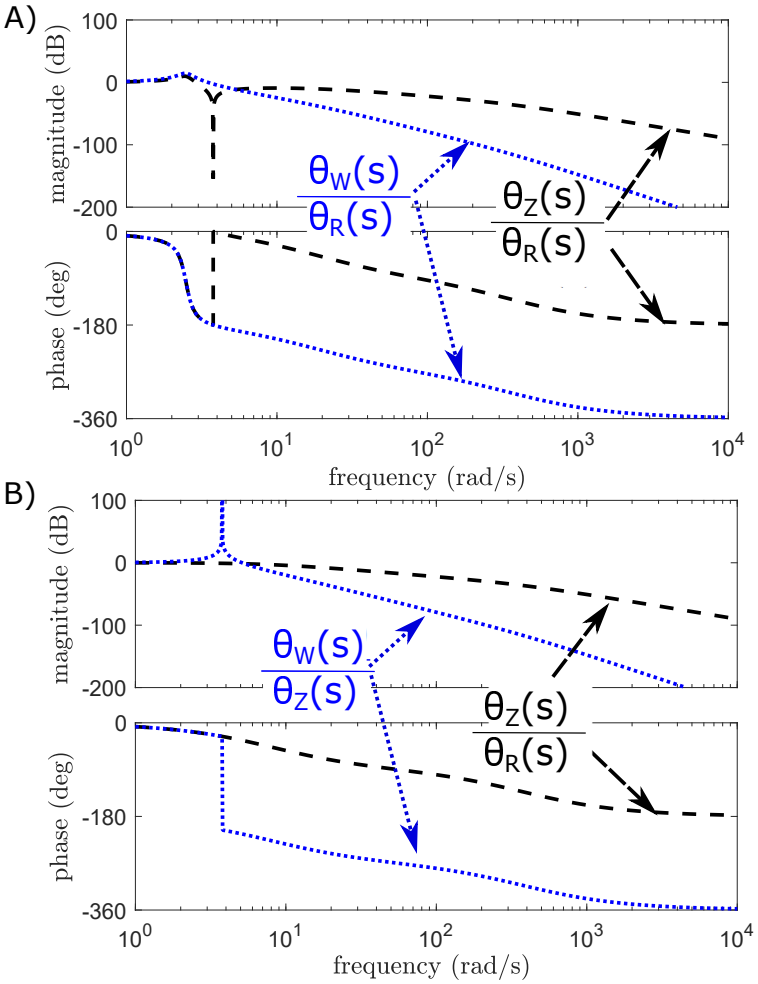

Figure 2.4: (A) The coupled system displays a null response in the response of θ_z and a steady response in θ_w to sinusoidal excitation in θ_r at $\omega_0 = 0.6$ rad/s. (B) The uncoupled system, on the other hand, displays a steady response in θ_z and an unstable response in θ_w.

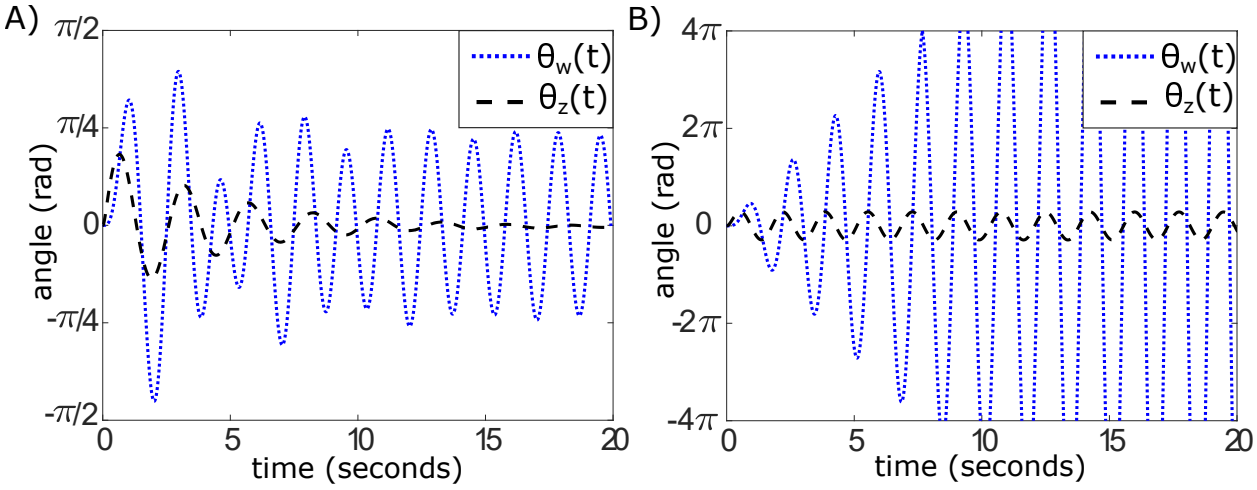

Figure 2.5: Time domain simulation results. (A) Coupled system, (B) Uncoupled system. Parameter values were selected as follows: $k_1 = 2.1$ N/m, $b = 0.27$ Ns/m, $m_1 = 0.00068$ kg, $m_2 = 0.2$ kg, $k_2 = 2.84$ N/m.

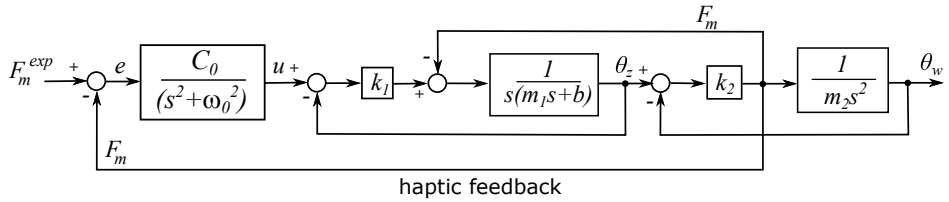

Figure 2.6: Block diagrams for the closed-loop controller based on the Internal Model Principle wrapped around the coupled system

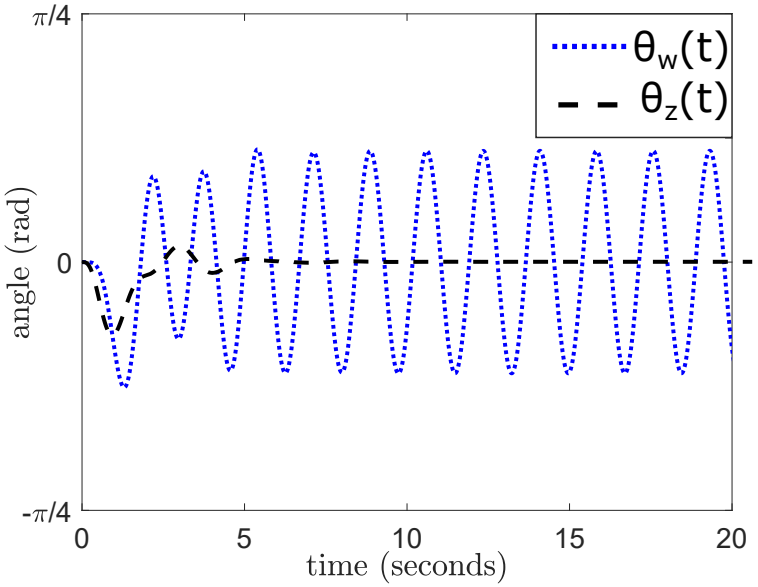

Figure 2.7: Time domain simulation results for the closed-loop system shown in Fig. 2.6. The value 1 was used for the single free controller parameter C_0.

computing the difference between the expected and actual haptic feedback, as shown in the block diagram in Fig. 2.6. An analysis of this loop shows that $\frac{E(s)}{F_m^{exp}(s)}$ also has transmission zeros at the roots of $(s^2 + \omega_0^2)$.

Again it follows that $e(t) \to 0$ for $F_m^{exp}(t) = \sin \omega_0 t$. Figure 2.7 shows results from a simulation of an internal model controller $C(s)$ closing a loop around the coupled system. $C(s)$ is simply a model or generator of steady oscillations characteristic of the spring-mass. When driven with $F_m^{exp}(t) = A_d \sin(\omega_0 t + \phi_d)$, where A_d and ϕ_d are a desired amplitude and phase, this controller will produce, after a brief transient, steady oscillations in the virtual spring-mass system with $\theta_z(t) \to 0$ (haptic device handle motionless) and $e(t) \to 0$. That is, all objectives are achieved: $\theta_W(t) = A \sin(\omega_0 t + \phi)$, with $A \to A_d$ and $\phi \to \phi_d$.

The control strategy based on the Internal Model Principle described above is also compatible with an adaptive controller that supports adjustment in control parameters C_0 or ω_0. Whether the neural substrates are available to support the computations suggested in the block diagram of Fig. 2.6 or some alternate computation produces similar behavior remains an open topic. In the meantime, we undertake a human participant study to test some of the hypotheses generated by the exposition above.

In our human subject experiment we evaluated three strategies "Relax", "Co-contract", and "Oppose" with the expectations that follow from our analysis above. First, we expect that oscillations in the coupled dynamics will decay in amplitude if the user relaxes their muscles ("Relax" strategy). A second approach to maintaining oscillations is co-contracting muscles (increasing impedance) in an attempt to hold the handle stationary ("Co-contract strategy"). In such case muscle action will be high and steady, not correlated to the sinusoidal motion of the oscillator. Both of these strategies do not correspond to Fig. 2.6 because the neural substrate is not generating a sinusoid. These strategies are better understood by viewing Fig. 3.2 where the strategy of relaxing corresponds to the human maintaining nominal k_1 and b and the strategy of co-contracting corresponds to increasing k_1 and b such that the human acts like a high gain position controller. Alternatively, the user may adopt the approach, we will call "Oppose", suggested by the Internal Model Principle: to simply balance the force feedback felt from the haptic device. Our analysis suggests that this strategy will also eliminate motion in the haptic device, resulting in sustained oscillations in the virtual spring-mass. This balancing the force feedback is what is shown in Fig. 2.6. It is important to note here that for all three strategies the transfer function shown in eq(2.4) is representative of all three cases of the coupled human wheel system and these strategies simply represent a construction of θ_r (in the case of "Oppose") or adjustments to b and k_1 (in either "Relax" or "Co-contract").

2.3 Methods

2.3.1 Participants and Apparatus

Experiments were conducted with 5 participants (3 male, 2 female) from the population of engineering students at the University of Michigan. All participants signed an informed consent according to an IRB approved protocol (HUM00148462). The angular position θ_Z of the haptic wheel (Encoder - US Digital E6S-2048-157), the angular position θ_W of the virtual wheel, an amplified, rectified measure EMG of surface electromyographic signal (Ottobock $13E200 = 60$) from the medial aspect of the forearm, and the current commanded to the motor (Maxon $RE - 40 - 148877$) were all recorded at 1KHz. The EMG signal was low pass filtered at 5Hz. All signals were collected using a Sensoray 626 and Simulink real-time at 1KHz. The haptic wheel is pictured in Fig. 3.1.

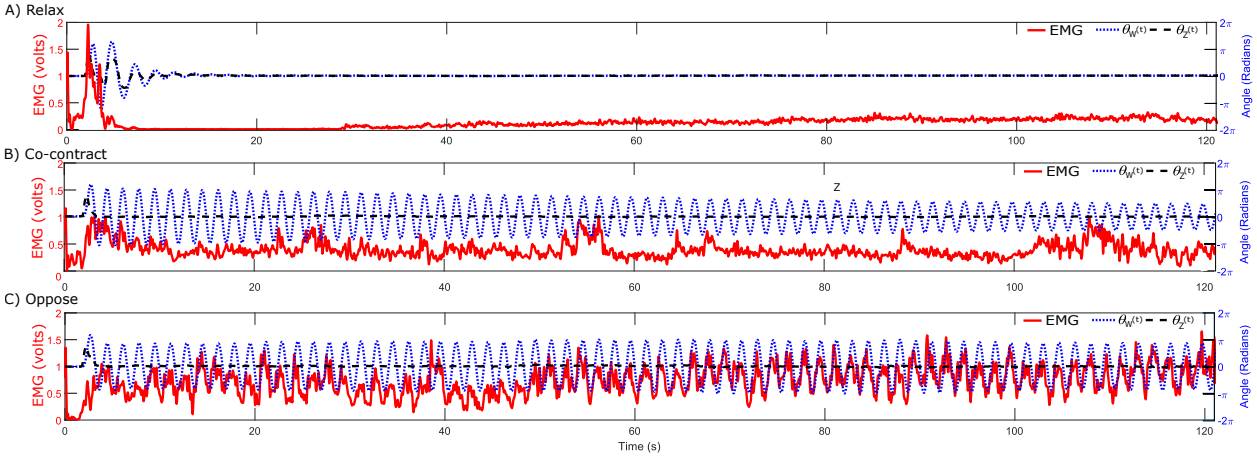

Figure 2.8: Raw Signals: EMG, Virtual Wheel $\theta_w(t)$, and Physical Wheel $\theta_z(t)$ position for Participant 4 (S4). The force $F_m(t)$ experienced by the user is proportional to the difference between $\theta_w(t)$ and θ_z(t)

2.3.2 Experiment Conditions

Each participant was instructed to grasp the haptic wheel, which was rendering a virtual spring-mass with a natural frequency f_n = 0.6Hz. A diagram of the coupled system is shown in Fig. 3.2. The participant was asked to displace θ_Z by about 160°), return θ_Z to 0° to excite the system, and then attempt to maintain oscillations under three instructions: “Relax”, “Co-contract”, and “Oppose”. The instructions under the “Relax” were to passively hold the wheel. Under “Co-contract”, the participants were asked to hold the haptic wheel stationary at 0° by contracting their arm muscles hard (holding the haptic wheel stiffly). In the “Oppose” strategy the instructions were to counteract the torque they felt by applying an opposing torque that would keep the wheel steady at about 0°. The duration of each trial was 120 seconds.

2.4 Results

2.4.1 Raw Signals

The raw signals for a sample participant (S4) are shown in Fig. 2.8 including EMG, the physical wheel position $\theta_z(t)$, and virtual wheel position $\theta_w(t)$ under all three control strategies. The oscillations decay rapidly under "Relax", decay slowly under "Co-contract", and are maintained (or only decay slightly) under "Oppose".

2.4.2 Fast Fourier Transform (FFT)

A single sided amplitude spectra obtained from the FFT from one subject (S4) is shown in Fig. 2.9 where a spike in the EMG signal present at the natural frequency (0.6 Hz) can be seen in the "Oppose" strategy and is not present in either the "Relax" or "Co-contract" strategies. Both the "Co-contract" and "Oppose" strategies have a large DC component (near $f = 0$). The oscillations in $\theta_W(t)$ were successfully generated at 0.6 Hz in the case of the "Co-contract" and "Oppose" conditions, whereas oscillations were not generated in the "Relax" strategy. The relax strategy does however have a smaller spike closer to $0.45Hz$ due to the dampened oscillations that were seen in Fig. 2.8. The amplitude at ω_0 in the EMG and $\theta_W(t)$ signals for all participants are shown in Table 2.1.

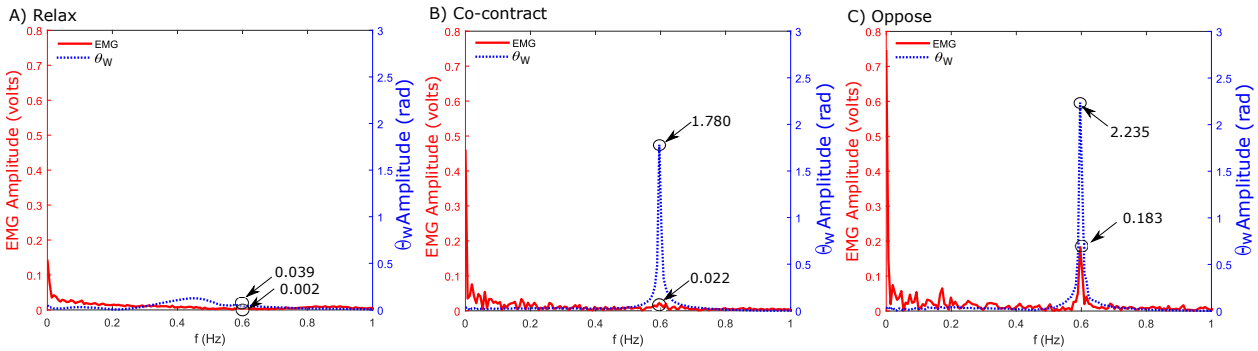

Figure 2.9: Fast Fourier Transforms: Single Sided Amplitude Spectrum for EMG and Virtual Wheel Position for Subject 4 (S4)

2.4.3 Signal Energy

To compare differences in the amount of control effort, the energy of the EMG and $\theta_W(t)$ signals was calculated in all conditions, and can be seen in Table 2.1. It is evident that the Energy in "Co-contract" and "Oppose" conditions is typically higher than "Relax", as expected. In addition, the energy in "Co-contract" is about twice that of the "Oppose" condition showing that the "Co-contract" strategy requires considerably more control effort.

		0.6Hz Peak		Signal Energy	
		EMG (volts)	θ_W (rad)	EMG (volts^2)	θ_W (rad^2)
S1	A) Relax	0.004	0.014	0.003	0.103
	B) Co-contract	0.269	1.928	2.577	3.226
	C) Oppose	0.395	3.959	1.097	8.462
S2	A) Relax	0.020	0.011	0.149	1.861
	B) Co-contract	0.478	1.377	1.983	1.219
	C) Oppose	0.833	2.339	1.695	3.223
S3	A) Relax	0.006	0.073	0.015	0.455
	B) Co-contract	0.291	5.903	1.567	23.94
	C) Oppose	0.194	9.950	1.982	163.2
S4	A) Relax	0.002	0.039	0.037	0.197
	B) Co-contract	0.022	1.780	0.235	2.350
	C) Oppose	0.183	2.235	0.632	3.927
S5	A) Relax	0.002	0.023	0.004	0.943
	B) Co-contract	0.130	1.994	0.573	2.359
	C) Oppose	0.108	2.089	0.234	4.534

Table 2.1: Amplitude at 0.6 Hz and signal energy associated with EMG and θ_W for all three strategies and all 5 participants.

2.4.4 Phase Plots

For each participant and strategy the derivative $\frac{d\theta_W(t)}{dt}$ was calculated and plotted against $\theta_W(t)$ as a function of time. The trajectories start at $(0, 0)$, spiral quickly outwards due to the large initial excitation, and then either spiral back towards $(0, 0)$ or maintain a circular oscillatory pattern. In figure 2.10 the phase plots calculated in this manner are shown for all participants and strategies. The "Relax" strategy trajectories quickly decay, the "Co-contract" trajectories decay slowly, and the "Oppose" trajectories decay slightly but are the best maintained. The differences between subjects during these conditions have to do with each subject having differing m_1, k_1, and b parameters as well as differing success in performing the control task. The take away from these results is all of the human subjects performed similarly in terms of general behavior. The one apparent difference is that S3's oscillations are large and tend to spiral outwards. This is likely due to S3 injecting energy into the system by having too large an input command; driving the system instead of just compensating for the haptic feedback.

2.5 Discussion and Conclusion

The correlation between surface EMG signals and virtual oscillator displacement was evident when our participants held the haptic device stationary by opposing the torque that they felt. However, this cannot be taken as direct evidence of a neural controller containing a sinusoid generator per the Internal Model Principle. But the alternative hypothesis involving the formation

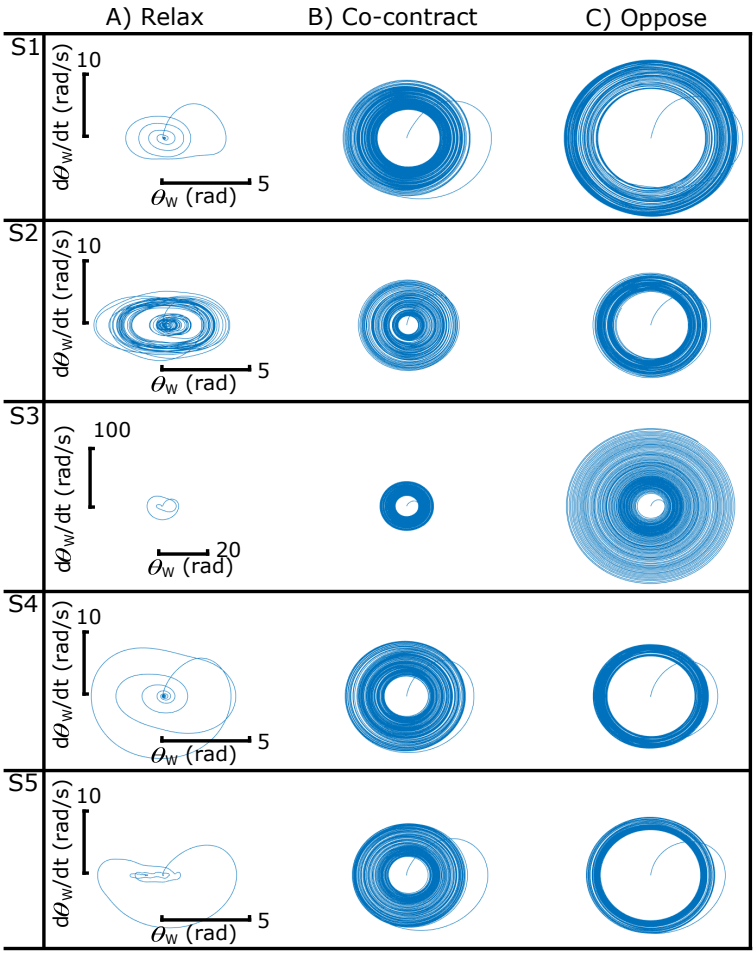

Figure 2.10: In this figure $d\theta_W(t)/dt$ is plotted against θ_W for all three strategies and all 5 participants cr(t)eating phase plots.

of an error using (delayed) haptic feedback would by comparison be very sensitive to parameter perturbations and noise. Our results also show that an approach involving increased impedance—which can either be construed as brute force suppression of haptic device motion or high gain error feedback on haptic device displacement—was by comparison a more costly approach. This energy comparison highlights the fact that a human's innate ability to make predictions and interpret haptic feedback naturally allows for a more economical strategy for movement. It should also be noted that the arm model we used in this work is a highly simplified approximation. For future work a more complex nonlinear model with more degrees of freedom could be explored. We are also interested in looking at better separating feed forward, feedback, and Internal Model Principle elements of human motor control, the effects of varying haptic feedback, and the effects of varying preview. In particular, the question of how the human builds its internal model is a nonlinear one, and there is evidence from a pursuit tracking task in weakly electric fish that this process may be quite fast—possibly on the order of 2-3 cycles of the sinusoidal stimulus [72]—indicating that nonlinear adaptive controller dynamics are likely important for short timescales and for small signal analysis.

CHAPTER 3

Respecting the Coupled Dynamics: Haptic Feedback Carries both Power and Information

3.1 INTRODUCTION

Certain haptic sensations, especially those that arise through contact with the environment, are accompanied by significant power exchanges compared to visual and auditory sensations. Portions of the body are backdriven by contact forces and the dynamics of body and artifact in the environment become coupled. Here we speak of instances in which haptic feedback is provided in the axis of control and instances in which the impedance of artifact and body are approximately matched. Such haptic feedback would perhaps more appropriately be called force or kinesthetic feedback. Note that *haptic rendering* aimed at making virtual objects seem real is almost always concerned with synthesizing haptic feedback in the axis of control. For example, haptic feedback from a virtual ball that one juggles would be presented in the axis used to maintain the juggle [58] and click-feel from a button is presented in the axis of the button press. Because the transfer of mechanical power gives rise to coupling between the dynamics of the body and artifact, one can say that the dynamics under control by the user are not those of the artifact, but the coupled dynamics of the body and artifact.

Paradoxically, the brain is faced with a greater challenge when controlling the coupled dynamical system that includes the combined body and artifact. There are new degrees of freedom to be managed—dynamic modes that involve exchanges of potential and kinetic energy between body and artifact. But something magical takes place when the body and artifact dynamics are coupled. A feedback loop is closed and the artifact becomes an extension of the body. The tool handle or machine interface disappears and the user gains a new means to effect change in their environment. This kind of magic is certainly at play when a skilled carpenter wields a hand-tool, a tennis player hits a ball with a racket, or a musician plays an acoustic instrument. The notion of a tool as an extension of the body has been explored in philosophical (phenomenological) studies of experience and consciousness [73] and through sensorimotor experimentation [19, 18]. More recently, the ability of the sensorimotor system to utilize coupled dynamics in sensing tasks has been explored

[17, 74].

Dynamic coupling between body and environment carries significant implications when attempting to isolate the contributions of haptic feedback to motor performance. In light of dynamic coupling, it becomes apparent that haptic feedback is not strictly an information signal. Many authors have noted that to turn off haptic feedback changes the motor task [75, 76, 42]. And a user will notice that the task dynamics change quite noticeably when haptic feedback is removed. Thus comparing performance in a visuomotor task with and without haptic feedback is comparing apples and oranges.

Further evidence for the importance of the coupled dynamics in the analysis of haptic rendering systems is available from the literature on coupled stability. The stability properties of a virtual environment change markedly once a user grasps the haptic device, even when the user applies no control action [77, 78]. The passive biomechanics of the user evidently contribute damping to the coupled dynamics. Thus a virtual environment whose model analysis would predict instability due to sampled data effects or other destabilizing processes is observed to be stable when a user grasps the haptic device. Evidently a flow of power toward the human user contributes to the stability margin. Higher grip forces are associated with even greater margins of stability, because higher grip forces are associated with higher impedance and greater dissapative effects [69].

The question then arises, how could a task without haptic feedback be modified so that it may be compared to a task with haptic feedback? Can two different motor tasks be devised whose performance can be compared in the sense of apples to apples, one with and the other without haptic feedback? If haptic feedback couples the dynamics of body and environment, and the motor task comprises control of the coupled dynamics, then perhaps when haptic feedback is replaced by visual feedback the coupled dynamics could somehow be preserved in the motor challenge. In this chapter a motor task without haptic feedback is presented that retained the coupled dynamics. The virtual environment was augmented (coupled) with a model of the user's biomechanics. System identification of the passive biomechanics informed the design of the new motor task.

The remainder of the chapter presents models of the virtual environment and biomechanics both in coupled and uncoupled configurations that form the basis of our analysis and experiment design. This chapter also presents the methods and results of an experiment designed to separate the contribution of haptic feedback in its information relay and dynamic coupling roles. The chapter concludes with a discussion of results and future work.

3.2 Model Development

The motor challenge we set for our participants was to excite and maintain oscillations in a virtual oscillator for 30 seconds and subsequently to relax for 30 seconds. Fig. 3.1 shows our

single-axis haptic device (a motorized wheel) and a schematic of the virtual oscillator (spring-inertia) rendered at the handle of the haptic device. We devised three conditions under which participants would drive oscillations, which we describe in a sequence of three models below. The conditions differ not only by whether haptic or visual feedback was provided, but also by the dynamics of the virtual environment being driven. In addition to the virtual oscillator, these models encompass the passive biomechanics and means by which a participant acts on the haptic device handle and through the handle on the virtual environment.

3.2.1 Hand Model

To model the finite impedance through which a human user acts on their environment, we adopt a simple mass-spring-damper model with parameters m_1 (mass), k_1 (stiffness), and b_1 (damping) driven by a motion source $r(t)$. This model has roots in the literature on human motor behavior, where it was at one time known as the equilibrium point hypothesis [79] or virtual trajectory model [80]. The second order mass-spring-damper model has also been shown to fit system identification data describing the driving point impedance collected under conditions in which the hand is mechanically backdriven [70, 69]. By virtue of the mass-spring-damper dynamics, the motion of the hand $z(t)$ will bend under load. In addition to the hand bio-mechanics the mechanics of the haptic device also have to be considered; mass m_1 and damping b_1 are representative of the combined mass and damping of the hand and device.

3.2.2 Coupled Hand-Oscillator Model

Let us consider the case in which a user is asked to drive sinusoidal motion in an undamped oscillator. Figure 3.2 shows a schematic of the user with motion source $r(t)$ modeling a neural signal (not measurable directly) along with the hand and handle position $z(t)$ in black. The hand drives motion $w(t)$ of a virtual mass m_2 through a virtual spring k_2. The physical apparatus and virtual environment is shown in Figure 3.1.

The oscillator (undamped spring-mass) (in blue outline) is rendered through a haptic device. The variable $z(t)$ describes both the hand and the grasped handle of the haptic device. Haptic feedback F_m is provided in the axis of control and the dynamics of the hand/arm are coupled to the dynamics of the oscillator.

At this point we can already make an important observation. An undamped oscillator will produce sustained oscillations if excited and then held still ($z(t)$ = 0, holding the handwheel stationary). If the user relaxes (CNS command $r(t) =$ constant), then energy stored in the oscillator will backdrive the biomechanics including the damper b_1 and the entire system will come to a standstill. The forces acting on $z(t)$ must be balanced in order to do this if m_1,b_1, and k_1 are finite.

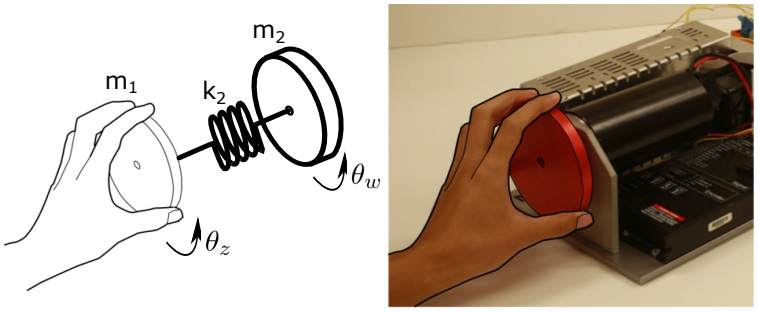

Figure 3.1: Experimental Apparatus and Virtual Environment. A single-axis haptic device was used to render a virtual spring-inertia comprising stiffness k_2 and inertia m_2.

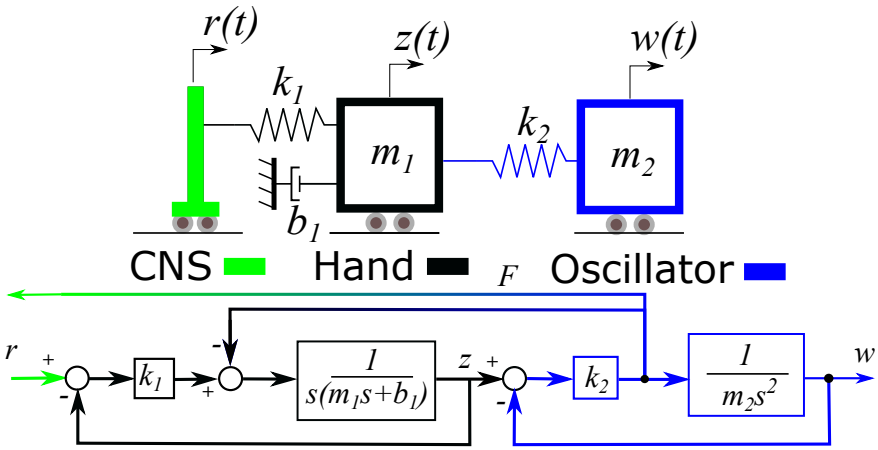

Figure 3.2: Coupled Hand-Oscillator Model. The spring k_1, damper b_1, and mass m_1 that together describe the backdrive impedance of the body are driven by a motion source $r(t)$ to produce displacements $z(t)$ at the hand. The oscillator is comprised of a stiffness k_2 and mass m_2. This translational schematic is standing in for a rotational system such as Fig 3.1. The corresponding block diagram is shown. Importantly, the diagram features a feedback signal F that represents the torque rendered through the haptic device to the dynamics of the body.

By linearity, a persistent sinusoidal excitation $r(t)$ at frequency $\omega_0 = \sqrt{k_2/m_2}$ will produce, at steady-state, a sinusoid at $\omega_0 = \sqrt{k_2/m_2}$ in $w(t)$. Thus if the user applies an open-loop drive to the system with sinusoidal motion at frequency $\sqrt{k_2/m_2}$ in $r(t)$, the hand and handle $z(t)$ will eventually cease motion while $w(t)$ will exhibit sinusoidal motion 180 degrees out of phase. If the user relaxes these forces are no longer balanced and k_2 will backdrive $z(t)$ until the damping in the human hand dampens out the oscillations in the undamped oscillator.

3.2.3 Decoupled Hand-Oscillator Model

In a second model we would like to describe the effect of turning off or removing haptic feedback. Thus we sever the haptic feedback channel F_m as pictured in Figure 3.3. In doing so we have severed not only the information in haptic feedback but also the force feedback that was

previously backdriving the the human hand. The signal $z(t)$ with which the motion source in the virtual environment drive the virtual oscillator (in blue) is drawn from the hand $z(t)$, as might be sensed using an encoder (ENC) on the haptic device handle. It is clear from the resulting block diagram that this is not mechanically equivalent to the Coupled Hand-Oscillator system because the coupled dynamics have not been preserved.

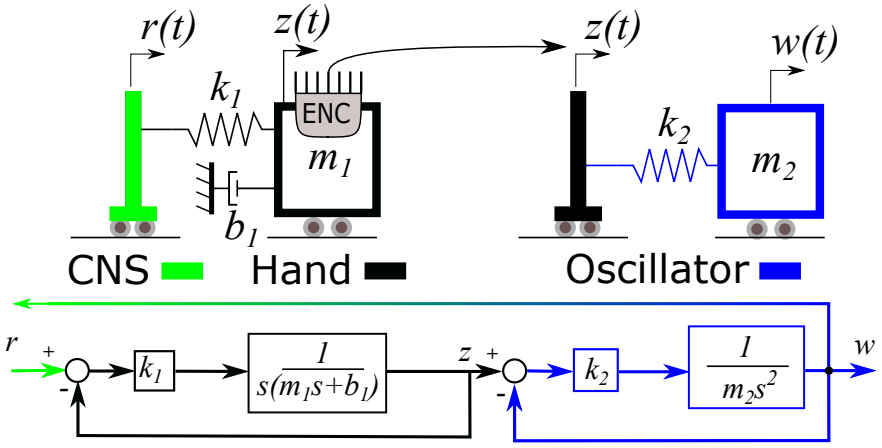

Figure 3.3: Decoupled Hand-Oscillator Model. Without coupling, or if the haptic device motor is disabled, the dynamics of the virtual spring-mass system is driven by the motion source $z(t)$, the displacement of the haptic device handle. Importantly, the diagram no longer features the feedback signal containing F as in Fig 3.2.

The behavior of this Decoupled Hand-Oscillator system under an (open-loop) sinusoidal excitation $r(t)$ at frequency $\omega_0 = \sqrt{k_2/m_2}$ will be very different than the behavior of the Coupled Hand-Oscillator. The hand is not loaded by the oscillator (no haptic feedback) and thus $z(t)$ will oscillate at frequency ω_0 in steady-state. When the virtual oscillator is then driven at its resonant frequency (the virtual motion source derives its motion $z(t)$ from the encoder on the haptic wheel), the amplitude of oscillation will grow. Then if driving motion in $r(t)$ ceases (the user relaxes), $z(t)$ will come to a standstill but the oscillator will continue to oscillate.

3.2.4 Coupled Virtual Hand-Oscillator Model

To create a motor task for the user that lacks haptic feedback but which is arguably equivalent to driving an oscillator with haptic feedback, we develop a model in which the coupled dynamics are preserved. But these coupled dynamics exist fully in the virtual environment and visual feedback is used in place of the missing haptic feedback. Thus in Figure 3.4, we have generated a model of the human hand bio-mechanics ("Virtual Hand", in red) and coupled it to the virtual oscillator (in blue). The actual human hand, now unable to feel torque feedback, drives the haptic device handle (whose inertia is already lumped in m_1). An encoder on the handle $z(t)$ is used to derive the signal $z^*(t)$

with which the virtual environment is driven. The "Virtual Hand" is now backdriven by the force F from the virtual oscillator.

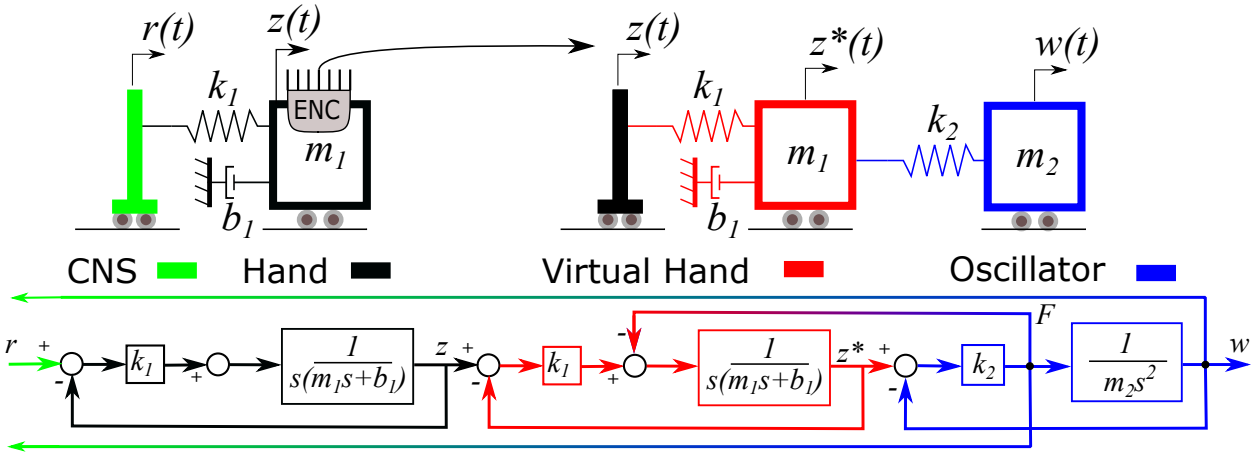

Figure 3.4: Coupled Virtual Hand-Oscillator Model. Haptic feedback has been removed and thus the mass-spring-damper biomechanics (in red) are no longer loaded by a reaction force from the oscillator. However, the double-mass task dynamics have been preserved by inserting a model of the hand (virtual hand, in black) into the virtual environment.

The behavior of the Coupled Virtual Hand-Oscillator system can be expected to mimic that of the Coupled Hand-Oscillator system. When a sinusoid at the resonant frequency ω_0 is applied at $r(t)$, the steady-state sinusoid $z(t)$ will drive a virtual environment (virtual hand, virtual oscillator) that is modeled after what was previously a coupled physical (hand) and virtual (oscillator) system. And when $r(t) =$ constant, energy stored in the oscillator will dissipate through the damper b_1.

3.2.5 System Identification for Hand Model

We hypothesize that due to the smaller rotation angle of the task in [78], we could utilize the previously identified mass m_1 and stiffness k_1 but would need to recalculate the damping coefficient b to obtain an appropriate model for our task. In this work, we will adopt the second order model $\tau = J\ddot{\theta} + b\dot{\theta} + k\theta$. Since m and k are known we can solve for b: $b = (\tau - k\theta - J\ddot{\theta})/\dot{\theta}$. To obtain data to generate our estimate of b we asked a single participant to grasp the haptic wheel handle without actively driving it. We then generated a sinusoidal motor command at an intensity that produced approximately 90 degree $(+/-)$ motion and recorded the encoder angle and input current i_c using a Hall Effect sensor (Tamura L01Z050S05). The motor constant for our Maxon Motor is $k_t = 60.3$ N-mm/A as identified by the datasheet. We then calculated output torque using $\tau_{out} = k_t i_c$.

Since, m_1 and k_1 have been selected, the observed phase difference between the motor command and hand wheel motion can be resolved by fitting b_1. The final bio-mechanical model of the hand is then given by $m = 0.180$ Nm/(rad/sec^2), $k = 2.558$ N-m/rad, and $b = 0.508$ Nm/(rad/sec).

Simulation Resonate: RMS of Signals	Hand	Virtual Hand	Oscillator
Decoupled Hand-Oscillator	1.110	x	36.26
Coupled Virtual Hand-Oscillator	1.110	0.147	0.941

Simulation Relax: τ_c of Oscillator Signal	Oscillator
Decoupled Hand-Oscillator	∞
Coupled Virtual Hand-Oscillator	1.952

Table 3.1: Simulation: Average RMS value of metrics (in rad) across all three conditions.

3.2.6 Control Strategies

In order to successfully accomplish the motor task outlined at the start of section II differing strategies are employed depending on the feedback available in each of three models outlined. In the case where haptic feedback was available (the Coupled Hand-Oscillator condition) maintaining oscillations required the participant to oppose haptic feedback in order to keep the handle still. This is because an excited spring-mass system with the link $z(t)$ held still will resonate with the same magnitude indefinitely (because there is no damping). The oscillations felt and opposed will be sinusoidal at the natural frequency of the virtual spring mass.

In the other two conditions, Coupled Virtual Hand Oscillator and Decoupled Hand-Oscillator, no haptic feedback was available and either an open loop or visual feedback based strategy had to be used. This corresponds to the same strategy as the Coupled Hand-Oscillator condition but without haptic feedback; the participant is attempting to oppose oscillations they can no longer feel. The correct action in this case is to move the handwheel in a sinusoidal motion at the natural frequency of the virtual spring mass. Visual feedback was provided to allow the participants to estimate whether they were causing the spring-mass system to resonate at its natural frequency. Alternatively, in the Coupled Virtual Hand-Oscillator condition this strategy can be interpreted as using visual feedback to keep the virtual hand still, effectively commanding the virtual hand to oppose haptic feedback.

3.2.7 Model Simulation

Given the damping estiamtion and the models presented in the previous section we can conduct a simulation comparing Decoupled Hand-Oscillator and the Coupled Virtual Hand-Oscillator conditions. The simulation results in Figure 3.5 were generated using the same Simulink models used for the human subject experiment in the following section but with the encoder signal $z(t)$ replaced by a sinusoid generator at the natural frequency of the spring mass oscillator. Figure 3.1 shows the results of the experimental measures on the simulation results.

The virtual oscillator had a mass of $0.18\ Nm/(rad/sec^2)$, a spring constant k of $2.5578\ Nm/rad$, and just enough damping b to remove Euler integration error. The amount of damping b was $T_s k = 0.0026\ Nm/(rad/sec)$ (where T_s was the sample time of $0.001s$). The natural frequency of this oscillator was $0.6Hz$.

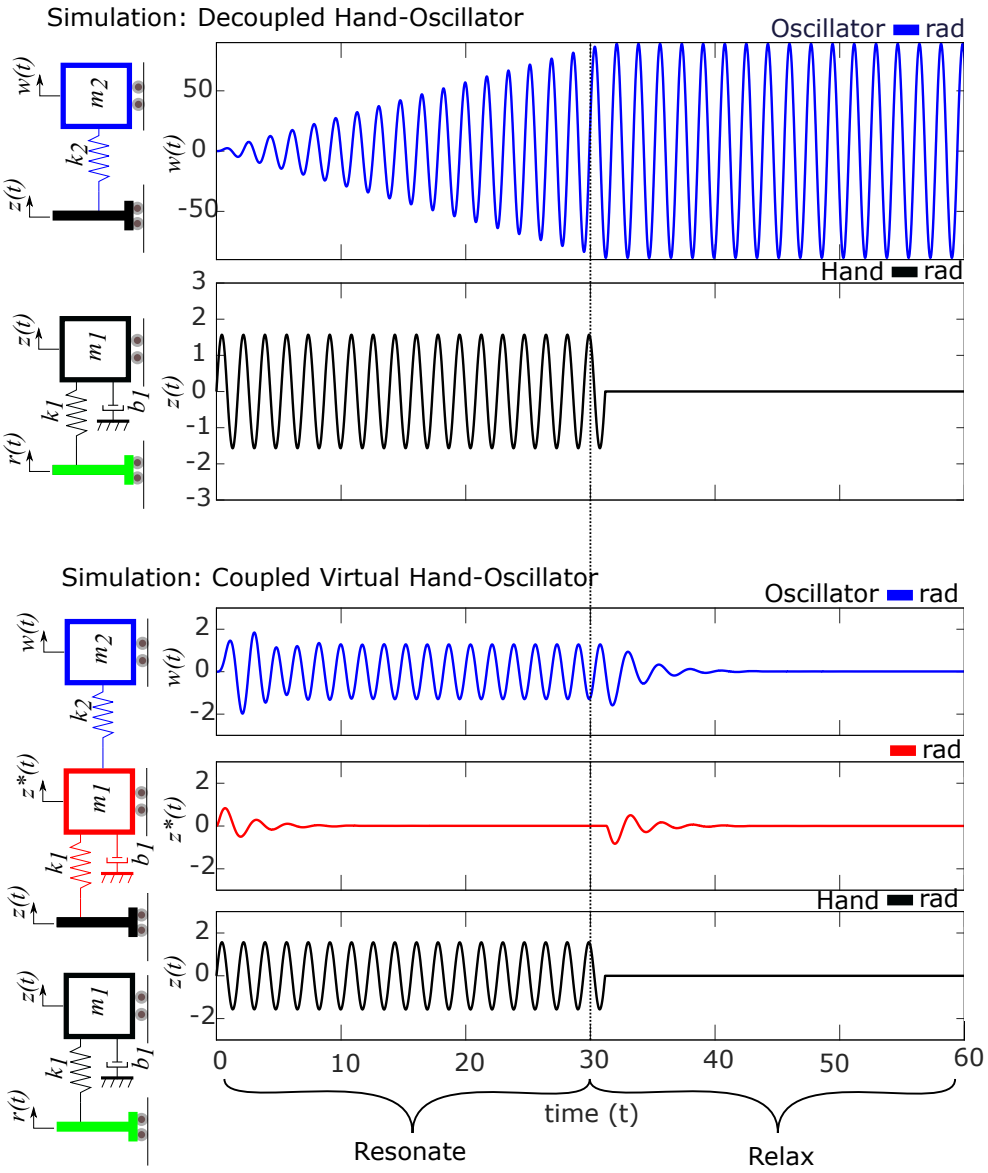

Figure 3.5: Simulation Results: The Decoupled Hand-Oscillator and Coupled Virtual Hand-Oscillator systems are simulated using a sinusoid generator. The first thirty seconds the system is excited at the natural frequency of the virtual spring mass and then the generator is shut off for thirty seconds.

3.2.8 Participants and Apparatus

Experiments were conducted with 5 male participants from the University of Michigan. All participants signed an informed consent according to an IRB approved protocol (HUM00148462). The angular position $z(t)$ of the haptic wheel (Encoder US Digital E6S-2048-157), the angular position $w(t)$ of the virtual oscillator, an amplified, rectified measure EMG of surface electromyographic signal (Ottobock 13E200=60) from the medial aspect of the forearm, and the current commanded to the motor (Maxon RE-40-148877) were all recorded at 1KHz. The EMG signal was low pass

filtered at 5Hz. All signals were collected using a Sensoray 626 with Simulink real-time at 1KHz. The haptic wheel is pictured in Fig. 3.1.

3.2.9 Experiment Conditions

In this experiment we compared the participant's ability to maintain resonance in a coupled spring mass with only one channel of information present; either visual information or haptic information. Visual information was substituted in the conditions where haptic feedback was unavailable and was displayed on a screen. However, in order for the conditions to be comparable, preservation of the coupled dynamics is needed but removal of haptic information is necessary; we now make use of the Coupled Virtual Hand-Oscillator model we developed earlier and pictured in Fig 3.4. Each participant was asked to resonate three different systems: 1) Coupled Hand-Oscillator 2) Decoupled Hand-Oscillator and 3) Coupled Virtual Hand-Oscillator. Each system was demonstrated and explained to the participant prior to a trial with demonstration and training time as appropriate. All participants were informed that the natural frequency f_n of the spring mass oscillator was 0.6Hz prior to the trials. The trial order was randomized.

The task given to each participant was to excite and maintain oscillations in a spring mass ('resonate' portion 30 seconds) followed by performing no motor action and relaxing ('relax' portion 30 seconds). Participants were instructed to induce an excitation by quickly turning the handle by about 90 degrees to the right and then back to center. For the remainder of the 'resonate' portion participants were then asked to maintain the oscillations by relying on either haptic feedback or visual feedback depending on which was available in the given condition. In these cases without haptic feedback the participants were instructed to move the handwheel in a sinusoidal motion (alternating from 90 to -90 degrees) at the natural frequency of the virtual spring mass using the visual feedback to adjust their magnitude and phase as needed. The visual feedback provided to the participants was in the form of laterally moving blocks similar to the right side of Fig 3.4).

3.2.10 Experimental Measures

Two separate measures were used to evaluate the perform under each instruction. For the first half of each trial, the resonate portion, the root mean square value (RMS) calculated. For the second half, the relax portion, the time constant τ_c was calculated.

3.3 Results

3.3.1 Sample Data

Representative data for a single participant is shown in Fig 3.6. The icons on the left side of the figure indicate which element of the spring-mass-damper is generating the signals shown to the immediate right.

3.3.2 Summary Data

3.3.2.1 Root Mean Square (RMS)

In figure 3.7 the average (across all 5 participants) RMS value of the resonate signals is shown. The virtual hand was present only in the Coupled Virtual Hand-Oscillator condition and therefore the corresponding RMS value is absent from the other two conditions in the graph. The symbol ∞ indicates that the oscillations in the virtual oscillator did not stabilize; they continued to grow so an RMS value was not determined.

3.3.2.2 Time Constant (τ_c)

To calculate τ_c the maximum value for the second half of the resonate phase was used (period of trial between 15 and 30 seconds). Figure 3.7 shows the results for all trials. The symbol ∞ indicates that a value could not be determined as oscillations did not decay.

3.4 Discussion and Conclusion

In this chapter we explored the idea that, rather than controlling object dynamics, the central nervous system controls the coupled dynamics of body and object. Force feedback synthesized by a haptic device, along with motion of the device handle, make up the two variables that couple user biomechanics and object dynamics. If haptic feedback is removed then the dynamic coupling is broken, even if the user retains an ability to drive the object dynamics. We devised an experimental condition that preserved the coupled dynamics yet removed force feedback by placing and coupling a model of the arm/hand (with parameters set by system identification) into the virtual environment. We asked our participants to first drive and maintain oscillations for 30 seconds ('resonate') and then to grasp the wheel but behave passively ('relax') for another 30 seconds. As expected, the performance of our participants driving the all-virtual coupled dynamic system (Coupled Virtual Hand-Oscillator) better matched the condition with haptic feedback (Coupled Hand-Oscillator) than the condition without haptic feedback (Uncoupled Hand-Oscillator). Coupled participant-virtual environment behavior (Fig. 3.6) matched predictions set up by simulation (Figure 3.5).

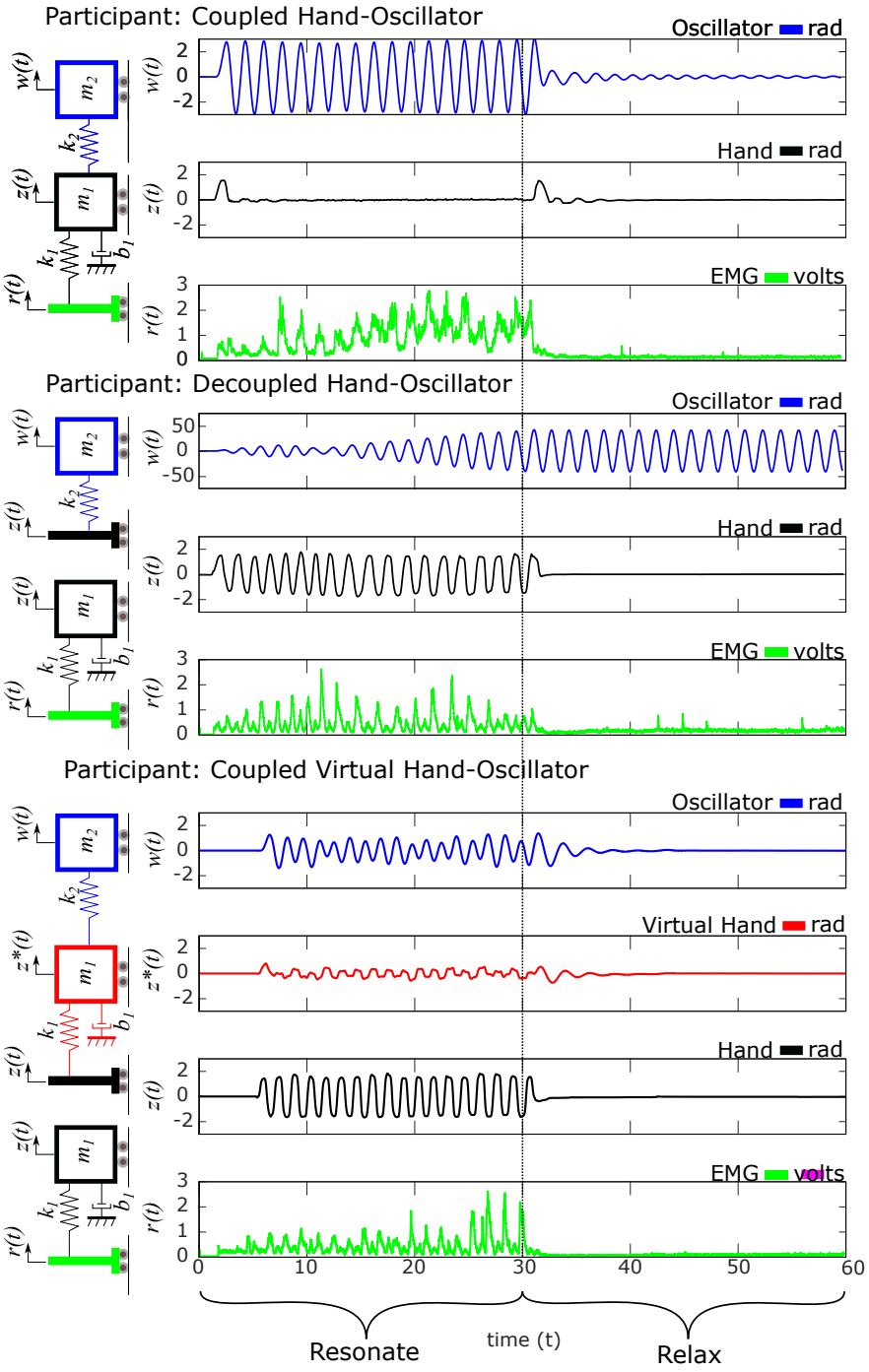

Figure 3.6: Single Representative Participant Results: This figure shows representative data from the human subject experiment. The participant attempts to resonate the system at the oscillator's natural frequency for the first 30 seconds and then relaxes for the next 30.

In particular, the same model describes the behavior of the coupled physical hand and oscillator as the coupled virtual hand and oscillator. In response to the oscillatory input generated by the participant in the first 30 seconds, the coupled system (whether coupled through the haptic device with haptic feedback or strictly in the virtual environment) responds with steady oscillations. The

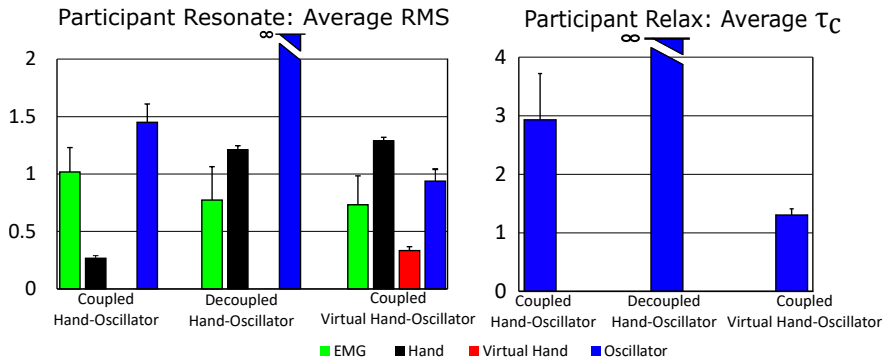

Figure 3.7: All Participants: means of metrics across all three conditions. Errors bars associated with each bar indicate variance. The amplitudes associated with the RMS values are in volts (EMG) and rad (hand, virtual hand, and oscillator).

uncoupled system responds with growing amplitude. When a participant relaxed, energy stored in the oscillator quickly dissipated, but only in the coupled-dynamics cases (see Figure 3.6). The EMG signals (green traces) indicated that our participants were following instructions, though when haptic feedback was present a greater muscle action was necessary to oppose the haptic feedback to keep the handle still once oscillations were initiated. In our future work we plan to assess task performance more closely and quantify the learning rate. It appears that our participants were adopting primarily open-loop strategies when visual feedback was substituted for haptic feedback. Anecdotally, the tasks involving visual rather than haptic feedback were more difficult to perform. Haptic feedback was easily incorporated in the sense of anticipatory control, in that our participants held the handle stationary simply by opposing the torque that they felt. By participant report, it was not as easy to quell oscillations in the virtual handle as it was in the physical handle. The fourth-order (double-mass) coupled dynamics were certainly more challenging to handle than the essentially second-order dynamics of the uncoupled system. Also, we did not set parameters in the virtual hand model according to data from individual system identification experiments. It would be interesting to assess whether our participants were adapting to changes in dynamics having to do with differences between the dynamics of their own hand and that of the virtual hand adopted for our experiments.

CHAPTER 4

An Internal Model Principle Based Approach to Modeling the Pursuit of Predictable Signals

4.1 Introduction

Relative to catching a baseball, catching a butterfly can be considered a difficult task—the motion of the butterfly is by comparison unpredictable. The features of parabolic flight previously internalized can be recalled to guide preparation for the baseball catch, whereas strategies for intercepting the butterfly must rely on continually available feedback. Internalizing observations and exploiting predictive models is accepted as an integral part of certain predatory behaviors in biology [3], to the point that behaving in an unpredictable fashion to avoid predation is considered an evolutionary response [1, 2]. Concrete evidence for predictive modeling by organisms has been provided by Roth et al. [4], who quantified differences in the behavior of glass knife-fish attempting to hide inside a predictably or unpredictably moving shelter: phase delay between the fish and shelter was significantly reduced when the the shelter moved according to a sinuoid rather than a sum of sinusoids. Evidence of predictive behavior in humans can be found in the precisely synchronized movements found in athletics and music performance [5].

The ability to internalize and recall predictable processes is said to rely on internal models in the field of human motor behavior [6, 7]. More specifically, the motor behavior field uses internal models to explain how humans extract desired behaviors from objects that have predictable responses to actions taken upon them [23]. Thus the *processes* in question are the dynamics of objects that can be handled—objects whose governing physics can be excited by the individual building the model. In other words, active perception is at play: the individual building the model can choose to excite the dynamics to test various hypotheses. *Objects* in this context include the body itself, and an ability to harness the dynamics of one's own body is thought to underlie the ability to harness object dynamics [23, 10, 24].

However, building models of predictable behavior is not restricted to objects that can be handled. Processes whose behavior can only be observed or perceived passively are also amenable to modeling. Naturally, the control objective differs with a model of a process over which one has no

control input. The object or process no longer plays the role of *Plant* in control engineering terms. Instead, the process output becomes a reference to be tracked or a disturbance to be rejected. As it turns out, the field of human motor behavior has introduced but not developed the internal model concept in the context of tracking or rejecting predictable signals or signals generated by external processes that can be modeled [8, 21, 25].

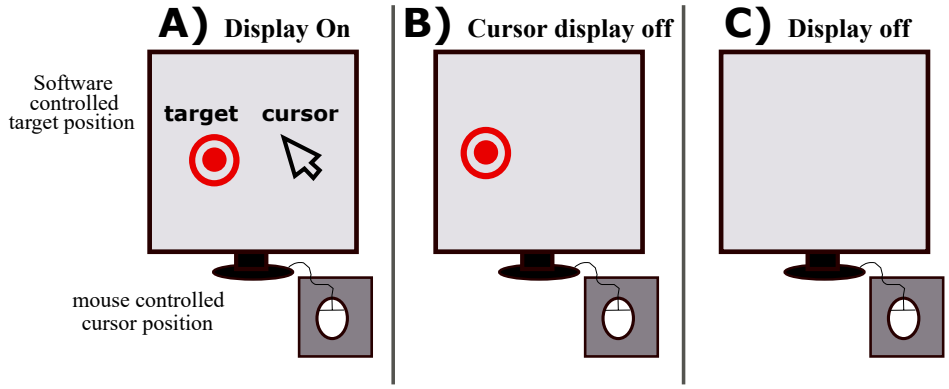

Figure 4.1: Experimental conditions. A) Visual feedback of both the target and the cursor are available to the participant. B) Only visual feedback of the target is displayed; the cursor is blanked. C) No visual feedback is displayed on the monitor; both the cursor and target are blanked.

Envision the following simple experiment: a cursor on a screen is controlled through a mouse to track the motions of a moving target, also presented visually on the screen [1]. If the target moves in a predictable manner, one can imagine completely eliminating errors associated with visual processing, feedback control, and muscle action. An internal model can be used to predict the target's motion an appropriate interval into the future to compensate for the delays. Furthermore, once the predictable pattern by which the target moves has been internalized, continuous visual input is no longer needed. The screen can go temporarily blank or visual attention can shift away without loss in tracking performance. Indeed, so-called "signal blanking" experiments have shown that visual access to a predictable signal can be temporarily denied without significant loss in tracking performance [13, 16, 34, 81, 82]. Similarly, tasks involving predictable haptic cues can be completed despite blanking of haptic stimuli [83, 84, 85, 86, 87].

Feedforward control is often credited for addressing delays associated with feedback. Indeed, the inclusion of a feedforward path in the control architecture speeds up system response. A feedforward path that includes a predictive model of the target motion together with an inverse model of the plant can even achieve perfect tracking. The predictive model of the reference removes delay inherent in human motor control while the inverse plant model accounts for phase delay

[1] The case in which both the cursor and target are visible is called *pursuit tracking*; the case in which only the error between target and cursor is shown is called *compensatory tracking* [27]. In this chapter we treat pursuit tracking.

introduced by the plant. Standard feedforward control, however, would not be able to explain the persistence of tracking performance in the case of signal blanking.

One means to describe an ability to track a temporarily invisible target is with the use of a model that *generates* the missing signal. The notion of a signal generator in the feedforward path was already suggested by McRuer in 1967 to explain situations in which pilots were presented predictable signals to track [27]. Krendel and McRuer used the term "precognitive control" to refer to an individual memorizing a predictable signal and internally generating its motion [88].

Control engineering provides an alternative to feedforward control and McRuer's precognitive control in the controller design directive known as the Internal Model Principle [32, 33]. A controller designed according to IMP eliminates tracking errors (or fully suppresses a disturbance) by placing a generating model of the predictable reference or disturbance signal in the control loop. Thus the Internal Model Principle is a directive for the design of controllers in the case of predictable reference or disturbance signals, treating precisely the case in which models are built under passive rather than active perception.

The Internal Model Principle (IMP) is specifically concerned with models of the reference signal in contrast to control-theoretic treatments in human motor behavior that invoke internal models of the process or plant under control [8, 7]. While the IMP has been used to guide control design within the control engineering community since the late 1960's, it has only recently been proposed for use in modeling human motor behavior [25, 89].

In this chapter we invoke the IMP to develop a model of human motor behavior, incorporating an explicit model of the process that generates a predictable reference signal in the feedback loop. This model explains perfect tracking, even in the face of temporary signal blanking. To handle the separate blanking of the reference and output feedback signals, we incorporate a second internal model in a feedforward path. After first presenting further background on the IMP, we present a small simulation study. Finally, we present results from a human participant study in which participants were tasked with tracking predictable sinusoids under signal blanking.

4.2 Background

4.2.1 The Internal Model Principle

The Internal Model Principle states that perfect tracking of a reference signal can be achieved by a stable system only when an explicit model of the reference dynamics can be found within the loop transfer function [32, 33]. In the sense that a Laplace transform or model $R(s)$ of a signal $r(t)$ *generates* the corresponding time-domain signal, by one useful interpretation of IMP, the reference signal is generated from within the control loop; it no longer needs to be sensed. Consider a controller $C(s)$ and plant $P(s)$ in the standard feedback control system (Fig. 4.2) that has achieved

perfect tracking of a sinusoid $r(t) = \sin(\omega t)$ in steady state. The error $e(t) = r(t) - y(t)$ has been nulled out and there is no excitation of the loop transfer function $C(s)P(s)$. It must then be the case that a *generator* of $r(t)$ resides within $C(s)P(s)$. Moreover, if $R(s)$ is part of $C(s)$, then the signal $u(t)$ exciting $P(s)$ has the appropriate amplitude and phase that induces $P(s)$ to produce $y(t) = r(t)$ in steady state. Now consider the case $y(t) \neq r(t)$. A non-zero error signal $e(t)$ drives the loop transfer function $C(s)P(s)$, but stability along with the existence of a signal generator within $C(s)P(s)$ requires that $e(t) \to 0$, or perfect tracking is eventually achieved.

The ability of the loop transfer function to generate the appropriate signal while driven with a null error signal can be used to describe human control performance in cases of *visual blanking*, where a moving target temporarily disappears yet continues to function as a reference. Quite plausibly, the human operator simply employs an *internal model* of the reference signal to generate the underlying signal during the period in which it is missing. The same kind of facility is available when the operator shifts attention away from visual input or looks away from a visual display. Thus a controller containing a model of the reference dynamics exhibits a memory-like behavior to handle periods during which the signal $r(t)$ is missing. If the reference can be described as sinusoidal motion at a certain frequency yet it is not available for visual tracking, the operator uses a sinusoid generator at that same frequency primed with the amplitude and phase that extracts a signal $y(t)$ from the plant that matches their best estimate of the amplitude and phase of the reference $r(t)$.

4.2.2 IMP Example

In this section we provide a brief tutorial example on IMP design for a predictable reference signal. For a longer discussion on IMP and an example that accommodates a predictable disturbance signal see [89]. In this chapter we treat the *pursuit tracking* problem, in which both the reference signal $r(t)$ (in the form of a moving target shown on a screen) and the system output $y(t)$ (a cursor shown on the screen) are available to the human operator. Thus we draw a dotted box representing the human around both the controller $C(s)$ and the summer in the standard feedback control system shown in Fig. 4.2. The transfer function from $R(s)$ to $E(s)$ is given by

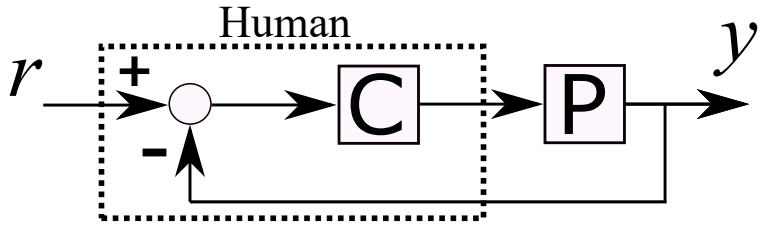

Figure 4.2: Standard feedback control block diagram. For an IMP based controller the poles of $C(s)$ include the poles of the reference signal generator $R(s)$.

$$\frac{E(s)}{R(s)} = \frac{1}{1 + C(s)P(s)}. \tag{4.1}$$

Let us represent $C(s)$ and $P(s)$ using ratios of their numerator and denominator polynomials whose roots are the zeros (subscript z) and poles (subscript p), respectively: $P(s) = \frac{N_P(s)}{D_P(s)}$ and $C(s) = \frac{N_C(s)}{D_C(s)}$. Substituting in Eq. 4.1 yields

$$\frac{E(s)}{R(s)} = \frac{D_C(s)D_P(s)}{D_C(s)D_P(s) + N_C(s)N_P(s)}. \tag{4.2}$$

Suppose $C(s)$ is designed based on the IMP and contains a model of a sinusoidal reference signal: $R(s) = \frac{\omega_m}{s^2+\omega_m^2}$. This means $C(s)$ must contain the poles of $R(s)$, or $D_C(s) = (s^2 + \omega_m^2)D_C^a$. Here D_C^a represents additional poles belonging to the controller that do not model the reference. In general, $C(s)$ can contain additional poles and zeros beyond those in $R(s)$ so long as the system remains stable. Substituting for D_C we have

$$\frac{E(s)}{R(s)} = \frac{(s^2 + \omega_m^2)D_C^a D_P(s)}{(s^2 + \omega_m^2)D_C^a D_P(s) + N_C(s)N_P(s)}. \tag{4.3}$$

Given that tracking error will tend to zero, note that the poles of $R(s)$, the roots of $(s^2 + \omega_m^2)$, are now in the numerator of the sensitivity function. The sensitivity function will then evaluate to zero at $s = \pm j\omega_m$, also known as transmission zeros.

In summary, the IMP imposes two stipulations: 1) the closed loop poles must be in the left half plane 2) the poles introduced by the reference signal must be contained in $D_C(s)$. If we assume the poles of $D_C(s)D_P(s)+N_C(s)N_P(s)$ lie in the left half plane, then the only potentially destabilizing element opposing the driving of $e(s)$ to zero are the poles contributed by $R(s)$. However, our choice of modeling the reference poles with $D_C(s)$ will lead to their cancellation, leaving only the poles of $D_C(s)D_P(s) + N_C(s)N_P(s)$, all of which lie in the left half plane by assumption.

4.2.3 A Hybrid Dynamical System with IMP Controllers

An IMP controller has the auspicious properties of generating the command necessary to produce perfect tracking in steady state. If steady state has not yet been reached, the controller will generate the command that drives the error downward by the stability argument. The input $e(t)$ must be computed, however, as the error between the reference $r(t)$ and the output $y(t)$; If either $r(t)$ or $y(t)$ are missing, then the signal $e(t)$ no longer represents tracking error. Thus to handle signal blanking, it is necessary to introduce modes of the control system that allow the system to use $e(t)$ only when it represents the difference between $r(t)$ and $y(t)$, and when it does not, switch to a mode that relies on the IMP controller as a signal generator without excitation.

In Fig. 4.3A, a version of the system in Fig. 4.2 is shown, in which P = 1, the IMP controller is given by $M(s)$, and the output is $r'(t)$. Nominally, the controller $M(s)$ has access to $r(t)$ and $r'(t)$ and uses these to compute $e(t)$. To handle the case in which either $r(t)$ or $r'(t)$ is not shown on the screen, we propose the introduction of two system modes A and B which together make up a hybrid dynamical system.

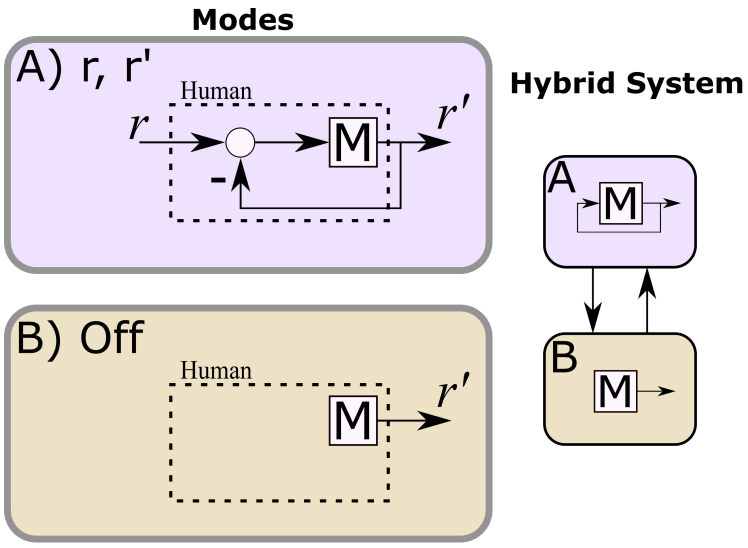

Figure 4.3: State machine featuring two modes: A) IMP controller $M(s)$ with feedback B) IMP controller $M(s)$ without feedback.

When $r(t)$ and $r'(t)$ are available, the system is in mode A) and feedback control can be used to drive the error to zero per the IMP. When either signal is not available the system is in mode B) and the controller $M(s)$ with an internal model of $R(s)$ continues to resonate at the last known amplitude and act as a signal generator.

In Fig. 4.4 the response of this simple system with $M(s) = \frac{\omega_m}{s^2+\omega_m^2}$ to a sinusoid of frequency ω_m is shown. The signal $r(t)$ is blanked halfway through the simulation. Even though $r(t)$ is not available, the system will nevertheless track $r(t)$ because $M(s)$ is a dynamic model of $r(t)$ and, once excited, becomes a generator of $r(t)$. If $r(t)$ continues to hold oscillations of constant frequency and amplitude, and perfect tracking has already been achieved (zero error), in the absence of disturbances, it no longer makes a difference which mode the system is in; the two modes perform identically. In Fig. 4.4, $r(t)$ was blanked after the system reached steady state. If blanking occurred earlier, the system in mode B would continue to oscillate but would exhibit steady state error equal to the error value just prior to blanking.

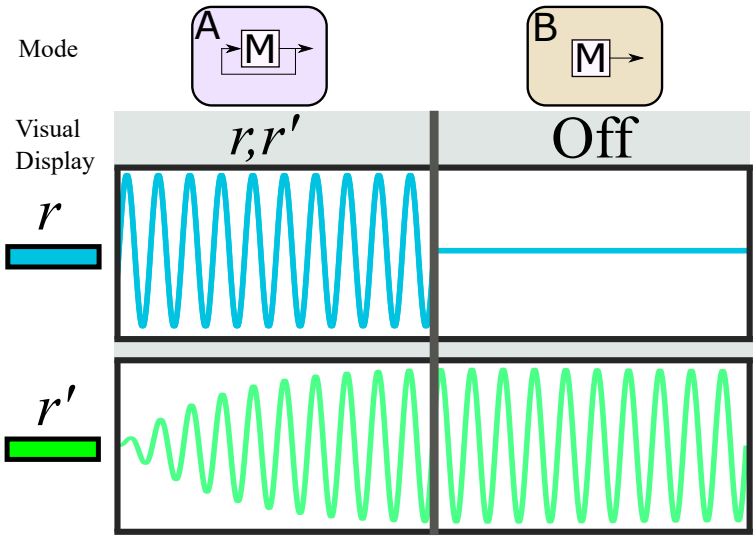

Figure 4.4: Simulation of a system designed according to IMP described as a hybrid dynamic model (a state machine with continuous modes). Note that the mode of the state machine changes halfway through the simulation. Tracking is maintained despite the change in availability of $r(t)$.

4.2.4 Our Proposed Model: The Feedforward Extended IMP Model

The IMP-based model proposed in this chapter utilizes two IMP controllers, or two controllers with embedded reference signal generators: $M(s)$ in a feedforward path and $C(s)$ in a feedback loop (see Fig. 4.5). In effect, we place the model highlighted in Fig. 4.3 in a feedforward path to augment the standard feedback system in Fig. 4.2. The feedforward path operator $M(s)$, like $C(s)$, contains a model of the reference signal generator and has a feedback loop closed around it. The input fed to $M(s)$ is the error between the reference $r(t)$ and its own output $r'(t)$. The controller $M(s)$ generates a command to the plant $P(s)$ that produces perfect tracking when $r'(t)$ matches $r(t)$.

To accommodate blanking of output feedback $y(t)$ or blanking of reference $r(t)$ and output feedback $y(t)$, we will compose a complete model in the form of a hybrid dynamical system. Mode I features a feedforward path with an IMP controller $M(s)$ added to the standard IMP control architecture. Mode II, relying only on the feedforward path, adds the ability to operate when $r(t)$ but not $y(t)$ is available. Finally, Mode III operates when both $r(t)$ and $y(t)$ are interrupted and both $C(s)$ and $M(s)$ act as signal generators without excitation. Thus IMP controllers $M(s)$ and $C(s)$ are equal to each other, are both surrounded by a feedback loop, and are both capable of generating the reference signal $r(t)$. The feedforward path through $M(s)$ and the feedback loop through $C(s)$ work together to produce tracking behavior from $P(s)$, even when the signals $r(t)$ and/or $y(t)$ are interrupted. Note that the only way for the feedforward branch to achieve perfect tracking without feedback from the plant is for $G(s)$ to be correctly matched a priori $G(j\omega_i) = P^{-1}(j\omega_i)$.

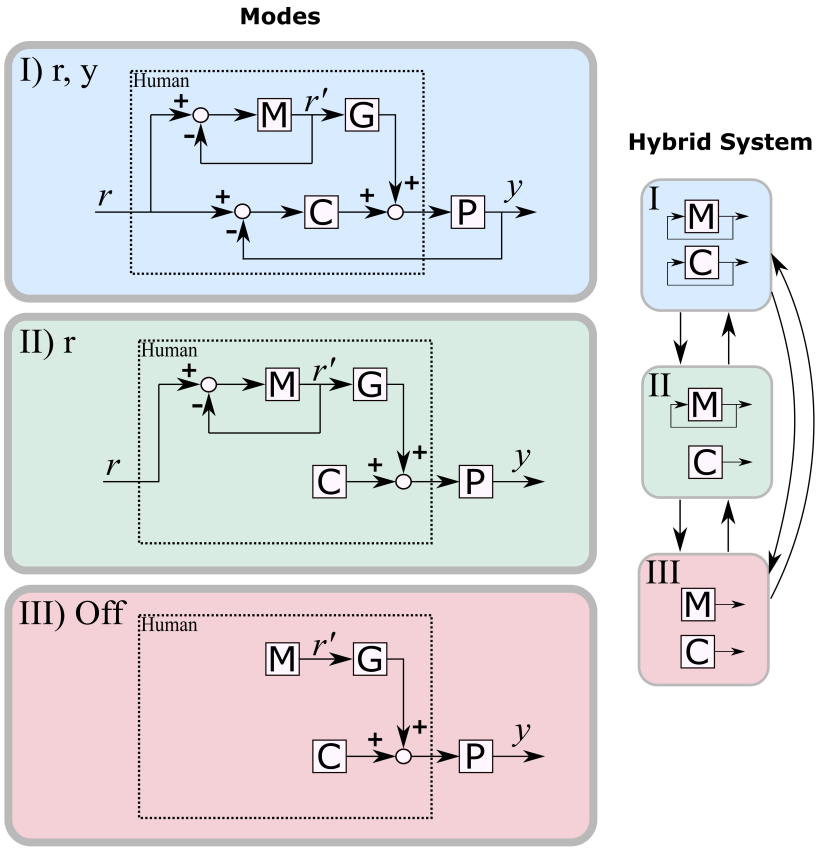

Figure 4.5: A hybrid dynamical model of predictable reference tracking with three distinct modes depending on signal availability. Mode I) uses two Internal Model Principle controllers $M(s)$ and $C(s)$ working in parallel when both $r(t)$ and $y(t)$ are available; mode II) uses an IMP controller $M(s)$ while $C(s)$ acts as a signal generator without excitation when only $r(t)$ is available; and mode III) uses both IMP controllers $M(s)$ and $C(s)$ acting as signal generators without excitation when neither $r(t)$ nor $y(t)$ are available.

4.2.5 Expected Model and Participant Behavior

Once the pattern of the predictable reference is internalized, a visual display should no longer be needed. The controller with an internal model of the predictable reference should be able to generate the appropriate signal to track the reference without access to external signals. To verify this expected behavior both the Feedforward Extended IMP Model and human participants will be tasked with tracking a single sinusoidal reference where the target and cursor are subject to blanking.

The first anticipated behavior is that temporary access to y(t) should enable the controller (simulated or human) to have a better understanding of the plant gain. The controller should internalize the appropriate gain to allow for better tracking performance when y(t) becomes unavailable. To test this hypothesis one would expect a significant improvement in tracking error during the $r(t)$ only condition after exposure to $y(t)$ as compared to the $r(t)$ only condition before exposure to $y(t)$. The second expected behavior is similar to the first, the same adaption effect of learning the appropriate gain should also be present in comparing the tracking error during Off intervals before and after exposure to $y(t)$. Lastly, it is expected that frequency and phase error behavior should be relatively constant throughout the experiment. The information needed to track the target is contained within $r(t)$, therefore is should be internalized within the first $r(t)$ interval and access to $y(t)$ should not be required for correct frequency and phase tracking.

4.3 Simulation of the Feedforward Extended IMP Model

4.3.1 Simulation Methods

In this simulation a single sinusoid will serve as a predictable reference, signal, which we will also call the target signal $r(t)$. A change in the availability of either the target $r(t)$ or cursor $y(t)$ on the screen will occur every 30 seconds. The order in which the visual information associated with the target $r(t)$ and cursor $y(t)$ are made available is shown in Table I and was chosen intentionally to highlight how the human-in-the-loop system responds as new information is added and subsequently blanked.

The simulated system is overmatched by design in order to see a contribution from the feedback controller in reducing the contribution of the feedforward path and perfectly track the reference. The IMP based model of a sinusoid (two marginally stable poles) requires a stabilization term (in $C(s)$ and $M(s)$) such that the closed loop poles are in the LHP: we selected the stabilizing term to be $(s+5)/(s+10)$.

4.3.2 Simulation Results

The Feedforward Extended IMP model shown in Fig. 4.5 presented was simulated using the parameters $G = \frac{3}{4}$ and $P = 2$ and results are shown in 4.6. These parameters are such that $G > |P^{-1}|$, meaning the feedforward loop is overmatched to the plant.

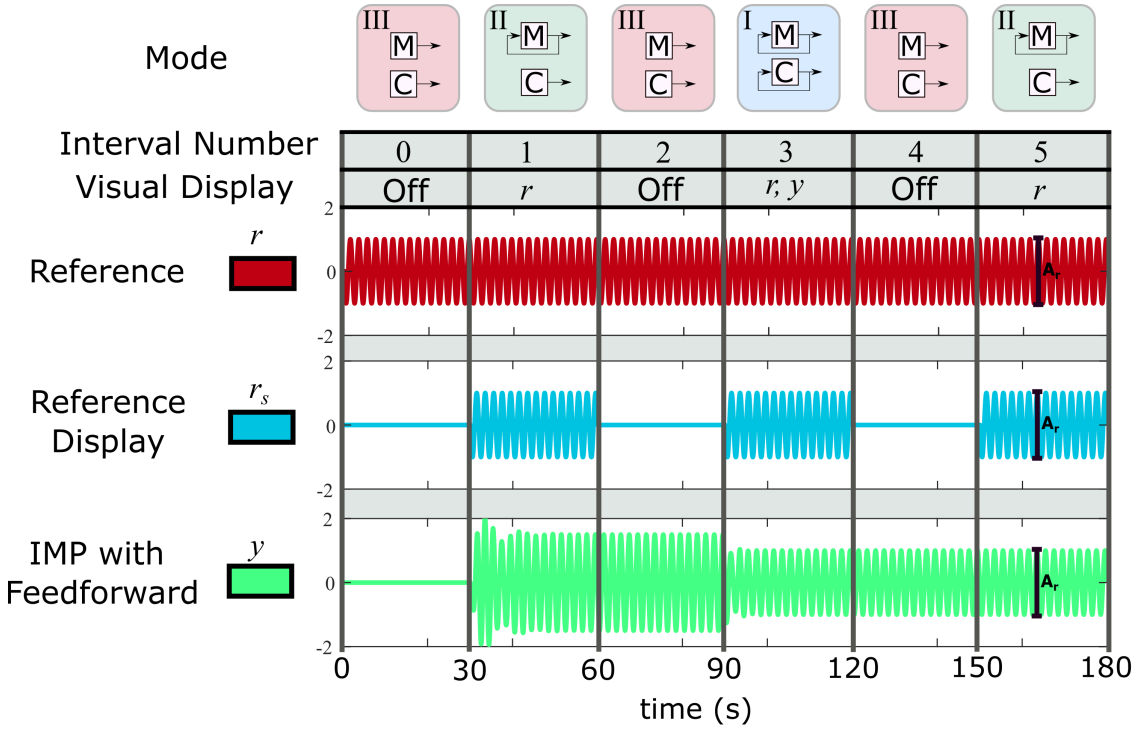

Figure 4.6: Results of IMP based model during signal blanking. Each 30 second interval is demarcated by a vertical grey bar; this indicates a change in the availability of $r(t)$ and/or $y(t)$.

4.3.3 Simulation Discussion

The first expected behavior is a reduced tracking error before and after y(t) is available. It clear by comparing the $r(t)$ intervals before and after exposure to $y(t)$ in Fig. 4.6 that the system it utilizing the incorrect gain, resulting in a large tracking error before exposure to $y(t)$. After exposure to $y(t)$ tracking error is corrected and the system is now tracking with the correct amplitude. The tracking amplitude of signal $y(t)$ is shown to match after exposure to y with a visual indicator labeled A_r in Fig. 4.6.

The second expected behavior also concerns the tracking error but with respect to the intervals with the 'Off' condition, where no visual display is available. Again, similar to the 'r(t)' intervals before and after exposure to $y(t)$, tracking error is reduced in the 'Off' intervals after exposure to $y(t)$.

Finally, the third expectation is that frequency and phase tracking should be fairly even throughout the experiment after an initial exposure to $r(t)$. After exposure to $r(t)$ only, the architecture is clearly able to generate a sinusoid with the correct phase and frequency. Further, the Feedforward IMP Model is able to generate an output despite subsequent removal of $r(t)$ or $y(t)$; it is able to act like a signal generator. It is important to note that a plant with a simple gain was chosen in this simulation. A more complicated plant could generate a change in phase that the system would only be aware of after y becomes available.

4.4 Human Participant Experiment

4.4.1 Experimental Methods

Participants signed an informed consent according to an IRB approved protocol (HUM00188115). The experiment was conducted remotely and only required access to a computer, mouse, and MATLAB.

The participants were asked to perform a pursuit tracking task in which they controlled a computer mouse, moving a cursor on the computer screen, in an effort to pursue a computer controlled target. The availability of visual display was changed throughout the experiment; the visibility of the target, cursor, or both were blanked during certain intervals. All three conditions tested are those shown in the previous thought experiment in Fig 4.1. All subjects were exposed to all conditions thus this is a within subjects experimental design.

Data was collected remotely using the participant's personal computer. In order to accomplish this, code was developed for MATLAB runtime; a free standalone MATLAB software that runs Matlab executables. Because data was not collected in lab setting a DAQ could not be used. As as such, data acquisition was limited to 60HZ.

The plant was selected to be a pure gain of 1.4 which the participant was not exposed to nor informed of before the experiment; it was expected that they would learn to compensate for this gain during the experiment. A preliminary training period where the plant gain was set to 1 was provided allowing the participant to gain familiarity with testing elements (target and cursor on screen and testing apparatus). After this preliminary training the gain associated with the plant was changed to 1.4 to remove knowledge of the learned plant gain.

Each participant was asked to perform two trials of the tracking task each lasting four and a half minutes with the visual display condition changing every thirty to forty seconds (randomized). The visual display changed according to the order 'C-B-C-A-C-B-C' with each letter indicating a condition as shown in Fig. 4.1.

The data set was separated into intervals corresponding to changes in visual display conditions. For each interval, three metrics were calculated: the root mean square error (RMSE) between the

cursor and target, the phase difference between the cursor and target, and the average frequency difference between the cursor and target. The mean and standard deviation of these metrics will be calculated and used for comparisons across intervals.

Finally, a survey was conducted to collect demographics (such as handedness and gender) about the participants, their computer setup (mouse sensitivity, screen resolution), and their experiences during the experiment.

4.4.2 Experimental Results

Data for a single representative participant is shown in Fig. 4.7. A summary of metric results for both trials and all participants is shown in Fig. 4.8. A T-test was run to compare trial one to trial two to see if any learning effects occurred. There were two significant results between trials one and two: an improvement in the mean of the phase difference ($p = 0.7043$) and an improvement in the standard deviation of the mean square error ($p = 0.0168$). Pooling trials 1 and 2 for the fifteen participants generated 30 data points for each interval whose distributions are shown in Fig. 4.8.

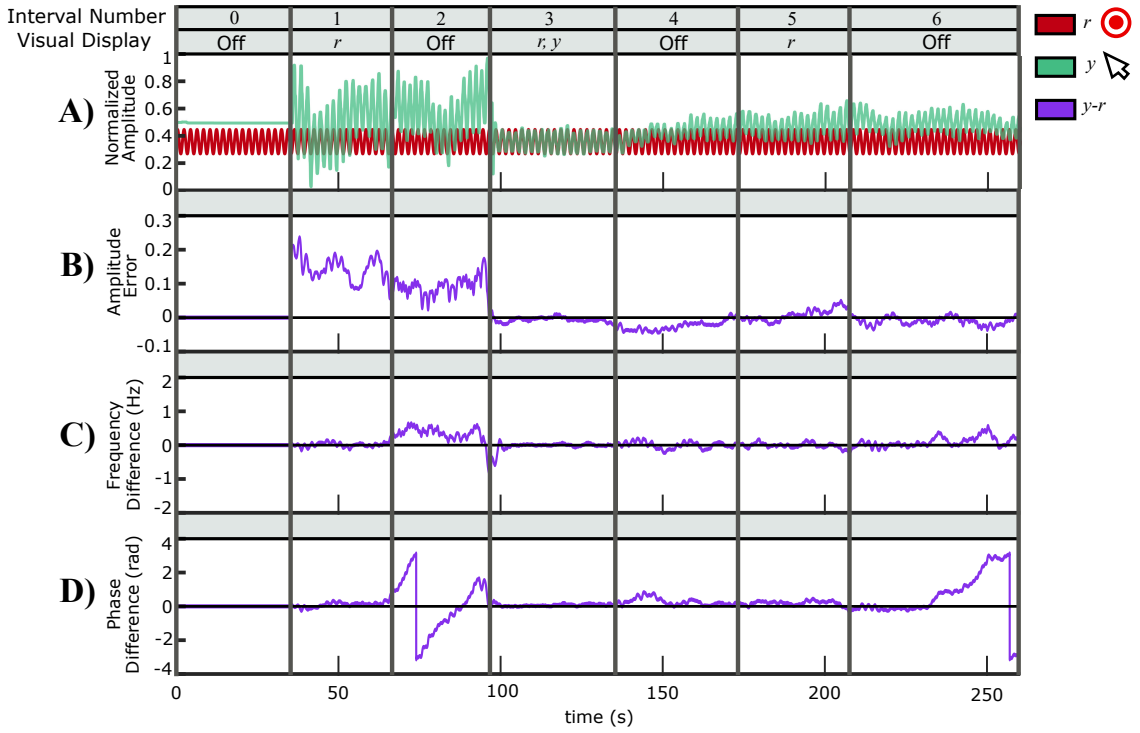

Figure 4.7: Representative subject time signals: A) The raw positional data of the target (red) and the participant controller cursor (green), B) Shows the amplitude associated with the highest frequency in the cursor data, C) The frequency difference between the target (oscillating at 0.5 Hz) and the cursor, and D) The phase difference between the target and the cursor.

A one sided T-test was performed on the difference in distributions associated with the 'r only' condition (intervals 1 and 5, pictured in Fig. 4.9) to determine if the difference in the distributions

had zero mean (indicating no improvement in error) or a positive mean indicating RMSE error improved. Similarly, a T-test was also performed to see if there was a significant improvement in RMSE error between the 'Off' intervals (intervals 2 and 4) this distribution is also pictured in Fig. 4.9. For the 'r only' intervals RMSE error was found to have a significantly improved mean (p = 0.0031) and standard deviation (p = 0.0012) but phase and frequency were not found to have significant differences. Similarly, for the 'Off' intervals RMSE error was found to have a significantly improved mean (p = 0.0001) and standard deviation (p = 0.0061) but phase and frequency were not found to have significant differences.

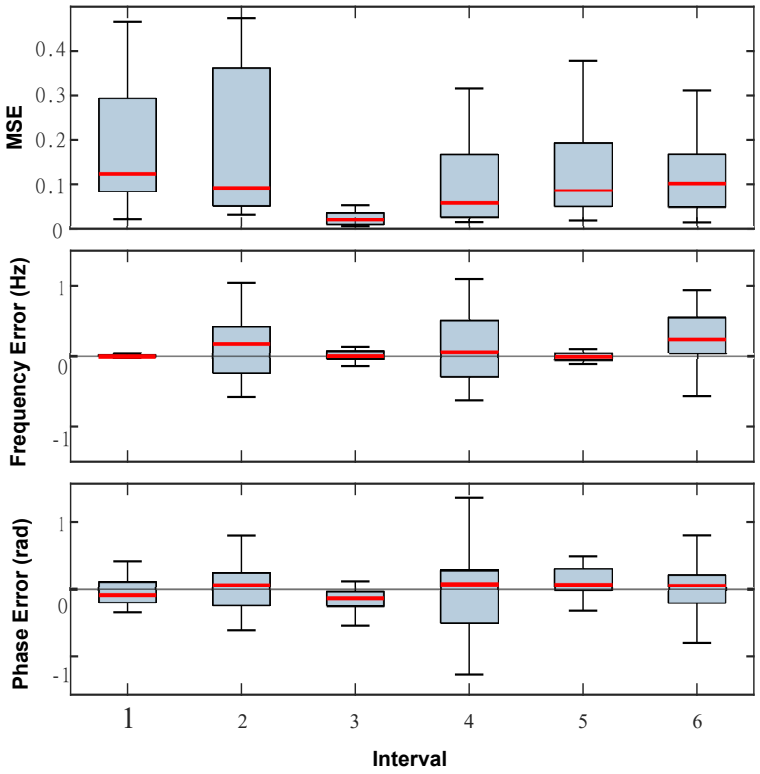

Figure 4.8: Summary Data: The box plots show average RMSE, frequency error, and phase error over all intervals, for all participants, and for both trials

T-tests were run on every interval for the frequency error and phase error metrics with the null hypothesis that the distribution has zero mean and the alternative hypothesis that the distribution has nonzero mean. For the frequency error metric, intervals 1 through 5 satisfied the null hypothesis and only interval 6 satisfied the alternative hypothesis (p = 0.0018). For the phase metric, intervals 1, 2, 4, and 6 satisfied the null hypothesis and intervals 3 (p = 7.57e-4) and 5 (p = 0.0074) satisfied the alternative hypothesis.

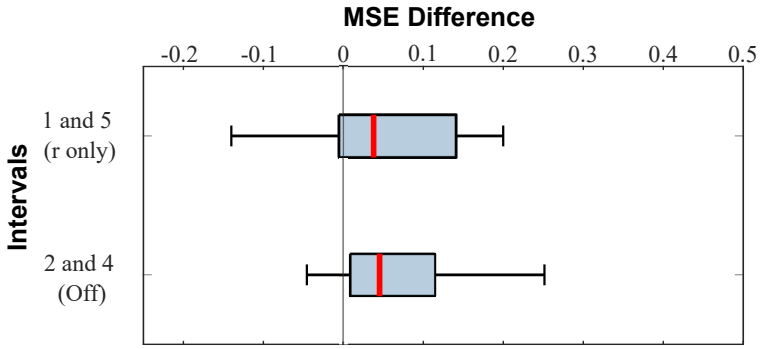

Figure 4.9: Boxplots showing the difference in RMSE performance before and after exposure to y, r condition

4.4.3 Survey Results

All fifteen participants were surveyed about age (25 to 35, mean 28.3), gender (M = 11, F = 4), handedness (R = 14, 1 L), and hardware set up (13 optical mice, 2 track pads).

Participants were asked about video game experience with precise mouse movements: six subjects reported a great deal of experience (once a week or more), one reported moderate experience (about once a month), four reported barely any experience (once a year or less), and four reported no experience.

Participants were also asked about what they found difficult in the experiment. Ten out of the fifteen subjects reported the condition where the target or cursor was invisible. Participants were also asked what they found easy about the experiment. Eleven out of fifteen subjects reported that the experiment in general felt easy, that the target was predictable, or that it was easier when the target and cursor were both visible.

4.4.4 Experimental Discussion

Statistical analyses were completed to verify three expected behaviors. The first expectation was a reduction in tracking error in the $r(t)$ only condition before and after exposure to $y(t)$ as was seen in the simulation results. The hypothesis is that without $y(t)$ the plant $P(t)$ is unknown therefore the the ability to generate correct amplitude should improve after being exposed to a display of $y(t)$. This effect is expected regardless if r is available or not. Here we consider exposure to y to be an intervention. The T-test conducted confirmed that the intervention had a significant effect on the mean and standard deviation of the error distribution. No significant results were found in terms of phase or frequency.

The second analysis conducted was to see if the reduction of error was also present within the 'Off' intervals as was seen in the simulation. The T-test conducted again confirmed that the intervention had a significant effect on the mean and standard deviation of the error distribution. No

significant results were found in terms of phase or frequency.

Finally, the third round of T-tests were conducted on every interval of the experiment for the metrics of phase and frequency error to see if both metrics tended to be distributed with zero mean. The majority of the intervals indeed satisfied the null hypothesis that both frequency and phase error had zero mean. For the frequency metric only interval 6 was found to have a significant non-zero mean. For the phase metric both intervals 5 and 6 were found to be significant.

4.5 Conclusion

In this chapter the IMP was motivated as a means for incorporating information about predictable reference signals within models of human motor behavior. The base architecture proposed by the IMP principle was extended to include a feedforward path and a second model of the predictable reference signal. Previous visual blanking experiments did not manipulate access to $r(t)$ and $y(t)$ independently, nor did they have the notion of a signal generator or the IMP in mind. To demonstrate the capabilities of an architecture capable of acting as a signal generator, simulations of the model and a human participant study were conducted in the face of blanking both $r(t)$ and $y(t)$. Finally, three expectations of system behavior were anticipated and confirmed in both simulation and by human participant experiment.

A feature within our proposed architecture that initially seems strange is that both M and C have the same design. If the system had a single model of the exogenous signal in the feedback loop its conception of the reference would be dependent on feedback. Intuitively, internalizing prior knowledge of the structure of the reference should be independent of feedback availability. For example, the periodicity of ocean waves from the beach can be observed visually and internalized. If one then entered the ocean blind-folded haptic feedback from waves could still anticipated. This is despite initially internalizing the periodicity via visual feedback rather than haptic feedback. To satisfy independence, both feedback and feedforward control paths should have access to an explicit model of the exogenous dynamics. It is also reasonable that there is transfer of knowledge between the two. For example, the difference in feedforward behavior pre- vs post intervention could be explained by a transfer of knowledge from what was learned by controller C to controller M.

A second feature of note is the feedback loop (around M) within the feedforward path because the physical interpretation is not readily apparent. The idea of self regulation without use of haptic, visual, or proprioceptive feedback is encapsulated in the theory of Corollary discharge. Corollary discharge is a mechanism by which internal copies of movement commands are generated. These signals are commonly thought to be used to differentiate self-generated movements from those imposed by the environment [90, 91].

For future work we would propose several extensions. First, an exploration into learning

effects under longer time spans. Longer timer intervals of exposure would likely correspond to stronger internal models resulting in stronger intervention effects. Second, incorporation of proprioception in the modeling section. Within the model this could be accomplished perhaps by adding an additional feedback path and an additional internal model of the reference. Thirdly, incorporation of proprioception in the human participant experiment. A limitation of this study was that proprioception could not be removed remotely. Although proprioceptive feedback was limited in this experiment, due to the small mouse movements, removing proprioceptive feedback and yielding similar results would make a stronger case for an IMP based modeling approach.

CHAPTER 5

The Effects of Haptic Feedback and Transition Type on Transfer of Control between Drivers and Vehicle Automation

5.1 Introduction

Self-driving cars have been proposed as a means to eliminate accidents that result from driver inattention and distraction. However, when driving situations arise in which the automation system can no longer guarantee safety, transfers of control back to a human driver become necessary. Lessons from domains such as aviation have shown that such transfers present challenges for human-machine teams. Highly automated systems support performance and reduce workload when operating in standard situations, but safety is not consistently maintained during off-nominal and time-critical situations [92, 93]. The human operator who is suddenly responsible for taking over control when automation system limits are exceeded often finds discrepancies between expected and actual system or environmental states. Insufficient awareness of the intention and actions of the automation (called "automation surprises") also makes control transitions difficult when anomalies occur Updated reference [53]. High degrees of automation often do not announce their intention nor require operator engagement [93, 94, 95]. This lack of feedback and awareness can lead to errors or misappropriations of responsibility during transfers of control [53, 54, 55]. Transitions involving such issues are often called "bumpy", and are implicated in compromises to safety [56, 57].

Similar challenges have been observed in driving. Even low-level automated systems such as Adaptive Cruise Control (ACC) have been reported to reduce the driver's situation awareness [96]. As the level of automation increases, so does the concern for keeping the driver "in the loop" [97]. This concern is not only a result of theoretical analysis and experimental validation, but also supported by naturalistic observations. For example, a recent analysis of videos of Tesla autopilot and Google self-driving cars called for designs that keep the driver engaged so that they are ready to take over control when necessary [98]. Operational experience has also shown that accidents and near-accidents are more likely to occur when humans are suddenly required to resume control of a vehicle [99].

A factor that further compromises safety during transitions of control is that distractions and

multitasking are very common in driving: a driver in an autonomous vehicle may be engaged in telephone conversations, texting, or usage of in-vehicle entertainment systems. Automation systems are generally designed and used to free driver attention and time for secondary activities, and these secondary activities further increase safety risks during control transitions beyond the effect of lack of feedback from the automation system and lack of involvement in the driving task [100, 101, 102].

A number of factors have been shown to affect the speed and quality of transitions from automated to manual driving. An early advance transition request helps improve the quality of transitions (measured by longitudinal acceleration and brake usage) [103]. The speed of transitions can be improved if the transitions are expected within a certain time interval [104]. In contrast, complex traffic situations have a negative impact on both the speed and quality of transitions [105]. Neither of these factors can be manipulated to better support transfers of control. The traffic situation is not under the control of the driver nor the automation; and likewise, the option to deliver early or expected transition requests is not always available. However, one factor that can be controlled is the level of operator engagement when the automation is in control and whether the system clearly announces its intentions. Accordingly, situation awareness of the driver can be improved with the use of displays. For example, a "haptic seat" that used vibrotactile motors embedded in the driver's seat to indicate the spatial position of approaching vehicles was shown to improve the speed and quality of control transitions for automated driving [106].

Conventionally, control transitions involve a transfer of authority as a lumped whole from one agent to the other that takes place over a short time period. Either the driver or the automation can initiate the transition. For example, transfers are rapid and whole in ACC, and typically initiated by the driver with a button press. Likewise, transfers are rapid and whole in automatic emergency braking, and initiated by the automation when an imminent collision is sensed. Schemes for transitioning control in which authority is transferred as a lumped whole over a short time period are called *traded* or *switching* schemes [107].

Alternative approaches to delegating control authority have been proposed in the interest of promoting transitions that are gradual and smooth. Rather than assigning control as a whole to one agent or the other, control authority is divided into portions and delegated such that each agent is partially in control at any given time. A shift or transition takes place gradually when the two portions are varied continuously over an interval of time. Schemes in which control authority is delegated in portions are called *control sharing* or *overpowering* schemes. In this chapter we use *overpowering* to emphasize the means by which transfers in control are managed, and highlight that there is no longer a switch to be thrown.

In the context of transitioning control between a human and automation, an example *overpowering* scheme is *input mixing* [108, 109]. In *input mixing*, an affine combination of the steering commands produced by the human driver and automation system is used to steer the vehicle. The

determination of weights in the affine combination can be made by the automation according to the sensed driving situation [108, 109]. Alternatively, the driver can overpower the automation in implementations of *input mixing* with fixed weights by steering in a manner that cancels an anticipated automation command.

Another *overpowering* scheme is *haptic shared control* [110, 111, 46, 112, 113, 114, 115]. In *haptic shared control*, the automation system imposes its control action through a motor on the steering wheel with a mechanical impedance roughly matched to nominal human impedance, giving the driver the means to override the automation. In effect, the driver edits the automation steering command, taking over a portion of control by acting with additional torque or by adopting a higher impedance. Sudden and potentially unexpected transfers of authority are replaced by gradual shifts.

Reputed advantages of *haptic shared control* include an increased situation awareness afforded by the driver's hands resting passively on the steering wheel while the automation is in control [116, 46, 117, 118, 114]. Haptic feedback can inform the driver about the automation's activity and intent. Research on *haptic shared control* has demonstrated that haptic feedback can simultaneously improve path following and secondary task performance while reducing demand for visual attention [111]. Further, *haptic shared control* has been demonstrated to support smooth shifts of authority in response to automation-induced faults, apparently by enabling the driver to detect faults and respond smoothly [113].

To date, most research on transitioning control between a human and automation has focused on tuning specific control paradigms and investigating the effects of different types of feedback. Few studies have included side-by-side comparisons of *switching* versus *overpowering* schemes or compared *haptic shared control* against alternatives. Moreover, few studies have assessed human-machine team performance when the automation system is not completely reliable. In this chapter we present results from a simulated driving study involving four schemes for transitioning control authority that involved either *switching* or *overpowering* transitions and were either accompanied or unaccompanied by haptic feedback in the form of torque on the steering wheel. Our intention in quantifying performance across these four control transitioning schemes in a single study was to isolate the effect of *switching* vs. *overpowering* and the effect of haptic feedback from other features in the human/automation interface. We consider nominal as well as off-nominal conditions. For half of the trials, we asked our drivers to perform a secondary tablet-based game task.

5.2 Methods

5.2.1 Participants

Twenty-four participants (16 male, 8 female) were recruited from the population of engineering graduate students at the University of Michigan. Data from one participant were excluded because

of simulator malfunction. Participants were between 20 and 30 years old (mean 24.9 years, SD 2.9 years) and self-reported as right-handed with normal or corrected-to-normal-vision, normal color vision and hearing, as well as having two or more years of driving experience (mean 6.4 years, SD 3.5 years). Participants were randomly assigned to two groups that differed with respect to transition type. 11 participants were assigned to the two schemes with transitions, and the remaining 12 were assigned to the two schemes with transitions.

The experiment took approximately 80 minutes to complete. Participants received a baseline compensation of $20. As an incentive, an additional $70, $40, or $20 was given to the three participants with the top performance. Participants were ranked based on their secondary task score, number of obstacles avoided, and their ability to minimize lateral error. Their overall rank was determined based on the sum of their rankings of each of these three metrics: e.g. if a participant ranked third, fourth, and fifth in the three criteria (compared to all other participants) their final score would be $3 + 4 + 5 = 12$. The three participants who had the lowest final scores were considered the best performers. Participants were only informed that their performance would be graded based on their performance of both tasks, that is both driving and the tablet game, but were not given specifics.

5.2.2 Apparatus

The experimental apparatus consisted of a custom fixed-base driving simulator with a motorized steering wheel. The vehicle dynamics and visual environment were computed on a HP Z400 Workstation desktop computer (Hewlett Packard, Palo Alto CA) with a Sensoray 626 data acquisition card (Sensoray, Portland, OR) using real-time Simulink (The Mathworks, Natick MA). In addition to the 15-inch diameter motorized steering wheel, the hardware setup included a speaker, a tablet computer (Nexus 7, running custom code for the secondary task), an emergency stop, and a 20-inch LCD monitor (see Fig. 5.1 A).

The simulated driving environment featured a gray road separated into two 5m wide lanes by a yellow dashed line. The centerline of the right lane was marked by a white line. The entire track was about 6100 meters in length and was created with straight sections and right and left-hand turns of various curvatures (see Fig. 5.1 C).

Twenty obstacles in the form of 2 m diameter cylinders (see Figure 5.1 B) were placed in the middle of the right lane and distributed approximately 200 m apart in areas in which the track had low curvature. The obstacles were colored either red or green to indicate whether the automation system would avoid them. Participants were told that red obstacles were recognized and handled by the automation; the participant did not have to intervene in order for the car to safely avoid red obstacles. Green obstacles, on the other hand, were not recognized nor handled by the automation. Thus, red obstacles were considered automation assigned (AA) and green obstacles were considered

human assigned (HA). In the following, we will refer to the two types of obstacles not by color but by the terms automation assigned (AA) and human assigned (HA). The drivers were also informed that in this study the road is considered fully available to the driver and it was understood that no other vehicles would be present; there was no penalty for moving to the adjacent lane.

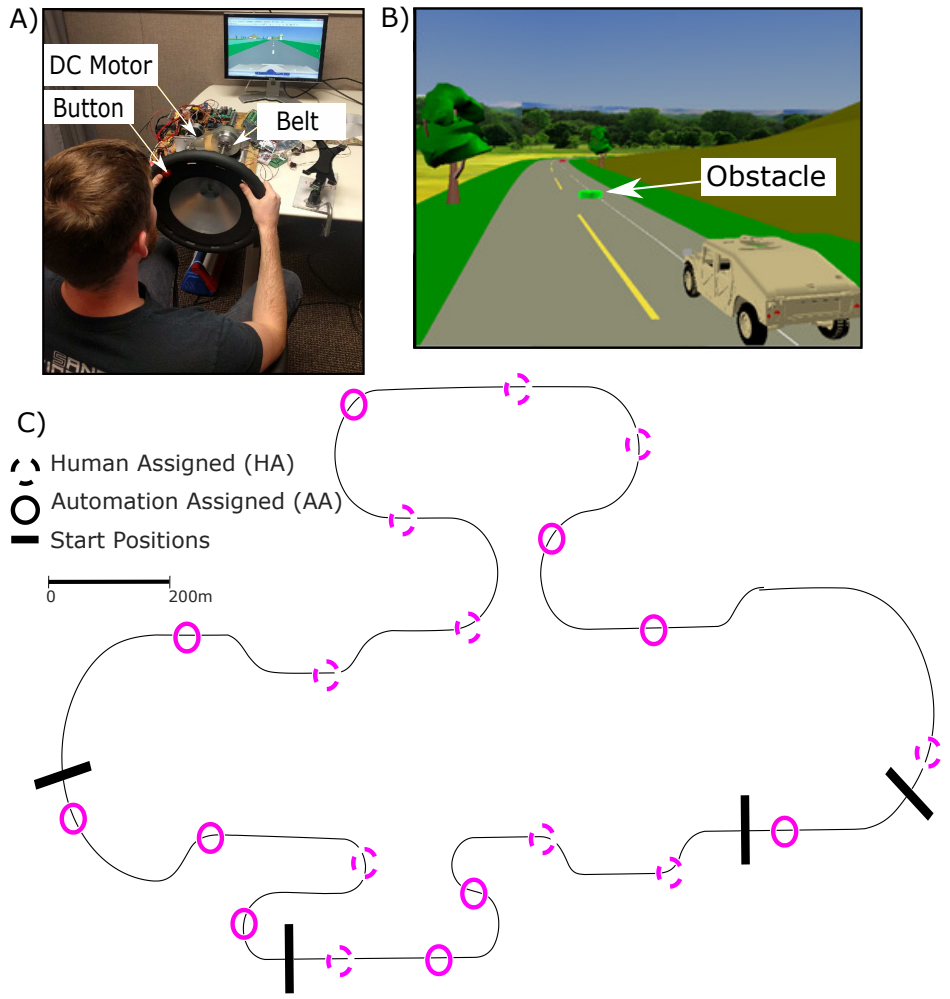

Figure 5.1: A) Hardware setup B) Virtual driving environment and C) Top view of the driving track (navigated clockwise)

5.2.3 Automation System

A standard bicycle model (see, for example [119]) was used to simulate the vehicle's motion on the track, describing the relationships between velocity, heading, current position, and future position. The vehicle speed was fixed at a constant value of 10 m/s; neither the driver nor the automation were able to vary the speed.

A path planner generated trajectories around the track prior to the start of the simulation. The center of the right lane was chosen as the planned path for all areas of the track that did not contain

an obstacle. To enable the automation to go around the obstacle to either side, two Gaussian curves were generated, one to either side of an obstacle. The generated path was then smoothed to avoid sharp corners at the points at which the Gaussian curves were joined to the lane centerline. For a given driving trial, which consisted of one lap around the track, the starting location was chosen randomly from one of four possible initial positions (see Fig. 5.1C).

The desired steering wheel angle was generated using a look-ahead controller. First, the closest point on the path to the vehicle's position was determined. Then the 'look-ahead point' was set a distance of 4 m further down the track. The desired steering wheel angle was chosen to head the vehicle towards the look-ahead point. A proportional-derivative (PD) controller commanded a torque signal proportional to the error (difference between the actual and desired steering wheel angle) and the error derivative. If haptic feedback was provided, the human felt the error as a torque on the steering wheel towards the center of the path. This can be interpreted as a virtual spring connecting the vehicle to the path. If haptic feedback was off, the automation command was passed through a dynamic model of the steering wheel before being sent to the virtual vehicle.

Finally, monotone auditory alerts were sent from a speaker to inform the driver of an upcoming obstacle. The auditory alert was graded, consisting of a single "beep" when the obstacle was 10 seconds away and a double "beep" when the obstacle was 3 seconds away. The auditory alert was sent for both AA and HA obstacles.

5.2.4 Secondary Task

The secondary task in this experiment was a tablet-based game. The tablet was mounted to the right side of the steering wheel and featured a touch screen. Red and blue arrows that pointed either left or right were displayed on the screen, one at a time (shown in Fig. 5.2). The participant was instructed to swipe in the direction of the blue arrow and to swipe in the opposite direction of red arrows. Each arrow stayed on the screen for three seconds or until a swipe was registered. At that point, the next arrow appeared. Participants earned one point for each correct response and lost one point if they swiped in the wrong direction. This externally paced visual task was selected to mimic the attentional demands involved in using a cellphone or in-vehicle navigation/entertainment system. The task was also chosen because it could be expected to use the same processing code (spatial) as the driving task and therefore to compete for mental resources [120]. Participants were required to keep their left hand on the steering wheel at all times and use only their right hand for the secondary task. They were also instructed to give highest priority to obstacle avoidance.

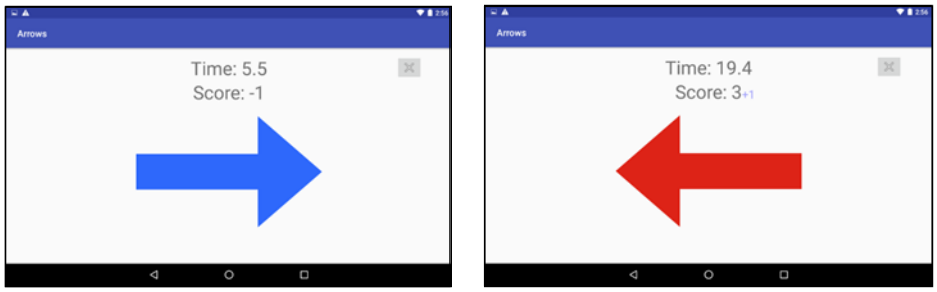

Figure 5.2: Screenshots of the secondary task that was presented on a tablet computer (in both cases above, the participant was required to swipe right)

5.2.5 Transitioning Schemes

We incorporated four schemes by which control could be transitioned between human and automation, each with transition timing determined by the human driver. The resulting four experimental conditions (transitioning schemes) are laid out in Table 1. The and schemes featured transitions (the driver could take over control authority or assign control authority to the automation by pressing a button on the steering wheel). The and schemes featured control (the driver could override the automation by applying additional torque on the steering wheel). The weights in and the impedance (proportional gain) in were held constant. Two of the four schemes featured haptic feedback (and) while and did not.

Table 1: Transitioning Schemes

		haptic feedback	
		Haptic Off	***Haptic On***
transition type	***Switching***	*Traded Control*	*Autopilot*
	Overpowering	*Input Mixing*	*Haptic Shared Control*

Table 5.1: Transition schemes by type and feedback availability

The path taken by the vehicle around an obstacle under a given scheme was determined by some combination of the commands issued by the human driver and automation. For the simulated automation, the command corresponded to a planned path. Assuming that the command by the human driver is not subject to feedback, it might also be represented as a planned path, as shown in Fig. 5.3. Given that each obstacle in our experiment was assigned to either the human or the automation, we might suppose that the assigned agent takes a smooth curve around the obstacle while the other agent drives straight through the obstacle. The vehicle path used in the schemes is determined by either the human or that automation (indicated by a solid line) with no contribution by the other agent (the dashed line or curve). In the schemes, both human and automation commands are combined (both shown as solid lines in 5.3), result in a path between the two planned paths. In

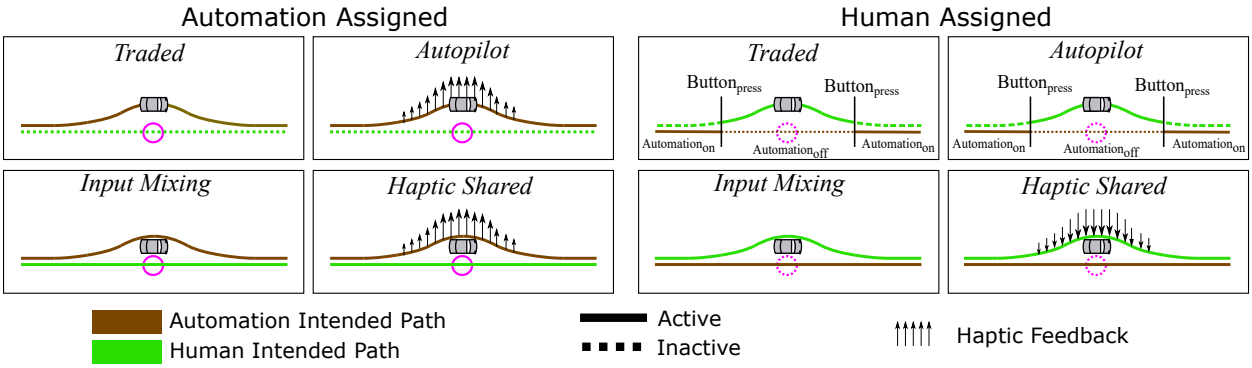

Figure 5.3: Expected result of composing planned human and automation paths by transitioning scheme and obstacle-handling assignment. Under the schemes (top row) only one of the automation planned paths (in brown) or human planned paths (in green) is active (solid) while the other is inactive (dashed) at any given time. Thus the vehicle follows either the automation or human planned path around the obstacle. For the human-assigned obstacles (right group of four panels), the driver pushes a button to disengage and re-engage the automation, whose path is nominally through the obstacle. Under the schemes (bottom row), the vehicle follows a combination of the human and automation planned paths. The arrows indicate the direction and magnitude of haptic feedback presented to the human driver. Note that and have identical behavior in response to HA obstacles, however they have different performance in response to AA obstacles. The intent of the comparison between these two schemes is to understand which performs better overall when AA and HA are jointly considered.

, the combination is the average of both inputs. In the combination depends on the extra torque applied or the increased impedance adopted by the driver.

5.2.6 Experiment Procedure

Upon arrival at the laboratory, each participant was consented according to a protocol approved by the University of Michigan Institutional Review Board (UMIRB ID: HUM00132703). Each participant was then given on-screen instructions on the primary and secondary tasks and the various control transition schemes.

Next, participants were trained for 5-10 minutes on the transition scheme they would experience first. They then completed two 10-minute scenarios with this scheme, one with and one without the secondary task. The same procedure was repeated for the second transition scheme in their condition. Each 10-minute scenario contained 20 obstacles: ten AA and ten HA obstacles intermixed. The total number of participants, trials, and obstacles by transition type are shown in Table 2.

After each scenario, the participant filled out the NASA Task Load Index (TLX) questionnaire to assess their perceived workload.

For each participant, the last scenario included an unexpected automation failure in which an AA obstacle was encountered but the automation did not execute an avoidance maneuver. At the

Table 2: Experiment Structure

		Participants	Trials	Obstacles
transition type	***Switching***	12	48	960
	Overpowering	11	44	880

Table 5.2: Experiment design

end of the experiment, a debriefing questionnaire was used to gather participant feedback on the various schemes.

5.2.7 Performance Metrics and Data Analysis

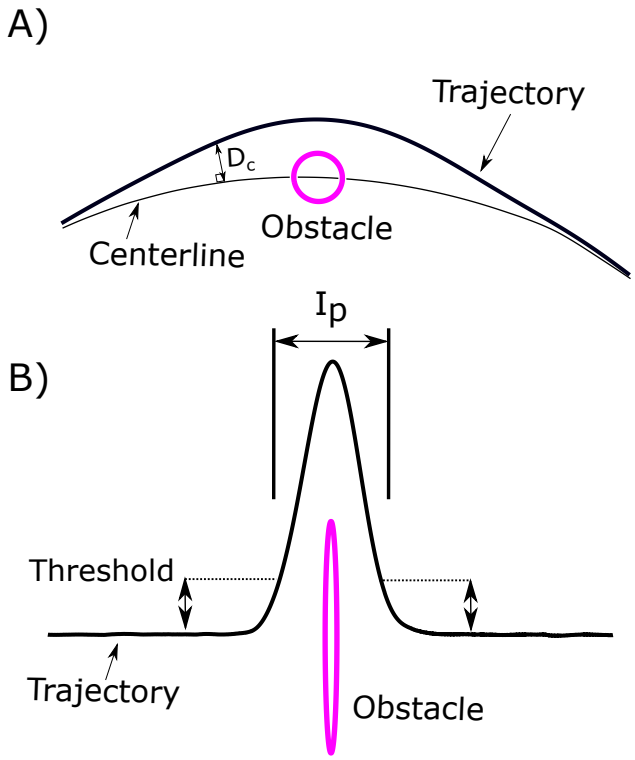

Figure 5.4: A) An example of a typical trajectory traced by the vehicle around an obstacle with the metric $D_C(t)$ indicated between the trajectory and lane centerline. B) The metric I_P is defined as the time interval between crossing a 1 m threshold from the lane centerline.

The present study employed a $2 \times 2 \times 2$ factorial design, with the three factors being: (vs.), (vs.) and secondary task (present vs. absent). The was varied between subjects while haptic feedback and secondary task were within subject variables.

The dependent measures were : (1) The number of Collisions; (2) the Distance To Centerline

$D_c(t)$ as a function of time (see Fig. 5.4A); (3) the Intervention Period I_p measured between points at which $D_C(t)$ crossed a 1 m threshold before and after passing an obstacle (shown in Fig. 5.4B); (4) the Mean Distance to Centerline $\overline{D_C}$, computed as the average of $D_C(t)$ over the period 10 seconds before to 10 seconds after the obstacle. Note the metric $\overline{D_C}$ is equivalent to the Mean Absolute Error between the vehicle path and the centerline. Other measurements included the game scores from the secondary task, NASA-TLX workload scores and subjective ratings of satisfaction and awareness of automation input, collected from a debriefing questionnaire.

The expected findings were: 1) a reduced number of collisions when control was employed and/or when haptic feedback was present; 2) less variance in the vehicle trajectories under control, compared to control; and 3) reduced workload when haptic feedback was present.

The collision rates were analyzed using mixed model binary logistic linear regression. Secondary task score, $\overline{D_C}$, I_P, NASA-TLX scores and subjective rating scores were analyzed using univariate analyses of variance (ANOVA). For all analyses, the significance level p was set at 0.05.

5.3 Results

5.3.1 Collisions

Performance differences on the simulated driving task were readily apparent in the comparison of collisions with automation assigned (AA) and collisions with human assigned (HA) obstacles. No collisions occurred with the 920 AA obstacles encountered, while ten collisions occurred with the 920 HA obstacles encountered (pooling trials with and without secondary task and pooling all four transitioning schemes; $p < 0.001$).

The ten collisions that occurred with HA obstacles were broken down further by transitioning scheme (see Fig. 5.3). Chi-squared tests were performed with transitioning scheme, haptic feedback, and secondary task as the fixed factors. The only significant main effect was observed for haptic feedback ($\chi^2(1) = 6.506, p = 0.011$, Cramér's $V = 0.124$). In the absence of haptic feedback, 9 obstacles were hit while, with haptic feedback present, there was only 1 collision. Transition type (or) had no significant effect on the percentage of obstacles hit: the two transitioning schemes (and) led to 4 obstacles being hit, and the two transitioning schemes (and resulted in 6 obstacles hit ($\chi^2(1) = 0.590, p = 0.442$). There was no effect for secondary task ($\chi^2(1) = 1.618, p = 0.203$), and no significant interactions were found.

5.3.2 Detection of unexpected automation failures

For 19 of the 23 participants, one of the obstacles in the last trial was labeled as an AA obstacle (colored red) but was actually treated by the automation as a HA obstacle (not avoided by the automation). These mislabeled obstacles are called unexpected automation failures and were set up

Human Assigned Obstacle Collisions

	Haptic Off	Haptic On
Switching	4 (1.82%)	0 (0.00%)
Overpowering	5 (2.08%)	1 (0.42%)

With Secondary

	Haptic Off	Haptic On
Switching	3 (2.73%)	0 (0.00%)
Overpowering	3 (2.50%)	1 (0.84%)

No Secondary

	Haptic Off	Haptic On
Switching	1 (0.92%)	0 (0.00%)
Overpowering	2 (1.67%)	0 (0.00%)

Table 5.3: Number of collisions occurring in the four transitioning schemes with HA obstacles.

to explore how participants respond to automation dropouts. Two participants did not notice the unexpected automation failures. Both cases took place in the presence of the secondary task. The remaining 17 participants noticed (determined via questioning post trial) the unexpected automation failures but either chose to not intervene at all or intervened too late and still collided with the obstacle.

5.3.3 Secondary Task Score

Secondary task scores accumulated over each 10-minute trial did not differ significantly across the various schemes for control transitions. However, when scores on the secondary task were assessed only in the vicinity of obstacles, significant differences were observed. Figure 5.5 shows the mean score (computed across all participants) on the secondary task, accumulated within a 50 m (5 second) window before the obstacle is passed and separated by obstacle type. The secondary task score was significantly lower with HA obstacles, compared to AA obstacles (3.30 vs. 4.93, $F(1, 846) = 314.929, p < 0.001$, Cohen's $d = 1.08$). Also, the presence of haptic feedback led to a significantly lower secondary task score (3.99 vs. 4.23, $F(1, 851) = 9.232, p = 0.002$, Cohen's $d = 0.142$).

5.3.4 Distance to Centerline $D_C(t)$

The Distance to Centerline $D_C(t)$ in the vicinity of all obstacles as a function of path length (or time, given the constant vehicle speed) is shown in Fig. 5.6 sorted by obstacle type (AA/HA) and by transitioning scheme. Trajectories are shown in overlay on separate axes for the four transitioning

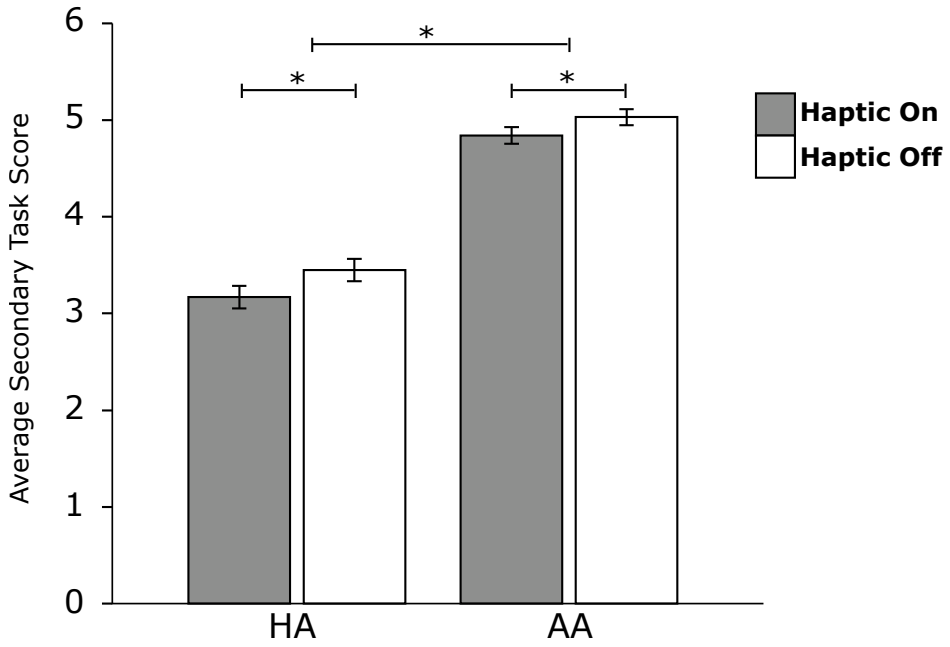

Figure 5.5: Average total secondary task score accumulated 0 to 5s before obstacles. Error bars indicate standard error.

schemes with the AA obstacles gathered in the left group of four graphs and the HA obstacles gathered in the right group of four graphs. For both the AA and HA obstacles, the four transitioning schemes are arranged in the same 2x2 layout. The ellipse shown indicates the minimum $D_C(t)$ required for a trajectory to clear the obstacle. A collision with an obstacle is then visible as an intersection of a trajectory and the ellipse. The average trajectory for each condition is shown as a single bold trace in magenta around the obstacle.

The mean distance to centerline $\overline{D_C}$ computed across transitioning schemes but separated by secondary task is shown in Fig. 5.7. The presence of the secondary task led to a significantly greater mean distance to centerline $\overline{D_C}$ (3.48m vs. 3.11m, $F(1, 822) = 77.977, p < 0.001$, Cohen's $d = 0.488$). No other main effects were observed between the transitioning schemes. However, two interaction effects were observed. and transitions did not lead to significantly different $\overline{D_C}$ when haptic feedback was present (3.30m vs 3.28m), but in the absence of haptic feedback, transitions led to a significantly smaller $\overline{D_C}$ (3.46m vs. 3.14m, $F(1, 882) = 12.618, p < 0.001$). A similar interaction was observed between secondary task and transition type, such that transitions led to a significantly smaller $\overline{D_C}$ (3.24m vs. 2.98m, $F(1, 882) = 4.314, p = 0.038$) only in the absense of the secondary task.

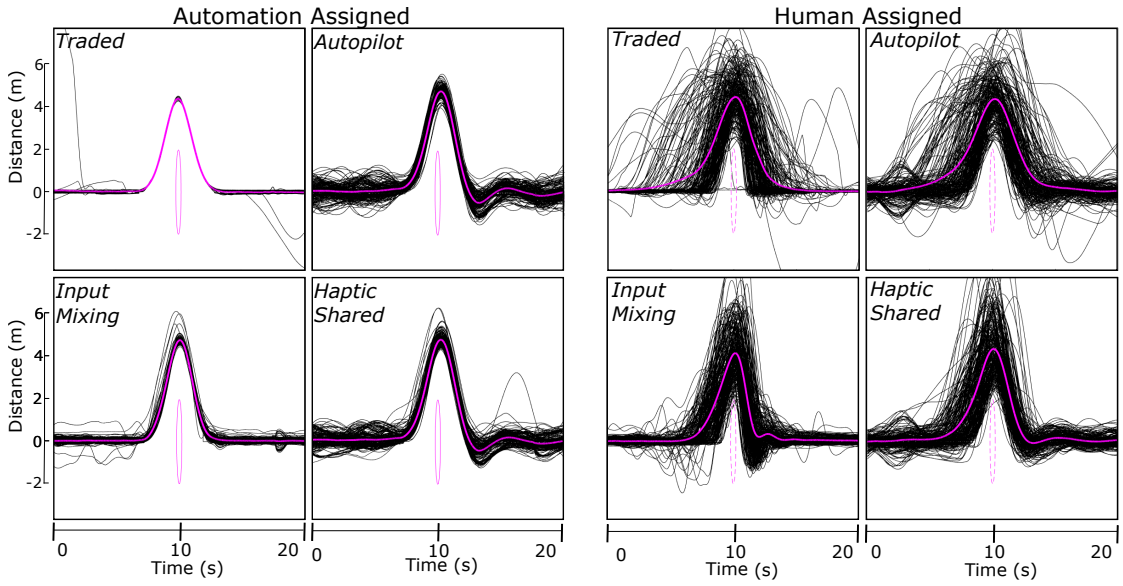

Figure 5.6: Distance to centerline $D_C(t)$ shown in overlay for all obstacles except for unexpected automation failures, separated by Obstacle Type and transitioning scheme. A) AA obstacles (shown to participant as red obstacles) and B) HA obstacles (shown to participant as green obstacles). The magenta trace is the average trajectory.

5.3.5 Intervention Period I_P

The average intervention period I_P as a function of transitioning scheme is shown in Fig. 5.8A. Main effects are indicated in Fig. 5.8B. There were main effects for transition type ($F(1, 880) = 5.137, p = 0.034$, Cohen's $d = 0.765$) and haptic feedback ($F(1, 880) = 53.824, p < 0.001$, Cohen's $d = 0.277$). I_P was significantly longer for transitions (mean = 5.27s, SD = 2.40s, SE = 0.11s) compared to transitions (mean = 3.80s, SD = 1.30s, SE = 0.05s). I_P was significantly longer also when haptic feedback was present (mean = 4.79s, SD = 2.02s, SE = 0.10s) than when haptic feedback was absent (mean = 4.23s, SD = 2.03s, SE = 0.10s).

5.3.6 NASA-TLX Score

The NASA-TLX score measures six dimensions of workload (mental demand, physical demand, temporal demand, overall performance, frustration level, and effort) using 0 - 20 rating scales. Participants reported increased physical demand and frustration level with control compared to control schemes (8.36 vs. 5.75, 6.00 vs. 3.40, respectively; both $p < 0.005$). They also reported increased workload in all six dimensions when the secondary task was present (average 9.61 vs. 3.29; all dimensions $p < 0.005$).

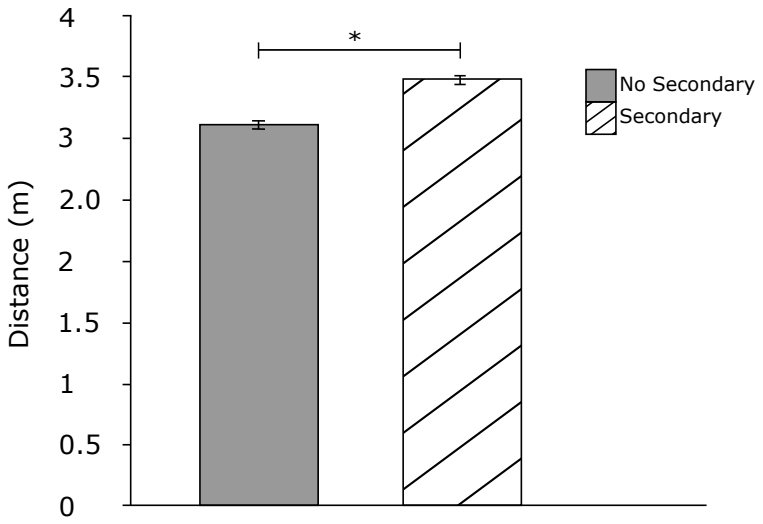

Figure 5.7: The mean distance to centerline $\overline{D_C}$ computed over a 20 second window centered at the obstacle. The error bars indicate standard error.

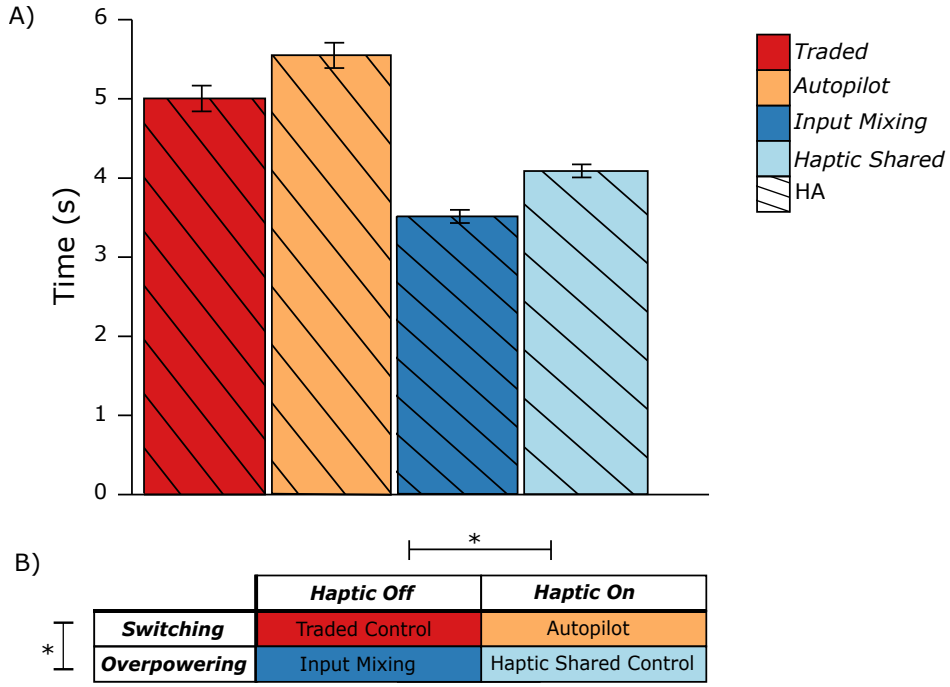

Figure 5.8: A) Average time interval I_P between 1 m threshold crossings before and after passing an HA obstacle. Error bars indicate standard error. B) Table indicating significant differences (*) across transition schemes

5.3.7 Subjective Ratings of Awareness of Automation Input

Participants' subjective ratings were based on a five-point Likert scale (Question: Please rate how aware you were of the automation's control input based on the haptic feedback from the steering wheel. 1-Very little, 5-Very much). They reported improved awareness of automation actions with haptic feedback (3.83 with versus 4.64 with) compared to no feedback (2.58 with versus 2.36 with) ($F(1, 44) = 35.20, p < 0.001$, Cohen's $d = 1.33$). The highest level of awareness was reported in the scheme (a significant interaction between haptic feedback and transitioning scheme: $F(1, 44) = 2.91, p = 0.095$).

5.4 Discussion

In this study, we compared the performance of 23 human-automation teams at following a winding road and avoiding obstacles under four schemes for transitioning between automatic and manual control. We expected that performance would improve when transitions were accomplished through overpowering rather than switching and when the actions of the automation were apparent through haptic feedback while driving around an obstacle.

The number of collisions was significantly reduced when haptic feedback was available to the driver. Only one of the ten collisions with obstacles assigned to the human (HA obstacles) occurred when haptic feedback was present (See Fig. 5.3). On the other hand, the number of collisions did not depend on whether transitions were or . Thus haptic feedback is associated with safer control of the vehicle, independent of transition type. In addition to safer control of the vehicle, an increased awareness of automation actions was associated with the presence of haptic feedback according to subjective ratings.

The distance to centerline $D_C(t)$ trajectories in the vicinity of obstacles indicate differences in driver behavior as a function of transition scheme (see 5.6. Perhaps the most salient, though not surprising feature is that trajectories around the AA obstacles (for which the automation was assigned avoidance responsibility) have the least variation under . This can be explained by the fact that the human driver was uncoupled, and the automation was in complete control of steering. The other schemes for AA obstacles show more variation because the automation had to back-drive the driver's hands through the coupled steering wheel while controlling the vehicle. The trajectories around HA obstacles show significantly more variation, especially under the two schemes. This likely resulted from a button press to invoke a discrete transfer of control from one agent to the other.

While the mean distance to centerline $\overline{D_C}$ did not differ as a function transition scheme, the time interval I_P at which the driver intervened to avoid an obstacle was affected by both transition scheme and haptic feedback. The average time interval I_P between threshold crossings longer for

the two schemes and when haptic feedback was provided (see Fig. 5.8).

Combined with the collision results, this indicates that requires longer intervention times without yielding any benefit in safety. Because faults are often sudden occurrences, schemes that support rapid transitions (such as button presses) may hold advantages. On the other hand, using the steering wheel as the interface for adjusting control authority might support smoother or earlier transitions.

One of the expectations for this experiment was that the benefits of overpowering and haptic feedback would be amplified when the driver was engaged in a secondary task [120]. Across all transitioning schemes, 7 collisions occurred while the driver was performing the secondary task, and 3 collisions occurred in the absence of the secondary task. However, this difference was not significant. One likely explanation for this lack of significance is that shifting attention between the primary driving and secondary tablet-based game task was accomplished in a timely manner thanks to the auditory alerts. Participants learned to glance at the driving scene upon hearing the audio alert to determine whether they were responsible for the obstacle ahead. They subsequently either shifted their attention to avoiding the obstacle or continued with the secondary task. Without the auditory alerts, participants would have to rely on haptic feedback to notice when the automation initiates an avoidance maneuver around an AA obstacle. And they would have to disengage from the secondary task on a regular and more frequent basis to scan the road ahead in order to detect HA obstacles.

While the number of collisions was not significantly affected by multitasking, participants did opt for wider trajectories around obstacles when the secondary task was competing for their attention, as indicated by the significantly larger mean distance to centerline $\overline{D_C}$ with secondary task (see Fig. 5.5).

Interestingly, the presence of haptic feedback resulted in poorer performance on the secondary task in the vicinity of obstacles (see Fig. 5.5). This suggests greater engagement in the primary task when automation actions were communicated, which can be considered a positive outcome.

One important question in this study was how performance might differ under the four control transition schemes in the face of unexpected automation failures (automation dropouts), when AA obstacles unexpectedly became the full responsibility of the human driver [53, 54]. Nineteen such obstacles were encountered by the 23 participants, and all resulted in a collision. This result suggests that, over time, participants became miscalibrated in terms of trust in an reliance on the system. In most cases, the driver noticed the failure, suggesting that their monitoring of the system did not suffer significantly; however they did poorly on the second task left for operators when automation is introduced - intervening in the case of system failures [93]. Participants either did not intervene at all or intervened too late. This finding replicates earlier work highlighting the risk of over-trust and over-reliance on automation, leading to a loss in preparedness after the automation has performed reliably for some time [54, 121]. Given recent accidents that have appeared during

testing of autonomous vehicles (e.g. the crash involving an Uber driverless car on March 18, 2018 in Tempe, Arizona), this problem is highly relevant and should receive more attention.

5.5 Conclusion

In conclusion, the current study demonstrated facilitates collaboration between a human driver and automation. The effectiveness of two features of , haptic feedback and transition by overpowering, was tested independently. Haptic feedback enhanced safety by improving the driver's awareness of automation input and the status of the vehicle. control was shown to improve the smoothness of intervention, compared to control. These benefits were robust even with the addition of a secondary visuo-manual task. Future work will seek a better understanding of conflicts between human and automation, as well as issues regarding the development or dissolution of trust in automation. Another future direction would be to explore if the effects of transition scheme are exacerbated in scenarios with higher difficulty including a higher vehicle speed, other vehicles, and additional obstacles. In addition, while driving performance in the simulator will not transfer to the road in absolute terms, we do expect relative performances across control schemes to transfer to the road.

CHAPTER 6

Conclusion

The study of how the sensorimotor system interacts with the world is a large field with many perspectives. The fields of control systems, human motor behavior, neuroscience, and haptics each provide unique insights and distinct sets of tools. In many cases these fields work on solutions to very similiar problems and may not be aware of their counterpart's efforts. The major goal of this dissertation has been to combine some of the insights and methodologies from the control systems, human motor behavior, neuroscience, and haptics communities to highlight conclusions that align these multiple ways of thinking.

The first contribution of my dissertation was to introduce the Internal Model Principle as a means for modeling human motor behavior. The Internal Model Principle was developed and continues to be used within the controls community but is largely unknown to motor behaviorists and the neuroscience communities. The IMP represents a promising modeling tool for predictive motor behavior that is consistent with the notion of Internal Models developed by the human motor behavior and neuroscience communities. Further, I demonstrated its usefulness by showing how the IMP may be used to model a haptic task: sustaining oscillations in a virtual spring.

My second contribution was to develop an extension to the standard IMP model for use in modelling human-motor behavior in response to signal blanking. The ability to track a reference signal despite blanking cannot be explained by well known approaches that utilize internal models of the plant (McRuer model) or feedforward control. I developed an extension of the standard IMP architecture that is capable of replicating observed human motor behavior during reference blanking. I also demonstrated through a human motor task that the behavior of my model is consistent with what one would expect from a human participant attempting to track a target despite blanking.

My third contribution was to highlight how haptic feedback carries the dual roles of power and information. When biomechanics become coupled to an artifact of the environment, such as grasping an object, the sensorimotor system now has to control the coupled dynamics. If the object is able to exert sufficiently strong force through haptic feedback upon the biomechanics it is then able to backdrive the biomechanics and thus close a mechanical feedback loop. A seperate feedback loop exists in the form of information. Haptic feedback exerted upon the body allows the sensorimotor

system to make decisions based on the perception of what is felt. In order to incorporate haptic technology in applications where the user may be backdriven such as prosthetics, exoskeletons, and driving, it is important that the distinction between information and power feedback loops is clear so that the correct dynamics are considered in the design of controllers. In addition to distinguishing the dual roles, I presented the results of a human participant experiment I conducted. In many cases experiments within the Haptics community are interested in how human behavior and perception differ when haptic feedback is turned on or off. However, as I illustrated, simply turning off haptic feedback will not preserve the dynamics of the system. In my dissertation I demonstrated a means of decoupling the participant from haptic information while preserving haptic power through a model of the coupled biomechanics.

The fourth and final contribution was a human participant study on a human-machine system conducted to assess how transitions affect performance within a human-machine scenario. In many driving simulation studies, a single control scheme is studied with the goal of understanding how a design parameter affects performance or with the goal of making a comparison to manual driving. My dissertation aimed to make a comparison across two of the most salient features among different human-machine controls schemes, namely, the abruptness of transitions (switching versus overpowering) and whether or not haptic feedback was available. During this study it was found that the presence of haptic feedback and continuous transitions both have some benefits on the performance of human-machine systems.

6.1 Limitations and Future work

Chapters 2 and 3: Modeling based on the Internal Model Principle

Limitations

- **Consideration of Proprioception**: A limitation of my work was the limited ability to experimentally control for the sense of proprioception. The sense of proprioception enables one to have a feedback signal with which to implement closed loop control on position despite the lack of haptic or visual information. This experimentally uncontrolled feedback signal that is difficult to remove presents a confound in attempting to determine the differences between feedforward and feedback control using the method of blanking. Notwithstanding, the magnitude of the sensation and reliability of proprioception is thought to correlate with the range of motion. The experiments conducted in this thesis all had a limited range of motion which, as a result, helped minimize but not eliminate the impact of proprioception.

- **Modeling of Transient Behavior**: The behavior analyzed in each study focused on steady state responses and trends in general behavior. Analysing transient behavior was beyond the

scope of this thesis and would likely require incorporation of additional modelling techniques.

Future Work

- **Modeling of proprioception**: The work presented in Chapter 4 could be extended to incorporate the sense of proprioception as an additional feedback loop. It could be investigated whether the additional loop, featuring a third IMP controller fed with proprioceptive error, would be representative of human motor behavior.

- **Investigate preview**: In addition to a target having predictable behavior, a target whose trajectory seems unpredictable can be anticipated if preview of the future target position is provided. Previous studies have shown that as preview distance of an unpredictable target is extended, the resulting human motor behavior performance becomes closer to what one would expect for a predictable target. Preview then allows for a level of performance that outperforms models of unpredictable signal tracking but falls short of models of predictable signal tracking. A future study could investigate the applicability of IMP based models in the study of human motor performance under varying levels of predictability and preview. I have made some progress towards this goal by previously completing the development of experimental setup enabling tracking experiments with varying levels of preview, haptic feedback, and automation.

- **Modeling of cerebellar ataxic patient behavior**: A future avenue of work would involve collaboration with John Hopkins to investigate the applicability of IMP based models for understanding the behavior of the cerebellar ataxic population. In particular, the focus would be to see if a corruption of an IMP based model architecture could explain observed human motor behavior.

Chapter 4: Power and Information

Limitations

Identify participant biomechanics A more robust model of the arm biomechanics could be utilized. The presented work presented a model with stiffness and damping values based upon a previous study. System identification of each participant's bio-mechanics would insure the virtual arm is consistent with each subject's biomechanics and may lead to better performance.

Future work

- **Utilize anesthetization**: In Chapter 3, the virtual arm was presented as an alternative to anesthetization, however the anesthetization case was not used as a point of comparison. The work presented could be built upon in the future to include a comparison of all three cases: the control condition, the virtual arm, and an anesthetized arm.

Chapter 5: Transitions of Authority

Limitations

- **Simulating a vehicle**: In chapter 5 the human participant study was conducted on a simulated vehicle. Being in a simulated environment is likely to cause differences in participant behavior compared to a real-life scenario. For example, recreating motor behavior in response to an obstacle that is realistic to a real-life scenario is hard to reconstruct in an ethical manner within a laboratory setting. Correspondingly, the real-world effect of the driver's level of stress on their response to cues from a human-machine interface is hard to assess. Beyond ethical concerns, a simulation is an approximation of a real world environment and consequently there will always be differences in between laboratory and real-world performance.

Future Work

- **Exploration of the parameter space for Haptic Shared Control**: After the study presented in this dissertation was completed, several collaborators at the University of Michigan continued to investigate the potential benefits of haptic shared control in a follow up study. Several upgrades were made to the simulation platform including utilization of a better visualization and vehicle dynamics platform (CarSim) and a better visual display (a three monitor setup). These researchers were interested in exploring how human participants responded to a shared control architecture where haptic feedback was presented in differing levels of strength and exploring three different automation modes: intended, idle, and adversarial [122].

BIBLIOGRAPHY

[1] T. Y. Moore and A. A. Biewener, "Outrun or Outmaneuver: Predator-Prey Interactions as a Model System for Integrating Biomechanical Studies in a Broader Ecological and Evolutionary Context," *Integrative and Comparative Biology*, vol. 55, no. 6, pp. 1188–1197, 2015.

[2] M. R. A. Chance, D. Sc, W. M. S. Russell, and D. Phil, "Protean Displays: A Form of Allaesthetic Behavior," *Proceedings of the Zoological Society of London*, vol. 132, pp. 65–70, 1959.

[3] M. Mischiati, H. T. Lin, P. Herold, E. Imler, R. Olberg, and A. Leonardo, "Internal models direct dragonfly interception steering," *Nature*, vol. 517, no. 7534, pp. 333–338, 2015.

[4] E. Roth, K. Zhuang, S. A. Stamper, E. S. Fortune, and N. J. Cowan, "Stimulus predictability mediates a switch in locomotor smooth pursuit performance for Eigenmannia virescens," *Journal of Experimental Biology*, 2011.

[5] M. C. Marieke Van der Steen and P. E. Keller, "The adaptation and anticipation model (ADAM) of sensorimotor synchronization," *Frontiers in Human Neuroscience*, vol. 7, no. MAY, pp. 1–15, 2013.

[6] D. M. Wolpert, Z. Ghahramani, and M. Jordan, "An Internal Model for Sensorimotor Integration," *Science*, vol. 269, no. SEPTEMBER, 1995.

[7] D. M. Wolpert, R. C. Miall, and M. Kawato, "Internal models in the cerebellum," *Trends Cog Sci*, vol. 2, no. 9, pp. 338–347, 1998.

[8] R. C. Miall and D. M. Wolpert, "Forward models for physiological motor control," *IEEE Trans Neural Netw*, vol. 9, no. 8, pp. 1265–1279, 1996.

[9] M. Kawato, "Internal models for motor control and trajectory planning mitsuo kawato," *Curr Opin Neurobiol*, pp. 718–727, 1999.

[10] R. Shadmehr and F. A. Mussa-ivaldi, "Adaptive Representation of Dynamics during Learning of a Motor Task," *The Journal of Neuroscience*, vol. 74, no. May, 1994.

[11] R. S. Johansson and G. Westling, "Roles of glabrous skin receptors and sensorimotor memory in automatic control of precision grip when lifting rougher or more slippery objects," *Experimental Brain Research*, vol. 56, no. 3, pp. 550–564, 1984.

[12] L. Snyder, "This way up: Illusions and internal models in the vestibular system," *Nature Neuroscience*, vol. 2, no. 5, pp. 396–398, 1999.

[13] B. Mehta and S. Schaal, "Forward Models in Visuomotor Control," *Journal of Neurophysiology*, pp. 942–953, 2002.

[14] J.-l. Vercher, "The oculomanual coordination control center takes into account the mechanical properties of the arm," *Experimental Brain Research*, no. February 1999, 2014.

[15] M. Shidara, K. Kawano, H. Gomit, and M. Kawatott, "Inverse-dynamics model eye movement control by Purkinje cells in the cerebellum," *Nature*, vol. 365, no. September, pp. 50–52, 1993.

[16] J. J. Orban de Xivry, M. Missal, and P. Lefèvre, "A dynamic representation of target motion drives predictive smooth pursuit during target blanking," *Journal of Vision*, vol. 8, no. 15, pp. 1–13, 2008.

[17] L. E. Miller, L. Montroni, E. Koun, R. Salemme, V. Hayward, and A. Farnè, "Sensing with tools extends somatosensory processing beyond the body," *Nature*, vol. 561, no. 7722, pp. 239–242, 2018.

[18] M. Martel, L. Cardinali, A. C. Roy, and A. Farnè, "Tool-use: An open window into body representation and its plasticity," *Cognitive Neuropsychology*, vol. 33, no. 1-2, pp. 82–101, 2016.

[19] A. Maravita and A. Iriki, "Tools for the body (schema)," *Trends in Cognitive Sciences*, vol. 8, no. 2, pp. 79–86, 2004.

[20] J. A. Kluzik, J. Diedrichsen, R. Shadmehr, and A. J. Bastian, "Reach adaptation: What determines whether we learn an internal model of the tool or adapt the model of our arm?" *Journal of Neurophysiology*, vol. 100, no. 3, pp. 1455–1464, 2008.

[21] D. McNamee and D. M. Wolpert, "Internal Models in Biological Control," *Annual Review of Control, Robotics, and Autonomous Systems*, vol. 2, no. 1, pp. 339–364, 2019.

[22] F. Lacquaniti and C. Maioli, "Adaptation to suppression of visual information during catching," *Journal of Neuroscience*, vol. 9, no. 1, pp. 149–159, 1989.

[23] J. B. Dingwell, C. D. Mah, and F. A. Mussa-ivaldi, "Experimentally confirmed mathematical model for human control of a non-rigid object," *J Neurophysiology*, vol. 91, pp. 1158–1170, 2019.

[24] K. A. Thoroughman and J. A. Taylor, "Rapid reshaping of human motor generalization," *Journal of Neuroscience*, vol. 25, no. 39, pp. 8948–8953, 2005.

[25] J. Huang, A. Isidori, L. Marconi, M. Mischiati, E. Sontag, and W. M. Wonham, "Internal models in control, biology and neuroscience," in *Proc IEEE Int Conf on Decision Control*, 2019, pp. 5370–5390.

[26] M. Mulder, D. M. Pool, D. A. Abbink, E. R. Boer, P. M. Zaal, F. M. Drop, K. Van Der El, and M. M. Van Paassen, "Manual Control Cybernetics: State-of-the-Art and Current Trends," *IEEE Transactions on Human-Machine Systems*, vol. 48, no. 5, pp. 468–485, 2018.

[27] D. T. McRuer and H. R. Jex, "A Review of Quasi-Linear Pilot Models," *IEEE Transactions on Human Factors in Electronics*, vol. 8, no. 3, pp. 231–249, 1967.

[28] F. M. Drop, D. M. Pool, H. J. Damveld, M. M. Van Paassen, H. H. Bülthoff, and M. Mulder, "Identification of the transition from compensatory to feedforward behavior in manual control," *Conference Proceedings - IEEE International Conference on Systems, Man and Cybernetics*, pp. 2008–2013, 2012.

[29] F. M. Drop, R. de Vries, M. Mulder, and H. H. Bülthoff, "The Predictability of a Target Signal Affects Manual Feedforward Control," *IFAC-PapersOnLine*, vol. 49, no. 19, pp. 177–182, 2016.

[30] K. Van Der El, D. M. Pool, H. J. Damveld, M. M. Van Paassen, and M. Mulder, "An empirical human controller model for preview tracking tasks," *IEEE Transactions on Cybernetics*, vol. 46, no. 10, pp. 2609–2621, 2015.

[31] K. van der El, D. M. Pool, M. M. van Paassen, and M. Mulder, "Effects of Preview on Human Control Behavior in Tracking Tasks With Various Controlled Elements," *IEEE Transactions on Cybernetics*, no. November, 2017.

[32] B. A. Francis and W. M. Wonham, "The internal model principle for linear multivariable regulators," *Applied Mathematics & Optimization*, vol. 2, no. 2, pp. 170–194, 1975.

[33] ——, "The Internal Model Principle of Control Theory," *Automatica*, vol. 12, no. 5, pp. 457–465, 1976.

[34] J. J. Orban de Xivry, M. Missal, and P. Lefèvre, "Smooth pursuit performance during target blanking does not influence the triggering of predictive saccades," *Journal of Vision*, vol. 9, no. 11, pp. 1–16, 2009.

[35] F. M. Drop, D. M. Pool, M. M. Van Paassen, M. Mulder, and H. H. Bulthoff, "Effects of Target Signal Shape and System Dynamics on Feedforward in Manual Control," *IEEE Transactions on Cybernetics*, vol. 49, no. 3, pp. 768–780, 2019.

[36] K. Van Der El, S. Padmos, D. M. Pool, M. M. Van Paassen, and M. Mulder, "Effects of preview time in manual tracking tasks," *IEEE Transactions on Human-Machine Systems*, vol. 48, no. 5, pp. 486–495, 2018.

[37] C. D. M. Jonathan B. Dingwell and Ferdinano A. Mussa Ivaldi, "Manipulating Objects With Internal Degrees of Freedom: Evidence for Model-Based Control," *Journal of Neurophysiol*, vol. 8, pp. 222–235, 2001.

[38] G. Maffei, I. Herreros, M. Sanchez-Fibla, K. J. Friston, and P. F. Verschure, "The perceptual shaping of anticipatory actions," *Proceedings of the Royal Society B: Biological Sciences*, vol. 284, no. 1869, 2017.

[39] C. Antfolk, M. D'alonzo, B. Rosén, G. Lundborg, F. Sebelius, and C. Cipriani, "Sensory feedback in upper limb prosthetics," *Expert Review of Medical Devices*, vol. 10, no. 1, pp. 45–54, 2013.

[40] J. E. Colgate, "Robust Impedance Shaping Telemanipulation," *IEEE Transactions on Robotics and Automation*, vol. 9, no. 4, pp. 374–384, 1993.

[41] N. Colonnese and A. Okamura, "Stability and quantization-error analysis of haptic rendering of virtual stiffness and damping," *International Journal of Robotics Research*, vol. 35, no. 9, pp. 1103–1120, 2016.

[42] R. Adams and B. Hannaford, "Stable haptic interaction with switched virtual environments," *IEEE Transactions on Robotics and Automation*, vol. 15, no. 3, pp. 465–474, 1999.

[43] J. C. Dean and A. D. Kuo, "Elastic coupling of limb joints enables faster bipedal walking," *Journal of the Royal Society Interface*, vol. 6, no. 35, pp. 561–573, 2009.

[44] A. M. Wind and E. J. Rouse, "Neuromotor Regulation of Ankle Stiffness is Comparable to Regulation of Joint Position and Torque at Moderate Levels," *Scientific Reports*, vol. 10, no. 1, pp. 1–9, 2020.

[45] A. J. Pick and D. J. Cole, "Dynamic properties of a driver's arms holding a steering wheel," *Proceedings of the Institution of Mechanical Engineers, Part D: Journal of Automobile Engineering*, vol. 221, no. 12, pp. 1475–1486, 2007.

[46] D. A. Abbink, M. Mulder, and E. R. Boer, "Haptic Shared Control: Smoothly Shifting Control Authority?" *Cognition, Technology and Work*, vol. 14, no. 1, pp. 19–28, 2012.

[47] K. B. Reed and M. A. Peshkin, "Physical collaboration of human-human and human-robot teams," *IEEE transactions on haptics*, vol. 1, no. 2, pp. 108–120, 2008.

[48] K. Reed, M. Peshkin, M. J. Hartmann, M. Grabowecky, J. Patton, and P. M. Yishton, "Haptically linked dyads are two motor-control systems better than one?" *Psychological Science*, vol. 17, no. 5, pp. 365–366, 2006.

[49] S. Gentry, E. Feron, and R. Murray-Smith, "Human-human haptic collaboration in cyclical fitts' tasks," in *2005 IEEE/RSJ International Conference on Intelligent Robots and Systems*. IEEE, 2005, pp. 3402–3407.

[50] N. Wegner and D. Zeaman, "Team and individual performances on a motor learning task," *Journal of General Psychology*, vol. 55, no. 1, pp. 127–142, 1956.

[51] D. Feth, R. Groten, A. Peer, S. Hirche, and M. Buss, "Performance related energy exchange in haptic human-human interaction in a shared virtual object manipulation task," *Proceedings - 3rd Joint EuroHaptics Conference and Symposium on Haptic Interfaces for Virtual Environment and Teleoperator Systems, World Haptics 2009*, pp. 338–343, 2009.

[52] M. I. Jordan and D. E. Rumelhart, "Forward models: Supervised learning with a distal teacher," *Cognitive Science*, vol. 16, no. 3, pp. 307–354, 1992.

[53] N. B. Sarter, D. D. Woods, and C. E. Billings, "Automation surprises," *Handbook of human factors and ergonomics*, vol. 2, no. 1926-1943, 1997.

[54] Raja Parasuraman and Victor Riley, "Humans and Automation: Use, Misuse, Disuse, Abuse," *Human Factors*, vol. 39, no. 2, pp. 230–253, 1997.

[55] Zhenji Lu, Riender Happee, Christopher D.D. Cabrall, Miltos Kyriakidis, and Joost C.F. de Winter, "Human factors of transitions in automated driving: A general framework and literature survey," *Transportation Research Part F: Traffic Psychology and Behaviour*, vol. 43, pp. 183 – 198, 2016.

[56] K. L. Mosier, "Automation and cognition: Maintaining coherence in the electronic cockpit," in *Advances in human performance and cognitive engineering research*. Emerald Group Publishing Limited, 2002, pp. 93–121.

[57] J. S. Rubinstein, D. E. Meyer, and J. E. Evans, "Executive control of cognitive processes in task switching." *Journal of Experimental Psychology: Human Perception and Performance*, vol. 27, no. 4, p. 763, 2001.

[58] M. M. Ankarali, H. Tutkun Sen, A. De, A. M. Okamura, and N. J. Cowan, "Haptic feedback enhances rhythmic motor control by reducing variability, not improving convergence rate," *J Neurophysiology*, vol. 111, no. 6, pp. 1286–1299, 2014.

[59] M. Buehler, D. E. Koditschek, and P. J. Kindlmann, "Planning and control of robotic juggling and catching tasks," *Int J Robot Res*, vol. 13, no. 2, pp. 101–118, 1994.

[60] P. Kulchenko and E. Todorov, "First-exit model predictive control of fast discontinuous dynamics: Application to ball bouncing," in *Proc IEEE Int Conf Robot Autom*. IEEE, 2011, pp. 2144–2151.

[61] R. Ronsse, K. Wei, and D. Sternad, "Optimal control of a hybrid rhythmic-discrete task: the bouncing ball revisited," *J Neurophysiology*, vol. 103, no. 5, pp. 2482–2493, 2010.

[62] S. Schaal and C. G. Atkeson, "Open loop stable control strategies for robot juggling," in *IEEE International Conference on Robotics and Automation*, vol. 3, 1993, pp. 913–918.

[63] F. Huang and R. B. Gillespie, "Haptic feedback and human performance in a dynamic task," in *10th Symp. On Haptic Interfaces For Virtual Envir. & Teleoperator Sys.*, 2002.

[64] J. C. Huegel and M. K. O'Malley, "Progressive haptic and visual guidance for training in a virtual dynamic task progressive haptic and visual guidance for training in a virtual dynamic task," in *IEEE Haptics Symposium*, 2010, pp. 343–350.

[65] X. Guo and M. Bodson, "Equivalence between adaptive feedforward cancellation and disturbance rejection using the internal model principle," *Int J Adapt Control Signal Process*, vol. 24, pp. 211–218, 2010.

[66] T. Yamashita, T. Nakamura, M. Ohtsuka, and T. Taniguchi, "Heuristic learning process observed in manual control of crane," *World Cong Intl Fed Autom Control*, vol. 14, no. 2, pp. 1041–1046, 1981.

[67] M. Loomis and S. Barbara, "Distal attribution and presence," *Presence*, vol. 1, no. 1, 1991.

[68] E. Burdet, R. Osu, and D. W. Franklin, "The central nervous system stabilizes unstable dynamics by learning optimal impedance," *Nature*, vol. 414, 2001.

[69] C. J. Hasser and M. R. Cutkosky, "System identification of the human hand grasping a haptic knob," in *10th Symp Haptic Interfaces For Virtual Envir Teleoperator Sys*, 2002.

[70] A. Hajian and R. D. Howe, "Identification of the mechanical impedance at the human finger tip," *J Biomech Eng*, vol. 119, pp. 109–114, 1997.

[71] B. Yu, R. B. Gillespie, J. S. Freudenberg, and J. A. Cook, "Identification of human feedforward control in grasp and twist tasks," in *2014 American Control Conference*, 2014, pp. 2833–2838.

[72] E. Roth, K. Zhuang, S. A. Stamper, E. S. Fortune, and N. J. Cowan, "Stimulus predictability mediates a switch in locomotor smooth pursuit performance for Eigenmannia virescens," *J Exp Biol*, vol. 214, no. 7, pp. 1170–1180, 2011.

[73] A. Clark, *Being There: Putting Brain, Body, and World Together Again*. The MIT Press, 1997.

[74] L. E. Miller, V. Ravenda, N. Bolognini, V. Hayward, A. Farne, V. Ravenda, S. Bahmad, E. Koun, and R. Salemme, "Somatosensory Cortex Efficiently Processes Touch Located Beyond the Body," *Current Biology*, pp. 1–8, 2019.

[75] F. C. Huang, R. B. Gillespie, and A. D. Kuo, "Human adaptation to interaction forces in visuomotor coordination," *IEEE Transactions on Neural Systems and Rehabilitation Engineering*, vol. 14, no. 3, pp. 390–397, 2006.

[76] D. Powell and M. K. O'Malley, "The task-dependent efficacy of shared-control haptic guidance paradigms," *IEEE Transactions on Haptics*, vol. 5, no. 3, pp. 208–219, 2012.

[77] D. W. Weir, J. E. Colgate, and M. A. Peshkin, "Measuring and increasing Z-width with active electrical damping," *Symposium on Haptics Interfaces for Virtual Environment and Teleoperator Systems 2008 - Proceedings, Haptics*, pp. 169–175, 2008.

[78] B. Yu, R. B. Gillespie, J. S. Freudenberg, and J. A. Cook, "Human control strategies in pursuit tracking with a disturbance input," *Proceedings of the IEEE Conference on Decision and Control*, vol. 2015-February, no. February, pp. 3795–3800, 2014.

[79] R. L. Sainburg, "Should the Equilibrium Point Hypothesis (EPH) be Considered a Scientific Theory?" vol. 19, no. 2, pp. 142–148, 2015.

[80] N. Hogan and D. Sternad, "Dynamic primitives of motor behavior," *Biological Cybernetics*, vol. 106, no. 11-12, pp. 727–739, 2012.

[81] P. R. Davidson, R. D. Jones, H. R. Sirisena, and J. H. Andreae, "Detection of adaptive inverse models in the human motor system," *Human Movement Science*, vol. 19, no. 5, pp. 761–795, 2000.

[82] R. J. Krauzlis and S. G. Lisberger, "A Control Systems Model of Smooth Pursuit Eye Movements with Realistic Emergent Properties," *Neural Computation*, vol. 1, no. 1, pp. 116–122, 1989.

[83] J. Medina, S. A. Jax, M. J. Brown, and H. B. Coslett, "Contributions of Efference Copy to Limb Localization: Evidence from Deafferentation," *Brain Research*, vol. 23, no. 1, pp. 1–7, 2010.

[84] J. C. Rothwell, M. M. Traub, B. L. Day, J. A. Obeso, P. K. Thomas, and C. D. Marsden, "Manual motor performance in a deafferented man," *Brain*, vol. 105, no. 3, pp. 515–542, 1982.

[85] L. Patino, V. Chakarov, J. Schulte-Mönting, M. C. Hepp-Reymond, and R. Kristeva, "Oscillatory cortical activity during a motor task in a deafferented patient," *Neuroscience Letters*, vol. 401, no. 3, pp. 214–218, 2006.

[86] P. Stenneken, W. Prinz, J. Cole, J. Paillard, and G. Aschersleben, "The effect of sensory feedback on the timing of movements: Evidence from deafferented patients," *Brain Research*, vol. 1084, no. 1, pp. 123–131, 2006.

[87] M. Billon, A. Semjen, J. Cole, and G. Gauthier, "The role of sensory information in the production of periodic finger-tapping sequences," *Experimental Brain Research*, vol. 110, no. 1, pp. 117–130, 1996.

[88] E. S. Krendel and D. T. McRuer, "A servomechanisms approach to skill development," *Journal of the Franklin Institute*, vol. 269, no. 1, pp. 24–42, 1960.

[89] R. B. Gillespie, A. H. Ghasemi, and J. Freudenberg, "Human Motor Control and the Internal Model Principle," *IFAC-PapersOnLine*, vol. 49, no. 19, pp. 114–119, 2016. [Online]. Available: http://dx.doi.org/10.1016/j.ifacol.2016.10.471

[90] C. T.B and M. Sommer, "Corollary discharge across the animal kingdom," *Nature Reviews Neuroscience*, vol. 9, no. 8, pp. 587–600, 2008.

[91] M. A. Sommer and R. H. Wurtz, "Visual perception and corollary discharge," *Perception*, vol. 37, no. 3, pp. 408–418, 2008.

[92] N. B. Sarter and D. D. Woods, "Pilot interaction with cockpit automation II: An experimental study of pilots' model and awareness of the flight management system," *The International Journal of Aviation Psychology*, vol. 4, no. 1, pp. 1–28, 1994.

[93] L. Bainbridge, "Ironies of automation," in *Analysis, Design and Evaluation of Man–Machine Systems 1982*. Elsevier, 1983, pp. 129–135.

[94] T. Ferris, N. Sarter, and C. D. Wickens, "Cockpit automation: Still struggling to catch up," in *Human Factors in Aviation*, E. Salas and D. Maurino, Eds. Elsevier Inc., 2010, pp. 479–502.

[95] B. D. Seppelt and J. D. Lee, "Keeping the driver in the loop: Dynamic feedback to support appropriate use of imperfect vehicle control automation," *International Journal of Human-Computer Studies*, vol. 125, pp. 66–80, 2019.

[96] N. A. Stanton and M. S. Young, "Driver behaviour with adaptive cruise control," *Ergonomics*, vol. 48, no. 10, pp. 1294–1313, 2005.

[97] N. Strand, J. Nilsson, I. M. Karlsson, and L. Nilsson, "Semi-automated versus highly automated driving in critical situations caused by automation failures," *Transportation research part F: traffic psychology and behaviour*, vol. 27, pp. 218–228, 2014.

[98] B. Brown and E. Laurier, "The trouble with autopilots: Assisted and autonomous driving on the social road," in *Proceedings of the 2017 CHI Conference on Human Factors in Computing Systems*. ACM, 2017, pp. 416–429.

[99] M. S. Young and N. A. Stanton, "Back to the future: Brake reaction times for manual and automated vehicles," *Ergonomics*, vol. 50, no. 1, pp. 46–58, 2007.

[100] N. Merat, A. H. Jamson, F. C. Lai, and O. Carsten, "Highly automated driving, secondary task performance, and driver state," *Human factors*, vol. 54, no. 5, pp. 762–771, 2012.

[101] J. C. De Winter, R. Happee, M. H. Martens, and N. A. Stanton, "Effects of adaptive cruise control and highly automated driving on workload and situation awareness: A review of the empirical evidence," *Transportation research part F: traffic psychology and behaviour*, vol. 27, pp. 196–217, 2014.

[102] A. Eriksson and N. A. Stanton, "Takeover time in highly automated vehicles: noncritical transitions to and from manual control," *Human factors*, vol. 59, no. 4, pp. 689–705, 2017.

[103] C. Gold, D. Damböck, L. Lorenz, and K. Bengler, ""Take over!" how long does it take to get the driver back into the loop?" in *Proceedings of the Human Factors and Ergonomics Society Annual Meeting*, vol. 57, no. 1, 2013, pp. 1938–1942.

[104] N. Merat, A. H. Jamson, F. C. Lai, M. Daly, and O. M. Carsten, "Transition to manual: Driver behaviour when resuming control from a highly automated vehicle," *Transportation research part F: traffic psychology and behaviour*, vol. 27, pp. 274–282, 2014.

[105] C. Gold, M. Körber, D. Lechner, and K. Bengler, "Taking over control from highly automated vehicles in complex traffic situations: the role of traffic density," *Human factors*, vol. 58, no. 4, pp. 642–652, 2016.

[106] A. Telpaz, B. Rhindress, I. Zelman, and O. Tsimhoni, "Haptic seat for automated driving: preparing the driver to take control effectively," in *Proceedings of the 7th International Conference on Automotive User Interfaces and Interactive Vehicular Applications*. ACM, 2015, pp. 23–30.

[107] F. Flemisch, D. A. Abbink, M. Itoh, M. P. Pacaux-Lemoine, and G. Weßel, "Joining the blunt and the pointy end of the spear: towards a common framework of joint action, human–machine cooperation, cooperative guidance and control, shared, traded and supervisory control," *Cognition, Technology and Work*, vol. 21, no. 4, pp. 555–568, 2019.

[108] S. J. Anderson and S. C. Peters, "An optimal-control-based framework for trajectory planning, threat assessment, and semi-autonomous control of passenger vehicles in hazard avoidance scenarios," *Int. J. Vehicle Autonomous Systems*, vol. 8, pp. 190–216, 2010.

[109] J. Anderson, S. Walker and K. Iagnemma, "Experimental Performance Analysis of a Constraint-Based Navigation Framework," *Transactions on Systems, Man, and Cybernetics–Part A: Systems and Humans*, pp. 1–10, 2014.

[110] M. Steele, R. B. Gillespie, and a. Arbor, "Shared Control Between Human and Machine: Using a Haptic Steering Wheel to Aid in Land Vehicle Guidance," *Human Factors and Ergonomics Society, 45th Annual Meeting*, 2001.

[111] P. G. Griffiths and R. B. Gillespie, "Sharing Control Between Humans and Automation Using Haptic Interface: Primary and Secondary Task Performance Benefits," *Human Factors: The Journal of the Human Factors and Ergonomics Society*, vol. 47, no. 3, pp. 574–590, oct 2005.

[112] F. Flemisch, D. Abbink, M. Itoh, M. P. Pacaux-Lemoine, and G. Weßel, "Shared control is the sharp end of cooperation: Towards a common framework of joint action, shared control and human machine cooperation," *IFAC*, vol. 49, no. 19, pp. 72–77, 2016.

[113] M. Itoh, F. Flemisch, and D. Abbink, "A hierarchical framework to analyze shared control conflicts between human and machine," *IFAC*, vol. 49, no. 19, pp. 96–101, 2016.

[114] F. Mars and P. Chevrel, "Modelling human control of steering for the design of advanced driver assistance systems," *Annual Reviews in Control*, vol. 44, pp. 292–302, 2017.

[115] C. Guo, C. Sentouh, J. B. Haué, and J. C. Popieul, "Driver–vehicle cooperation: a hierarchical cooperative control architecture for automated driving systems," *Cognition, Technology and Work*, 2019.

[116] D. M. M. M. Petermeijer, Sebastiaan A. Abbink, "The effect of haptic support systems on driver performance: A literature survey," in *IEEE Transactions on Haptics*. IEEE, 2015, pp. 467–479.

[117] F. Mars, D. Mathieu, and J.-M. Hoc, "Analysis of human-machine cooperation when driving with different degrees of haptic shared control," *IEEE Transactions on Haptics*, vol. 1412, no. c, pp. 1–1, 2014.

[118] R. Nishimura, T. Wada, and S. Sugiyama, "Haptic Shared Control in Steering Operation Based on Cooperative Status Between a Driver and a Driver Assistance System," 2015.

[119] J. Kong, M. Pfeiffer, G. Schildbach, and F. Borrelli, "Kinematic and dynamic vehicle models for autonomous driving control design," in *IEEE Intelligent Vehicles Symposium, Proceedings*, 2015.

[120] C. D. Wickens, "Multiple resources and mental workload," *Human factors*, vol. 50, no. 3, pp. 449–455, 2008.

[121] J. D. Lee and K. A. See, "Trust in automation: Designing for appropriate reliance," *Human factors*, vol. 46, no. 1, pp. 50–80, 2004.

[122] A. Bhardwaj, Y. Lu, S. Pan, N. Sarter, and B. Gillespie, "The Effects of Driver Coupling and Automation Impedance on Emergency Steering Interventions," *IEEE Transactions on Systems, Man, and Cybernetics: Systems*, vol. 2020-October, pp. 1738–1744, 2020.